Radioguided interventions and surgery: Interventional Nuclear Medicine

Rietbergen, D.D.D.

RADIOGUIDED INTERVENTIONS AND SURGERY

Interventional Nuclear Medicine

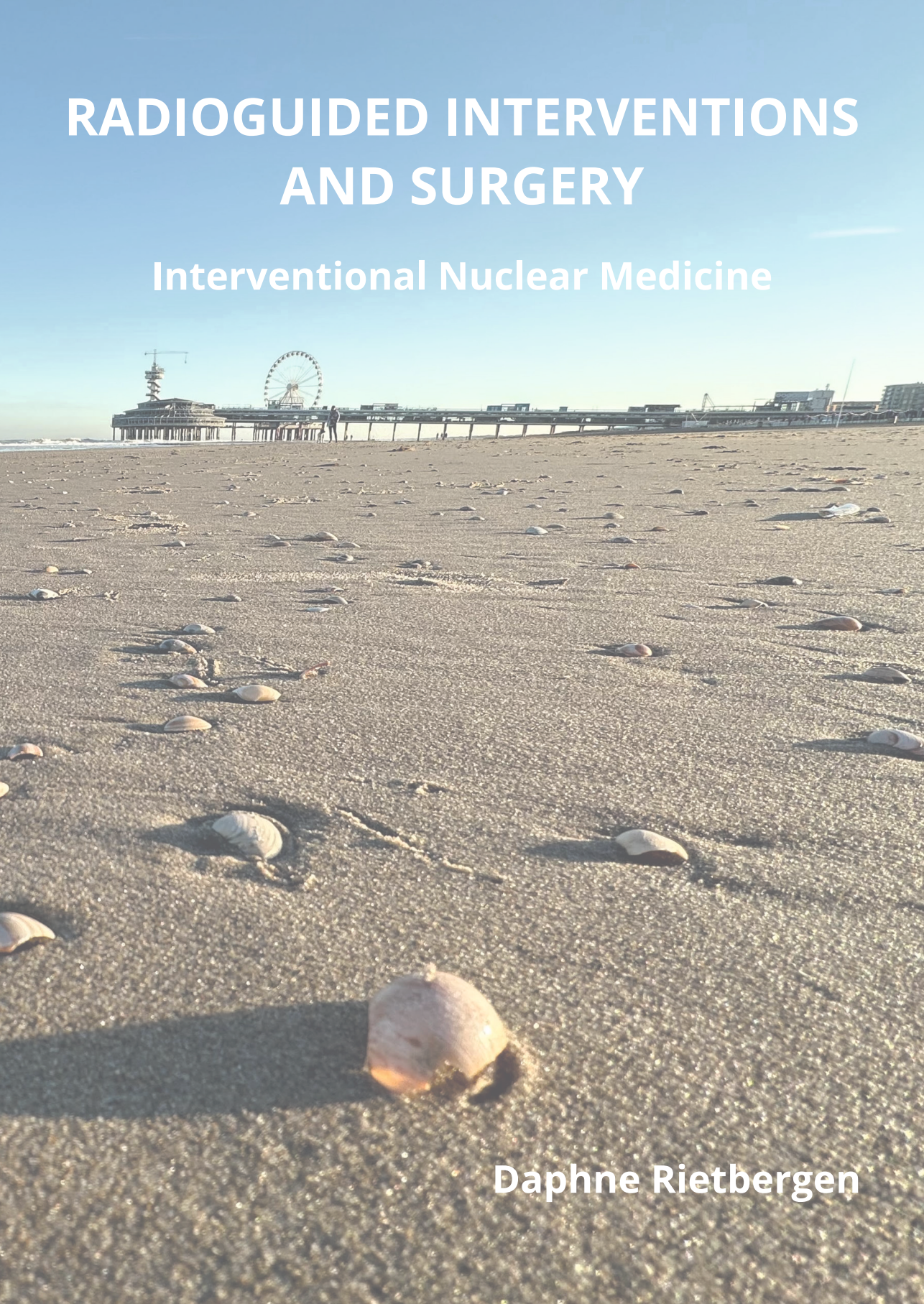

Daphne Rietbergen

Radioguided interventions and surgery

Interventional Nuclear Medicine

Daphne Rietbergen

Radioguided interventions and surgery. Interventional Nuclear Medicine

ISBN: 978-94-93391-66-6

Printed by Proefschriftspecialist | proefschriftspecialist.nl
Coverphoto: Daphne Rietbergen
Layout and design: Dagmar Versmoren, persoonlijkproefschrift.nl

Financial support: Curium Pharma, Sirtex Medical Europe GmbH

Radioguided interventions and surgery

-INTERVENTIONAL NUCLEAR MEDICINE-

Proefschrift

ter verkrijging van
de graad van doctor aan de Universiteit Leiden,
op gezag van rector magnificus prof. dr. ir. H. Bijl,
volgens besluit van het college voor promoties
te verdedigen op donderdag 21 november 2024
klokke 11.30 uur

door
Daphne Danielle Desire Rietbergen
geboren te Den Haag
in 1981

Promotiecommissie

Promotor:	Dhr. prof. dr. F.W.B. van Leeuwen
Co-promotor:	Mw. dr. T. Buckle
	Dhr. dr. R.A. Valdés Olmos
Overige leden:	Dhr. prof. dr. J.A. van der Hage (Secretaris)
	Dhr. prof. dr. H. van der Poel, Urology, NKI-AvL
	Dhr. prof. dr. J. Braun
	Mw. dr. D. Oprea-Lager, Nuclear Medicine, RadboudUMC
	Mw. dr. L.M. Pereira Arias-Bouda

Concordia res parvae crescent

(door eensgezindheid groeien kleine dingen)

-

Festina lente

Content

1

General introduction

Preoperative imaging of solid tumors is the cornerstone of adequate staging in the diagnosis of cancer. Patient with cN0 or preoperative staging imaging without lymph node involvement (iN0M0), patients undergo curative surgery. In solid tumors, the sentinel node (SN) procedure helps to define if micrometastatic lymph node are involved leading to adequate staging and suited treatment choices.

During surgical procedures, the surgeon explores the operation field for target lesions of interest; the primary tumor as well as the SN. In the bloodied operating field, small targets, like the SN, are not always easy to find. Especially not in areas with difficult anatomy or richly vascularized and nerve-supplied areas. Searching for this SN in these challenging areas can lead to unnecessary removal of healthy tissue with associated morbidities, incomplete or longer duration of surgery.

Accurate preoperative imaging, surgical planning and intraoperative tools to guide the surgeon to the lesion of interest can overcome these problems. Traditionally, radioguidance has been the standard of care for the SN procedure but this approach has limitations for SN biopsy in areas of complex anatomy like head/neck and the pelvis. In this context hybrid SN tracers have shown to give best of both pre- and intraoperative lesion detection. **Section 1** of this thesis is focused on clinical application with combined pre- and intraoperative imaging, using the hybrid SN tracer ICG-^{99m}Tc-nanocolloid, alone or in comparison to other radioactive tracers, for new potential clinical indications. This section pay also attention to ^{99m}Tc-Tilmanocept, a new generation SN tracer.

Chapter 2, provides an overview of interventional nuclear medicine using existing and novel tracers and various detection modalities discussing the needs for and key indications of radioguided surgery (e.g., lymphatic mapping, maker administration and targeted tracer development) related to chemical and engineering initiatives.

In **Chapter 3 and 4,** other radiocolloids of different particle sizes are compared with the hybrid tracer ICG-^{99m}Tc-nanocolloid which is based on the most used colloid particle size in Europe. In the clinical study, described in **Chapter 3**, lymphoscintigraphic drainage patterns, including SN and non-SLN appearing of ^{99m}Tc-Senti-Scint and the standard used tracer ICG-^{99m}Tc-nanocolloid are compared in patients with melanoma of the head and neck and truck.

In **Chapter 4**, drainage patterns, SN visualization and non-SN visualization of a rather new kid on the bloc, ^{99m}Tc-Tilmanocept, a manose receptor binding tracer, are presented and discussed for SN procedures in patients with breast cancer and melanoma.

Based on a prospective pilot study in patients with muscle invasive bladder cancer, **Chapter 5** describes the feasibility of SN targeting using the hybrid tracer indocyanine green (ICG)^{99m}Tc-nanocolloid for preoperative imaging and simultaneous intraoperative radioguidance and fluorescence guidance.

In **Section 2**, innovations within the field of radioguided surgery are described.

In a preclinical proof-of-concept setting, **Chapter 6** describes the sensitivity of using a freehand SPECT mobile gamma camera with 3D navigation to identify ^{99m}Tc-HDP positive lesions at bone scintigraphy. Further, the potential use for future radioguided biopsy osseous and non-osseous applications is discussed.

In **Chapter 7**, the preclinical tracer development of a novel hybrid tracer for liver surgery is described. This approach is based on fluorescence guided minimally invasive hepatobiliary surgery for liver cancer, including the use of preoperative imaging to visualize the lesions well in advance.

Section 2 concludes with future perspectives in radioguided surgery as discussed in **Chapter 8**, which also includes additional suggestions for expansion of the hybrid surgical guidance concept in robot-assisted surgery.

Section 1

Image guided surgery
and interventional
Nuclear Medicine

2

Interventional Nuclear Medicine

A focus on radioguided intervention and surgery

Adapted from:
Daphne D. Rietbergen, Matthias N. van Oosterom, Gijs H. KleinJan, Oscar R. Brouwer, Renato A. Valdés Olmos, Fijs W. van Leeuwen, Tessa Buckle.

The Quarterly Journal of Nuclear Medicine and Molecular imaging 2021;65:4-19

Abstract

Within interventional nuclear medicine (iNM) a prominent role is allocated for the sub-discipline of radioguided surgery. Unique for this discipline is the fact that an increasing number of clinical indications (*e.g.,* lymphatic mapping, local tumor demarcation and/or tumor receptor targeted applications) have been adopted into routine care. The clinical integration is further strengthened by technical innovations in chemistry and engineering that enhance the translational potential of radioguided procedures in iNM. Together, these features not only ensure ongoing expansion of iNM but also warrant a lasting clinical impact for the sub-discipline of radioguided surgery.

Introduction

In contrast to (conventional) interventional radiology – wherein target identification is defined by its anatomic or morphological features – interventional nuclear medicine (iNM) relies on underlying biological and pathophysiological features of diseases. More specifically, in nuclear medicine imaging of target specific molecular features in the human body (so called molecular imaging) is facilitated through the use of radiotracers. The ability of specific visualization of local tracer uptake in iNM facilitates molecularly targeted biopsy procedures (*e.g.,* breast specific gamma imaging)[1,2] or targeted therapy *via* local delivery of radioisotopes (*e.g.,* radioembolization).[3] Furthermore, radioguidance can help guide surgical resections (*e.g.,* PSMA-targeted salvage lymph node resections)[4]. The latter is also better described as the iNM sub-discipline of radioguided surgery.

Radioguided surgery has already been applied for decades and represents the most widely applied type of molecular-targeted image-guided surgery. The increasing surge of image-guided applications have strengthened the field of radioguided surgery *via* concomitant development and clinical availability of both novel (disease-specific) tracers and detection modalities. This review provides an overview of the needs for and key indications of radioguided surgery and discusses the related chemical and engineering initiatives.

Basic surgical needs

For surgically treated diseases, diagnosis and proper staging, surgical intervention and follow-up define the therapeutic process (Figure 1). Molecular imaging and NM are especially relevant during both diagnosis and the surgical intervention as: 1) the preoperative diagnostic scan allows target definition and staging of the patient; 2) immediate imaging provides a "scout scan" that confirms lesion-specific tracer uptake as well as the number of surgical targets; and 3) intraoperative imaging facilitates identification of relevant structures and confirmation of their removal. In the workflow preceding radioguided interventions, NM physicians rely on preoperative diagnostic scans as well as the "scout scan" used to define the surgical targets. Both are important as surgical planning revolves around roadmaps based on radiotracer uptake created using preoperative scintigraphy, SPECT and/or PET scans (the latter two are commonly complemented with CT to provide anatomical context besides attenuation correction). During surgery, imaging can be used to supplement the surgeons' ability to assess the target tissue (Figure 2). Open procedures provide the opportunity for palpation of the target lesion, allowing tactile feedback to complement visual interpretation of the surgical field (Figure 2A, B). One can imagine that tactile feedback is not an option for laparoscopic procedures (Figure 2C), meaning that the guidance provided by imaging becomes more dominant in these minimally invasive interventions.

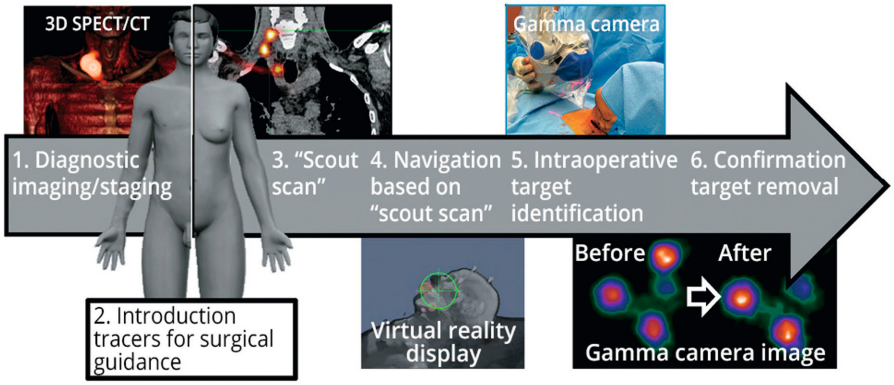

Figure 1. Workflow radioguided surgery. Example of the workflow in a head-and neck cancer patient from diagnostic imaging using (3D) SPECT/CT of the head-and-neck region (1), tracer administration performed by the nuclear medicine physician (2), SPECT/CT scout scan prior to surgery (3), preoperative navigation based on preoperative imaging using a virtual reality display (4), intraoperative localization of the target lesion using a portable gamma camera (5) to intraoperative confirmation of target removal based on the acquired image before and after the intervention (6).

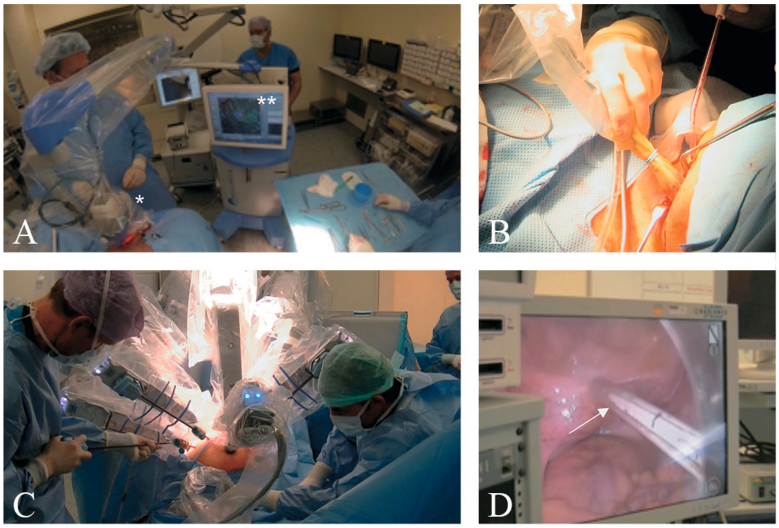

Figure 2. Radioguided surgery in practice. An example of A) mobile gamma-camera (*) based radioguidance applied in "open" head and neck surgery. The visualized SN is depicted on the screen (**) and intraoperative imaging can be applied prior to and post resection to validate accurate removal; B) intraoperative radioguidance using a conventional gamma probe in head and neck surgery. Herein the gamma probe is used to scan the wound bed, creating an acoustic readout with respect to the tracer uptake; C) application of radioguidance in a robot assisted laparoscopic setting wherein a laparoscopic gamma probe can be inserted through the assistant portal not in use by the robot, enabling D) intra-abdominal use (white arrow highlights the gamma probe).

To complement the surgeon's eyes and/or that of the laparoscopic/endoscopic camera, alternative modalities may be used to specifically detect tracer-accumulating targets (Figure 1,2). Depending on the country wherein the procedure is applied, this form of interventional imaging may be performed by a nuclear medicine physician or the surgical staff. The impact and relevance of such image guidance modalities, however, may vary per indication or stage of the procedure. At a macroscopic level, guidance can have a relatively low spatial resolution, as long as it has a high sensitivity and the signals minimally suffer from attenuation by tissue *i.e.* radioactive signals especially when focusing on the diseased tissue and its microscopic margins, these features remain of value, but real-time detection and a high spatial resolution become more critical, especially when surgeons re-examine the surgical field to confirm radical removal of radiotracer containing targets (so called R0-resection) sensitivity is leading. In case of tissue sparing resections, however, resolution could have a more prominent role.

Clinical indications for radioguided surgery

Radioguided surgery (Figure 2) has been successfully applied in a variety of clinical indications that can be divided among three distinct pathways, all of them based on the accumulation of an administered radiotracer in a target or index lesion, namely: local administration of a radiotracer followed by lymphatic diffusion, administration of a radioactive marker that is designed to be (partially) retained at the injection site, and systemic administration of a radiotracer that specifically accumulates in the target lesion. As each method has different strengths and limitations, these will be discussed separately.

Local administration of a radiotracer followed by lymphatic diffusion

It has been well known that fluid that is administered within the interstitial space of tissue predominantly drains *via* the lymphatic system. A concept that has been explored to identify lymph nodes basins that are related to a specific anatomical location is so-called lymphatic mapping. The ability to accurately detect areas that accumulate radioactivity in these areas has driven the identification of the lymph nodes directly draining from the tumor, the sentinel nodes (SNs). Assuming that metastases would sequentially spread through lymph nodes in the lymphatic system, examination of the SNs would allow identification of early invasion in locoregional lymph nodes. The SN biopsy procedure provides a particularly valuable tool to identify early metastatic spread (micrometastases <2 mm in diameter) in node negative patients, while sparing them from a potentially unnecessary radical lymph node dissection with all its morbidities. In addition, the SN approach provides means to identify aberrant drainage patterns; drainage routes that one does not expect based on the documented patient anatomy and is helpful in anatomic difficult areas.

For radioguided surgery a radiocolloid is locally administered and its drainage to SNs varies from <1% to approximately 7% of the administered amount of radiotracer, as demonstrated for melanoma.[5] Tracer migration and accumulation is preoperatively monitored using planar lymphoscintigraphy, frequently used in combination with SPECT/CT. Performing imaging at different timepoints allows the generation of roadmaps wherein SN(s) are differentiated from higher echelon nodes (nodes that contain radiotracer that has diffused beyond the SN). Intraoperatively, the SNs identified by imaging are targeted under guidance of gamma-probes and/or -camera's (Figure 2), which can be complemented with blue dye, depending on the indication and local strategy. Hereby especially the use of intraoperative gamma cameras has helped identify residual SNs *in situ e.g.,* in the form of cluster nodes.[6]

These abilities to specifically target SNs during surgery have led SN procedures to globally become a part of breast cancer and cutaneous melanoma surgery. Other routine implementations of the SN principle are found in penile and vulvar cancer. That said there is an ongoing discussion with regard to the clinical value of lymph node dissections. For example, the MSLT-2 trial (N=1755) revealed no melanoma-specific survival benefits when comparing immediate lymphadenectomy with active ultrasonography surveillance of the nodal basin.[7] For clinically node-negative patients with an increased risk of nodal metastases (G3, stage ≥T2 for penile cancer and <4 cm for squamous cell carcinoma of the vulva), SN procedures are recommended. Here, management of inguinal lymph nodes is crucial for prognosis and helps reduce the complication rates by minimizing the amount of inguinal lymph nodes dissected.[8,9] Beyond breast cancer,[10-18] melanoma[5,19] and penile/vulvar cancer,[8,9,20-22] SN detection in other malignancies, such as prostate,[23-27] head and neck cancer,[28-33] esophagus, lung, bladder and renal cancer[34-37] (Table 1),[5,8-122] is generally performed in research setting or as local standard treatment.[30,38]

Table 1. Radiotracers clinically used for image-guided surgery purposes. Modified from van Leeuwen et al.,[36] van Oosterom et al.[37]

Clinical procedure	Indications	Tracer
Sentinel lymph node biopsy (SN)[5,8-35,37-67]	Breast cancer Head and neck cancers Melanoma Prostate cancer Penile cancer Testicular cancer Vulvar cancer Cervix cancer Endometrial cancer Bladder cancer Esophagus cancer Colorectal cancer Anus cancer Gastric cancer Lung cancer Thyroid cancer	^{99m}Tc-nanocolloid, ICG-^{99m}Tc-nanocolloid, ^{99m}Tc-Senti-Scint, ^{99m}Tc-phytate colloid, ^{99m}Tc-tin colloid, ^{99m}Tc-sulfur colloid, ^{99m}Tc-rhenium colloid, ^{99m}Tc-antimony trisulfide, ^{99m}Tc-tilmanocept, ^{99m}Tc-dextran 500, ^{89}Zr-nanocolloid
Radioguided occult lesion localization (ROLL)[61,68-82]	Pulmonary lesions (*e.g.,* lung cancer) Thyroid cancer Endometriosis Renal cancer Ovary cancer Colorectal cancer Breast cancer Melanoma Lymphoma	^{99m}Tc-MAA, ICG-^{99m}Tc-nanocolloid
Radioguided seed localization (RSL)[83-88]	Breast cancer	^{125}I-seeds

Table 1. *Continued*

Clinical procedure	Indications	Tracer
Metabolic targeted resections - FDG[37,72,89-97]	Breast cancer, Thyroid cancer Ovarian cancer Cervical cancer Gastric cancer Lung cancer Head and neck cancer Adrenocortical cancer Melanoma Squamous cell Carcinoma Colorectal cancer Lymphoma Adenocarcinoma Endometrial carcinoma Plasmacytoma Urothelial carcinoma Sarcoma Eccrine porocarcinoma Testicular cancer Esophageal cancer	^{18}F-FDG
Metabolic targeted resections - L-DOPA[98]	Neuroendocrine tumors	^{18}F-L-DOPA
Metabolic targeted resection - Iodine or similar[37,98,99]	Thyroidectomy, Parathyroid adenoma, Thyroid carcinoma	^{99m}Tc-pertechenetate, ^{201}TlCl, ^{131}I, Na^{123}I
Metabolic targeted resections - Phosphorus[100]	Glioma	^{32}P buffered phosphate ion solution
Physiological targeted resections[37,101]	Thyroid cancer	^{99m}Tc-DMSA
Hydroxyapatite targeted resections[102-107]	Bone lesions	^{99m}Tc-MDP, ^{99m}Tc-HDP
Mitochondrial uptake targeted resections[69, 72, 108-115]	Breast cancer Brain tumor Parathyroid adenoma Parathyroid hyperplasia Parathyroid cancer	^{99m}Tc-sestamibi (MIBI)
Inflammatory targeted resections[90,116,117]	Extranodal lymphoma Granulomatous Inflammation Pancreatitis	^{67}Ga-citrate, ^{18}F-FDG

Table 1. *Continued*

Clinical procedure	Indications	Tracer
PET-guided biopsy[118-120]	Intrathoracic lesions Bone lesions Lymph nodes	^{18}F-FDG
Perfusion[121,122]	Brain tumors	^{131}I-diiodofluorescein
	Ureteral stent placement	^{99m}Tc-DTPA

Over the years, the widespread global implementation of the SN procedure has revealed some unsolved issues. In particular, the false-negative rates currently limit the routine implementation of SN procedures in indications such a cancer of the pelvic area. Evidently, the location of radiotracer deposition defines its connection to the lymphatic drainage pathways. Hence, improving the connection between the tumor extend and lymphatic coverage by the tracer deposition, could help make sure all lymphatic drainage pathways are covered. While sounding logical, this is still debated for *e.g.,* breast cancer, oral cavity cancer and prostate cancer.[18,33,24] This is illustrated by the differences in the applied techniques for tracer administration in breast cancer; these include intratumoral or peritumoral and intradermal, subdermal, subareolar and periaerolar injections. Although, oncological outcomes do not seem to be influenced by the route of administration, in multifocal lesions (peritumoral injections) discordance rates of 21% and 39% were found for respectively the axilla and internal mammary chain after performing both lymphoscintigraphy using a superficial injection and repeated lymphatic mapping following tumor-related injection (being intratumoral or surrounding the tumor) in the same patient.[15,17] Moreover, there is evidence that different parts of the breast show different drainage patterns.[15] Similar observations have been made for prostate cancer where the intraprostatic location of the tracer deposits was shown to determine the drainage routes.[24,65]

Next to the influence exerted *via* the administration route, physical blockage of lymphatic drainage, by tumor, as the result of trauma or previous local therapy or due to systemic therapy, could also impact the accuracy of the procedure. Any form of lymphatic blockage that occurs after the lymphatic seeding of metastases can possibly reroute the lymphatic drainage from the primary tumor, rendering the SN procedure inaccurate.[10, 21] In fact, literature indicates that the risk of missed disease after negative SN biopsy ranges from 1% to 4% in patients with T1 tumor and up to 15% in patients with T3.[14] Last but not least, "failure" to surgically resect the SNs identified on preoperative imaging also impacts the accuracy of the procedure. Here two scenarios may be explored: 1) the surgical team cannot identify the SN (or resects a higher echelon node instead), or 2) the SN cannot be safely resected

because it would lead to unacceptable iatrogenic morbidity (due to its locations). Both occur, but with the ever-advancing image guidance technologies, leaving SNs behind due to the risk of complications as result of the surgical resection seems to be the most likely threat.[25]

Administration of a radioactive marker that is designed to be (partially) retained at the injection site

In analogy to *e.g.,* the needle guided placement of guidewires, needle-guided delivery of radioactive substances or materials can also be used to mark specific tissues. In fact, the non-migrating fractions of the radiocolloids used in SN procedures can be used to demarcate the primary lesion or its margins.[33] Building on this, the use of physically larger microspheres (*e.g.,* ^{99m}Tc-microagregate albumin) can reduce the lymphatic drainage and can thus be used to improve the local tracer retention.[16] This concept has resulted in the radioguided occult lesion localization (ROLL) approach;[61,68-82] (Table 1);[5,8-122] an approach that has been applied in primary cancer and for metastatic lesions.[73,81,82] In lung cancer, this approach showed a 95% reliability for surgical successful localization and excision of small nodules and could be used to prevent open thoracotomy in 50% of patients because of benign origin.[80] Downsides of ROLL are that the procedure leads to excision of larger tissue volumes, and application can be complex in patients with multiple lesions or lesions that are non-assessable with a needle.[72]

Tissue marking of lesions with short living radionuclides such as ^{99m}Tc ($t_{1/2}$=6 h) provides a means to guide surgery within a 20-hour time window but has limited value beyond that. Longer living radioisotopes such as ^{125}I ($t_{1/2}$=59.4 days) have potential to extend this period. The need to reference the original location of a lesion has driven the implementation of radioguided seed localization (RSL), a procedure that uses sealed titanium capsule (4x0.8 mm: fits within a 18G needle) containing a non-therapeutic dose of ^{125}I. RSL has principally been applied in breast cancer patients receiving neoadjuvant treatment[123] (Table 1).[5,8-122] A recent study including 272 patients indicated that RSL results in higher tumor-free margin rates than wire-guided excision and ROLL in nonpalpable breast tumors. Advantages of RSL over wire localization are flexibility in timing (up to 5 days prior to surgery), improved definition of the incision site, and the ability to intraoperatively detect the targets. The use of ^{125}I-seeds also helps provide an axilla-conserving dissection solution for the increasingly popular neo-adjuvant strategies that are able to tailor systemic and locoregional treatment in breast cancer patients. The MARI (marking axillary lymph nodes with radioactive iodine seeds procedure; Table 1)[5,8-122] has helped realize a false-negative rate of 7% in predicting complete histopathological response in patients with tumor positive axillary nodes.[83] More recently, an 82% reduction in axillary lymph node dissections (N=159) was realized using an algorithm

combining ^{18}F-FDG PET/CT (pretherapy staging and stratification of the axilla) and the MARI-procedure (post-therapy staging).[87,88]

The most obvious limitation of using needle-based tissue demarcation for surgical guidance is the complexity associated with placing the needle in the center of the lesion or at specific points in the lesion borders. Given that today's image-guided needle placement approaches mostly rely on traditional radiological imaging *e.g.,* ultrasound, CT or MRI, this could mean pockets of diseased tissue are missed, resulting in positive surgical margins. Here iNM-guidance concepts based on systemic tracer administration such as those used in molecular-targeted biopsy could provide better outcome in the future[118-120] (Table 1).[5,8-122] Fei et al. provide a good overview of PET guided indications, (*e.g.,* brain tumors, bone lesions, breast, chest, head and neck, abdominal and pelvic tumors and bone and soft tissue malignancies).[96] Alternatively, scintigraphic guidance can be used *e.g,.* in the form of Molecular Breast Imaging (MBI).[97,115] Lee et al. found MBI has a superior specificity compared to mammography, and breast ultrasonography 90.93%, 90.66%, and 87.09%, respectively.[93] The overall rationale is that molecular guidance helps to improves the diagnostic yield of stereotactic biopsy sampling. Such percutaneous targeting concepts become especially appealing when they are integrated with "GPS-like" navigation concepts exploited with ultrasound modalities or the freehand SPECT technology.[29,54,124] The latter is a novel small field of view SPECT scanning technique that can be used to create a 3D image of the tracer distribution during the intervention by using optical tracking of the location and the orientation in space of a small gamma camera.[125]

Systemic administration of a radiotracer that specifically accumulates in a target lesion

Specific targeting of diseased areas that cannot be highlighted *via* SN procedures or using local demarcation techniques could benefit from targeting approaches that rely on systemic tracer administrations. Herein a distinction can be made between the use of metabolic tracers (Table 1)[5,8-122] and receptor-specific overexpression at the membrane of diseased cells (Table 2).[37,69,94,101,104,126-166] Theoretically, the same tracers that are used for diagnostic purposes, or analogues thereof, can also be used to facilitate surgical guidance. Relying on accumulation following systemic administration, may, however, mean signal intensities can be relatively low. As a consequence, more than with the above discussed SN procedures, achieving a high enough target-to-non target or signal-to-background ratio (TNR or SBR) can be challenging.

Table 2. Receptor targeted approaches image-guided surgery. Modified from van Oosterom et al.[37]

Clinical procedure	Indications	Tracer
Receptor targeted resections	Prostate [4,126-131]	^{99m}Tc-PSMA I&S, ^{111}In-PSMA I&T, 111In-capromab pendetide, ^{125}I-B72.3
	Renal [132,133]	^{124}I-cG250
	Colorectal cancer [94,104,134-141]	^{99m}Tc-IMMU-4 Fab', ^{111}In-B72.3 (CYT-103), $^{125/131}$I-B72.3, ^{125}I-CC49, ^{125}I-HuCC49ΔCH2 ^{125}I-A5B7, ^{125}I-CL58, ^{125}I-17-1A, ^{124}I-Hu-A33
	Gastric cancer [94,142,143]	$^{125/131}$I-3H11, ^{125}I-B72.3
	Breast cancer [94,142 143]	^{125}I-B72.3, ^{125}I-F023C5, ^{125}I-NR-LU-10
	Ovarian cancer [94,144,145]	^{99m}Tc-H17E2, ^{99m}Tc- SM3, ^{111}In-B72.3 (CYT-103), ^{125}I-B72.3, ^{125}I-CC49, ^{131}I-OC125
	Pancreatic cancer [94,144,145]	^{125}I-CC49
	Neuroendocrine tumors [37,69,101,146-166]	^{111}In-pentetreotide, ^{68}Ga-DOTA-NOC, ^{68}Ga-DOTA-TATE, ^{68}Ga-DOTATOC, [^{99m}Tc-EDDA/HYNIC] octreotate, ^{99m}Tc-HYNIC-octreotide ^{125}I-Tyr 3-octreotide, ^{125}I-Lanreotide, $^{123/125/131}$I-MIBG ^{99m}Tc-MIBI

Established methods of radioguided surgery rely on gamma-emitting tracers and is *e.g.* applied in prostate [4,126-131], renal [132,133],colorectal [94,104,134-141],gastric [94,142,143], breast [94,142,143], ovarian[94,144,145], pancreatic cancer [94,144,145] and in neuroendocrine tumors and meningioma[37, 69,101,146-166] (Table 2). In neuroendocrine benign and malignant diseases, metabolic imaging often is used to guide the surgeon to the target of interest. [37, 69, 94, 101, 146-166] ^{99m}Tc-MIBI (scintigraphy and SPECT) is used to highlight hyperfunctional tissue, and ectopic or mediastinal glands (70-95%).[167] Highlighting the hyperfunctional tissue, helps avoid bilateral cervical exploration by the surgeon and is known to be superior in terms of cure and complication rates.[168-170] Use of radiotracers can also show value for other neuroendocrine tumors *e.g.,* gastro-entero-pancreatic neuroendocrine tumors (GEPNETs), pheochromocytoma (PC) or paraganglioma (PGL). The majority of these neuroendocrine tumors express somatostatin receptors (SSR) which targets with radiolabeled somatostatin analogs (NET) or ^{123}I-MIBG (PC, PGL), depending on the expressed somatostatin receptor.[162,166] Wang et al. reported a significantly reduced 5-year recurrence rate in meningioma patients that underwent ^{99m}Tc-HYNIC-octreotide directed surgery, compared to patients who were operated solely based on preoperative MRI (13.3% *vs*. 30%). This approach could facilitate the detection of primary tumors as well as lymphatic metastasis.[171] A feasibility study by Kaemmerer *et al.* showed that 94% of ^{68}Ga-DOTA-NOC or ^{68}Ga-DOTA-TATE positive lesions were detected by a 511 keV gamma probe, 69% with PET-CT and 50% with surgical palpation (golden standard), in which the radioguided surgery approach resulted in change in operation approach in 56%.[155] Hereby a target-to-background threshold of 2.5 was used to warrant surgical resection.[165]

In prostate cancer patients (N=31) with recurrent disease a dual-tracer approach that combined preoperative imaging (^{68}Ga-PSMA-11 PET) with intraoperative ^{99m}Tc-PSMA-radioguided surgery (RGS) during radical prostatectomy was shown to allow removal of all lesions visualized on preoperative ^{68}Ga-PSMA-11 PET. Moreover, ^{99m}Tc-PSMA-RGS enabled the detection of additional metastases as small as 3 mm in two patients. The sensitivity, specificity and accuracy of this technique was reported to be respectively 83.6%, 100% and 93.0%. This resulted in a biochemical recurrence free survival rate of 41.9% and a treatment free rate of 64.5% at one-year post surgery.[129]

In addition to the use of dedicated gamma-emitting radiotracers, there have been a number of exploratory studies that made use of the widely applied metabolic PET-tracer ^{18}F-FDG for radioguided surgery, either *via* 511 KeV gamma-tracing, Beta-tracing or Cerenkov imaging in either head and neck, cervical or thyroid cancer patients.[91,172-174] In a study that included 12 thyroid cancer patients undergoing a total thyroidectomy along with a modified radical neck dissection Kim et al reported that tumors could be localized by Cerenkov imaging using a PET probe in real time.

It was especially interesting that in one patient lesions that were not observed on preoperative PET could be detected intraoperatively with Cerenkov imaging, while in a second patient additional lymph nodes that were not identified on preoperative ultrasonography could be intraoperatively detected with Cerenkov imaging.[91]

As for the other surgical guidance approaches, also receptor targeted imaging has its limitations. For instance, the ability to identify lesions based on their receptor expression has a strong volume dependency. In general, it is assumed that PET, the clinical nuclear medicine modality with the highest spatial resolution and sensitivity, can miss small lesions with low uptake. As a result, micrometastases and/or diluted pockets of diseased tissue may be missed, especially when the receptor density is low. Another limitation is the fact that the discussion to go for a surgical intervention is often made based on week- or month- old diagnostic scans *e.g.,* ^{68}Ga-PSMA PET, meaning that there can be a discordance in the lesions targeted, which can lead to confusion in the operating room. Finally, "failure" to surgically identify and resect the lesions is a real risk given the relatively low quantity of tracer that can be accumulated in a lesion as result of receptor-based binding.

An important issue in the development of new radioguided surgery procedures and the use of beta-emitting radionuclides is the occupational exposure of the surgical staff (isotopes with high-energy emissions may limit the clinical application due to dose limit for occupational exposure).[175]

Technical innovations that are advancing the field of radioguided surgery

Trends in tracer development

While various radiotracers have been clinically used for radioguided surgery purposes (Table 1);[5,8-122] the success of radioguided surgery indications is fully dependent on the ability to accumulate or retain radioisotopes in a specific area of interest, meaning that the implementation is very much driven by the chemical properties of the tracer. In fact, the chemical properties of a radiotracer dictate both the sensitivity and specificity. The impact of these chemical properties is underlined by the fact that many research groups have generated alternative tracers with the intent to improve the accuracy of existing procedures. For example, ^{99m}Tc-nanocolloid and ^{99m}Tc-tilmanocept for SN biopsy,[176] or radiotracers that enable expansion of the field towards other indications; *e.g.* ^{99m}Tc-PSMA I&S in PSMA-RGS in recurrent prostate cancer and ^{99m}Tc-HYNIC-octreotide for intraoperative identification of meningiomas.[129,151,159,171] Next to the, perhaps obvious, (radio)chemical refinements that are required to advance the intrinsic tracer performance, chemical efforts in this area have also focused on improving the dosing[177] and formulation of tracers (based on *e.g.* particle density or injection volume) [23] and the expansion

of radiotracers with imaging labels that may be detected by modalities other than radioguidance, *e.g.* fluorescence-guidance ICG-^{99m}Tc-nanocolloid or FITC-^{125}I-CEA-mAb[27,66] (Table 3).[66,178-183]

Table 3. Clinically applied hybrid tracers.

Clinical procedure	Indications	Tracer
Sentinel lymph node biopsy [178-182]	Breast cancer, Oral cavity cancer Head and neck cancer Penile cancer Vulvar cancer Melanoma	ICG-^{99m}Tc-nanocoloid ^{125}I-methylene blue
Targeted resections [66,183]	Brain tumors Parathyroid adenoma Colorectal carcinoma Clear cell renal cell carcinoma Metastatic melanoma Rectal cancer Head and neck cancer	^{131}I-Fluorescein ^{68}Ga-IRDye800CW-BBN ^{123}I-Methylene blue FITC-^{125}I- CEA mAb ^{111}In-DOTA-Girentuximab-IRDye800CW ^{124}I-cRGDY-PEG-C

Efforts in tracer refinement for radioguided lymphatic mapping procedures are emphasized by the quest for radiotracers that only accumulate in the SN and that do not migrate to higher echelon nodes. Here different avenues are being explored, *e.g.,* particle size restricted migration speed[16] or targeting of receptors expressed in lymphatic ducts and lymph nodes.[184] As a general rule, it can be assumed that particles <50 nm (such as ^{99m}Tc-HSA, ^{99m}Tc-antimony, or ^{99m}Tc-tilmanocept[11,19,67]; Table 1)[5,8-122] show faster washout rates from the injection site and therefore disperse more rapidly to the SN but also to higher echelon nodes, while particles >100 nm in size (*e.g.*, ^{99m}Tc Sulphur colloid, ^{99m}Tc-MAA and ^{99m}Tc-Scentiscint;[16, 185] Table 1,[5,8-122]) display slower migration and longer retention in the SN. The latter results in visualization of a higher number of nodes in delayed images compared to the number of nodes identified in early scintigraphy images. Colloidal particles with an average size range of 50-70 nm (*e.g.* ^{99m}Tc-nanocolloid) are therefore thought to be the best compromise between fast lymphatic drainage and optimal retention in the SN.[185] These assumptions were underlined in a comparative study in 215 patients with operable breast carcinoma wherein Paganelli *et al.* compared three ^{99m}Tc labeled tracers of different particle sizes (^{99m}Tc antimony sulfide [<50 nm], ^{99m}Tc-nanocolloid [<80 nm] and ^{99m}Tc-MAA [200-1000 nm]).[16] This study revealed that colloidal particles with a larger size were most successful in detecting only one or two sentinel nodes, even at 14-16 h after tracer administration. Despite the different options offered, in Europe the choice of radiocolloid is mainly dictated by availability and price, favoring ^{99m}Tc-nanocolloid.[16,185]

In the current setting, accurate SN imaging is dependent on tracer migration through the lymphatic system following local injection and subsequent uptake in macrophages. This setting can be stipulated to provide an ideal platform for receptor targeted tracer approaches that allow identification of micrometastases that are otherwise undetectable with *e.g.,* PET. As such, it has been argued that receptor targeted tracers could help to identify disease more specifically. Unfortunately, these efforts have not always proven to be successful. For example, comparative lymphatic mapping studies between either the targeted tracers ^{99m}Tc-Rituximab (antibody-based radiopharmaceutical that binds to the CD20 receptor on B-cells)[184,186] or ^{99m}Tc-tilmanocept (a small dextran-based colloid with DTPA and mannose moieties conjugated to its structure that binds CD206 receptor specific to reticuloendothelial cells)[11,19,47,67] and the untargeted ^{99m}Tc-sulfur colloid in patients with breast cancer or melanoma did not show improvement in the identification of tumor-positive SNs or a reduction in the number of false-negative SN biopsy results.[19] In contrast to applying receptor-targeted tracers during lymphatic mapping procedures, intravenously applied receptor-targeted tracers have shown great potential in identifying macrometastases using *e.g.,* PSMA- and somatostatin-specific tracers.[38,129,155]

While different radioisotopes have successfully been used in radioguided procedures (Table 1),[5,8-122] radiochemical efforts have been mainly focused on creating ^{99m}Tc-tracer analogues. Not only does the use of this isotope limit the radiation burden for the surgical staff, it also allows the use of existing pre- and intraoperative radioguidance modalities. Furthermore, the 6h half-life provides flexibility in logistics as both one- and two-day protocols can be used.[128,129,187] When PET is preferred in first-line diagnostics, tandem use of a diagnostic PET-tracer and specific tracer for radioguided surgery that both target the same receptor can be applied. For instance, combined use of ^{68}Ga-PSMA-11 and ^{99m}Tc-PSMA-11 can be used to facilitate PSMA-PET and to support PSMA-targeted resections.[129] Alternatively, re-injection of a PET-tracer could allow intraoperative beta- or Cerenkov imaging.[173,174] In such a case, however, one should consider the radiation dose and the half-life of the radioisotope.[52]

Perhaps the most innovative step made within the field of radiochemistry related to image-guided surgery is the generation of dual-labeled, or hybrid, tracers that contain both a fluorescent- and a radiolabel (Table 3).[66,178-183] The clinically implemented hybrid tracers again focus on the use of gamma-emitting radioisotopes such as ^{99m}Tc and ^{111}In and $^{123/124/125/131}$I. While not always in line with clinical demand, in the preclinical setting the development of hybrid tracers for the purpose of radioguided surgery is expanding rapidly, with many exotic radioisotope-dye-targeting vector options (including peptide-, antibody- or even nanoparticle-based vectors) under investigation and often also exploring PET-radioisotopes such as ^{64}Cu

and ^{68}Ga.[188] Although hybrid concepts today focus on the extension of radioguided surgery with *e.g.,* fluorescence- guided surgery, the simultaneous use of different imaging signatures could also be used to help visualize complementary imaging features during surgery.[179]

The overall trend in tracer development seems to be that the most straightforward/ uncomplicated tracer designs find the widest clinical use. It is also becoming increasingly clear that 1) the introduction of *e.g.,* a fluorescent label has a direct impact on the tracer performance (affinity, kinetics, biodistribution[189-192]), 2) that different imaging labels may yield different detection sensitivities[190] and 3) complementary imaging signatures can be used for multiplexing applications.[179]

Engineering

The implementation of engineering advances is widespread and can benefit a range of indications. The most important determinants for these detection modalities are: 1) the radioisotope that is used (*e.g.,* a gamma probe designed to detect ^{99m}Tc is able to detect all ^{99m}Tc-containing radiotracers); 2) the specific surgical method: open, laparoscopic, or robot-assisted surgery, and 3) the availability of preoperative imaging.[37] The first requirement separates most of the radioguided surgery technologies between application towards SPECT-based (*e.g.* ^{99m}Tc, ^{125}I, ^{111}In) and PET-based (*e.g.* ^{18}F, ^{68}Ga, ^{124}I) radioisotopes[94] (Table 1, Table 2, Table 3).[5,8-122,126-166,178-183] The second requirement indicates if a detection modality is best optimized for usage during open surgery (*e.g.,* handheld camera) or laparoscopic (robot assisted) surgery (*e.g.,* laparoscopic probes). Preoperative imaging, as indicated by the third requirement, is an essential piece of information during surgery, allowing the surgeon to evaluate the extent of the disease to be treated. Where applications with SPECT- or PET-based isotopes have a direct link with preoperative imaging, other applications can benefit from indirect bremsstrahlung imaging (*e.g.,* emitting beta radiation only,[193] radioisotopes emitting a combination of gamma, beta+ and/ or beta- radiation (*e.g.,* ^{131}I, ^{133}I, ^{64}Cu;), or hybrid tracer designs (*e.g.,* emitting both gamma radiation and fluorescence light).

Radioguidance modalities for low-energy (<150 keV) gamma emitting tracers, especially ^{99m}Tc, remain the most widely applied.[37] Most recent engineering efforts have focused on tailoring existing gamma-probe modalities towards modern surgical needs (Figure 1), such as minimal invasive (robot-assisted) surgery. One prime example is the DROP-IN gamma probe (Figure 3A),[95] a tethered small-sized gamma probe for radioguidance within robotic surgery.[194] Designed to be handled within the abdominal space, using highly maneuverable robotic instruments used by surgeon, this DROP-IN probe allows the surgeon to autonomously scan in many complex orientations.[4,26] Due to detector sizes, the application of portable gamma cameras remains mostly focused on open surgery procedures and is often

combined with the use of a gamma probe as well.[35] However, exception from this rule is shown for example by Brouwer et al. (Figure 3B),[95] using a portable gamma camera to simultaneously image the ^{99m}Tc-harboring SNs and a ^{125}I-seed fixed at the tip of a laparoscopic gamma probe to facilitate intraoperative lesion localization during laparoscopic testicular cancer surgery.[195] Yet another technical enhancement is provided by the freehand SPECT technology (Figure 3C, D).[95] This technology allows acquisition of an intraoperative SPECT scan using optically tracked gamma-probes or -cameras to render 3D views (*i.e.* augmented or virtual reality) of the radionuclide uptake during surgery.[34] This application has been described for both open and laparoscopic procedures, showing applications (Figure 3 C-G)[95] in: various SN applications (*e.g.,* breast cancer,[12,54,196] gynecology,[197] head and neck cancers,[12,31,32,34,198,199] melanoma,[32,200,201] penile cancer[63] and prostate cancer[63]), ROLL applications (*e.g.,* for pulmonary lesions[77]), RSL procedures (*e.g.,* breast cancer[85]), NET tumors,[202] parathyroid adenoma,[113] PSMA-targeted prostate salvage procedures,[203] and for visualization of various bone lesions.[105] Uniquely, the same tracking technology used to generate the freehand SPECT scans can also be used to navigate a gamma-probe in the preoperative SPECT(/CT) road map, thereby facilitating a 'GPS-like' navigation workflow.[204] There have been a number of studies that underline the use of preoperative SPECT/CT scans as basis for the navigation of a gamma probe in SN applications using (ICG-)^{99m}Tc-nanocolloid (*e.g.,* breast cancer, melanoma, penile cancer, prostate cancer and thyroid cancer[69,204,205]), removal of neuroendocrine tumors using ^{123}I-MIBG (*e.g,.* paraganglioma[69,204,205]) and resection of parathyroid adenoma using ^{99m}Tc-MIBI.[69,204,205] In these indications the real-time read-out of the gamma probe helps to compensate for navigation inaccuracies that are a fundamental issue in soft-tissue applications.[206] This approach was later expanded with the integration of ultrasound and fluorescence.[29,55,63,124,207-209]

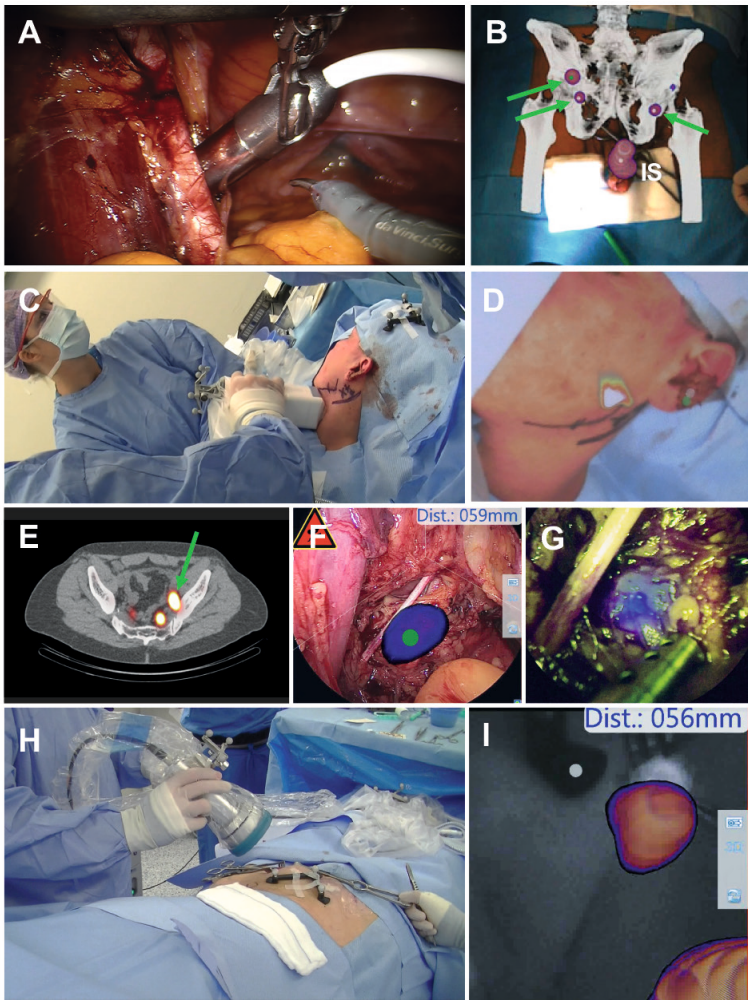

Figure 3. Engineering advances in radioguided surgery. A) Use of a DROP-IN gamma probe for robot-assisted radioguided surgery (*e.g.,* prostate SN or Tc-PSMA procedure) wherein the DROP-IN probe is inserted through a standard 12 mm trocar and handled using the laparoscopic surgical instruments while guidance is based on an acoustic readout. B) Intraoperative augmented reality overlay of a preoperative SPECT/CT (depicting the injection site (IS) and the SNs (arrows) used during penile cancer surgery. C) Acquisition of an intraoperative freehand SPECT scan using a handheld gamma camera during a head and neck SN procedure. D) Augmented reality overlay of the freehand SPECT results (rainbow coloring) on the surgical field prior to excision, depicting the SN location. E) Preoperative SPECT/CT depicting the SN (arrow) in a prostate cancer patient. F) Corresponding intraoperative navigation of the fluorescence laparoscope based on intraoperative freehand SPECT of the SN (middle) revealing the distance between the tip of the laparoscope and the SN target.[95] G) Confirmation that the target has been reached provided by fluorescence imaging showing the SN in blue.[95] H) Intraoperative navigation of a fluorescence camera dedicated to open surgery based on preoperative SPECT/CT in a penile cancer patient during a SN biopsy procedure. I) Navigated fluorescence imaging with augmented overlay of the SN and estimated distance towards the SN.

For detection of high energy gamma rays (511 keV) or beta-rays, alternative modalities are required. The ability to utilize the 511 keV annihilation gamma rays emitted by PET tracers has received most attention.[210] However, requiring large and heavy collimation (typical probe diameter 25-35 mm), means application of these probes is not widespread and restricted to open surgery. Recently there has been a reemergence of beta-probes that can be used to directly detect beta+ particles as emitted by the PET-based radioisotopes, or even beta- particles as emitted from radioisotopes more often considered as "therapeutic" (*e.g.,* ^{90}Y).[211,212] Where older designs often still required heavy-metal collimation or a more complicated dual-detector design to suppress background noise as a result of the gamma-ray background (*i.e.* 511 keV annihilation gammas and/or bremsstrahlung gammas), advances in the detector technology have eliminated this need.[213] As such, these beta-detectors can contribute to a much smaller and lighter probe design. This property has also opened avenues towards exploration of beta probes in laparoscopic or even robot-assisted laparoscopic procedures.[214] Similarly, there have also been efforts to explore the use of beta-cameras[215,216] and even freehand beta scans.[217,218]

In all applications of radioguidance an intuitive display of the counts or images, relative to the patient anatomy is in demand. A radioguidance readout can be placed in the surgical context by combining it with optical images, surgical navigation and/or additional modalities such as fluorescence (Figure 3 H-I).[95] To that end, some authors report on visualizing 2D portable gamma camera images as an augmented reality overlay on the patient anatomy, by a built-in optical camera.[57,69,219] As a next step, the above discussed "GPS-like" navigation concepts (based on preoperative SPECT/CT, [204] PET/CT [120] or intraoperative freehand SPECT [34]) use augmented and virtual reality visualizations in an attempt to integrate the in-depth 3D scan details in the surgical workflow. These technologies provide the surgeon with 3D information where his/her surgical instruments are relative to the surgical targets.

In a different approach to provide an intuitive display during radioguidance, combined with the increased clinical implementation of hybrid tracers, engineering efforts have also focused on the integration of hybrid (or "multiplexing") sensors in radioguidance detection modalities. An example is the opto-nuclear probe,[62,220,221] a gamma probe that can also trace ICG fluorescence by using acoustic and numerical read-out. Such hybrid modalities have even shown to be successful in a freehand imaging and navigation workflows, providing both 3D SPECT and 3D fluorescence.[222] In a more experimental setting this hybrid concept was later explored with the integrated use of gamma and fluorescence cameras, providing visual information of both imaging modalities *in vivo*.[223]

Despite the fact that many of the technological advances described in this review show great promise beyond the traditional open surgery gamma probe, in most cases the real clinical impact of these devices still requires more detailed evaluation.

Conclusion

The radioguided surgery sub-discipline of iNM has been steadily evolving over the last decades, guided by the outcome of clinical studies as well as the translation of new (chemical or engineering) technologies into the clinic. A prime example of the extension of the field is the recent introduction of ^{99m}Tc-PSMA targeted salvage surgery, which elegantly combines a chemical innovation with radioguidance concepts previously validated during SN approaches. It is success stories like these that motivate clinicians and researchers active within nuclear medicine and surgery to create technologies that meet the clinical demand. Overall, the technological developments in the field of radioguided surgery indicate future developments will most likely be directed towards: 1) further expansion to disease specific tracers; 2) hybrid detection concepts that combine radioguidance with *e.g.*, fluorescence imaging; 3) integration of image guidance in minimally invasive (*e.g.*, robotic) procedures; and 4) use of surgical navigation concepts (including augmented and virtual reality displays).

References

1. Fowler AM. A molecular approach to breast imaging. J Nucl Med 2014;55:177–80.
2. Urbano N, Scimeca M, Tancredi V, Bonanno E, Schillaci O. 99mTC-sestamibi breast imaging: current status, new ideas and future perspectives. Semin Cancer Biol 2020;S1044-579X(20)30008-0.
3. Abdel-Rahman O, Elsayed Z. Yttrium-90 microsphere radioembolisation for unresectable hepatocellular carcinoma. Cochrane Database Syst Rev 2020;1:CD011313.
4. van Leeuwen FW, van Oosterom MN, Meershoek P, van Leeuwen PJ, Berliner C, van der Poel HG, *et al.* Minimal-Invasive Robot-Assisted Image-Guided Resection of Prostate-Specific Membrane Antigen-Positive Lymph Nodes in Recurrent Prostate Cancer. Clin Nucl Med 2019;44:580–1.
5. Kapteijn BA, Nieweg OE, Muller SH, Liem IH, Hoefnagel CA, Rutgers EJ, *et al.* Validation of gamma probe detection of the sentinel node in melanoma. J Nucl Med 1997;38:362–6.
6. Hermann K. Radioguided Surgery – Current Applications and Innovation Directions in Clinical Practice. Berlin: Springer; 2016.
7. Faries MB. Completing the Dissection in Melanoma: Increasing Decision Precision. Ann Surg Oncol 2018;25:585–7.
8. Hakenberg OW, Compérat EM, Minhas S, Necchi A, Protzel C, Watkin N. EAU guidelines on penile cancer: 2014 update. Eur Urol 2015;67:142–50.
9. Kamel MH, Khalil MI, Davis R, Spiess PE. Management of the Clinically Negative (cN0) Groin Penile Cancer Patient: A Review. Urology 2019;131:5–13.
10. Albert A, Huyghe I, Stroobants S, Tjalma WA. Three Different Locations of a Sentinel Node Highlight the Importance of Performing a Sentinel Node Biopsy in Breast Cancer Recurrence. Breast Cancer (Auckl) 2016;10:1–3.
11. Baker JL, Pu M, Tokin CA, Hoh CK, Vera DR, Messer K, *et al.* Comparison of [(99m)Tc] tilmanocept and filtered [(99m)Tc]sulfur colloid for identification of SLNs in breast cancer patients. Ann Surg Oncol 2015;22:40–5.
12. Bluemel C, Schnelzer A, Okur A, Ehlerding A, Paepke S, Scheidhauer K, *et al.* Freehand SPECT for image-guided sentinel lymph node biopsy in breast cancer. Eur J Nucl Med Mol Imaging 2013;40:1656–61.
13. Chondrogiannis S, Ferretti A, Facci E, Marzola MC, Rampin L, Tadayyon S, *et al.* Intraoperative hand-held imaging γ-camera for sentinel node detection in patients with breast cancer: feasibility evaluation and preliminary experience on 16 patients. Clin Nucl Med 2013;38:e132–6.
14. Hindié E, Groheux D, Brenot-Rossi I, Rubello D, Moretti JL, Espié M. The sentinel node procedure in breast cancer: nuclear medicine as the starting point. J Nucl Med 2011;52:405–14.
15. Noushi F, Spillane AJ, Uren RF, Cooper R, Allwright S, Snook KL, *et al.* High discordance rates between sub-areolar and peri-tumoural breast lymphoscintigraphy. Eur J Surg Oncol 2013;39:1053–60.
16. Paganelli G, De Cicco C, Cremonesi M, Prisco G, Calza P, Luini A, *et al.* Optimized sentinel node scintigraphy in breast cancer. Q J Nucl Med 1998;42:49–53.

17. van der Ploeg IM, Nieweg OE, van Rijk MC, Valdés Olmos RA, Kroon BB. Axillary recurrence after a tumour-negative sentinel node biopsy in breast cancer patients: A systematic review and meta-analysis of the literature. Eur J Surg Oncol 2008;34:1277–84.
18. Wiatrek R, Kruper L. Sentinel lymph node biopsy indications and controversies in breast cancer. Maturitas 2011;69:7–10.
19. Silvestri C, Christopher A, Intenzo C, Kairys JC, Kim S, Willis A, *et al.* Consecutive Case Series of Melanoma Sentinel Node Biopsy for Lymphoseek Compared to Sulfur Colloids. J Surg Res 2019;233:149–53.
20. Cabanas RM. An approach for the treatment of penile carcinoma. Cancer 1977;39:456–66.
21. Kroon BK, Horenblas S, Estourgie SH, Lont AP, Valdés Olmos RA, Nieweg OE. How to avoid false-negative dynamic sentinel node procedures in penile carcinoma. J Urol 2004;171:2191–4.
22. Leijte JA, van der Ploeg IM, Valdés Olmos RA, Nieweg OE, Horenblas S. Visualization of tumor blockage and rerouting of lymphatic drainage in penile cancer patients by use of SPECT/CT. J Nucl Med 2009;50:364–7.
23. Acar C, Kleinjan GH, van den Berg NS, Wit EM, van Leeuwen FW, van der Poel HG. Advances in sentinel node dissection in prostate cancer from a technical perspective. Int J Urol 2015;22:898–909.
24. Buckle T, Brouwer OR, Valdés Olmos RA, van der Poel HG, van Leeuwen FW. Relationship between intraprostatic tracer deposits and sentinel lymph node mapping in prostate cancer patients. J Nucl Med 2012;53:1026–33.
25. Meershoek P, Buckle T, van Oosterom MN, KleinJan GH, van der Poel HG, van Leeuwen FW. Can Intraoperative Fluorescence Imaging Identify All Lesions While the Road Map Created by Preoperative Nuclear Imaging Is Masked? J Nucl Med 2020;61:834–41.
26. Meershoek P, van Oosterom MN, Simon H, Mengus L, Maurer T, van Leeuwen PJ, *et al.* Robot-assisted laparoscopic surgery using DROP-IN radioguidance: first-in-human translation. Eur J Nucl Med Mol Imaging 2019;46:49–53.
27. van der Poel HG, Buckle T, Brouwer OR, Valdés Olmos RA, van Leeuwen FW. Intraoperative laparoscopic fluorescence guidance to the sentinel lymph node in prostate cancer patients: clinical proof of concept of an integrated functional imaging approach using a multimodal tracer. Eur Urol 2011;60:826–33.
28. Alex JC. The application of sentinel node radiolocalization to solid tumors of the head and neck: a 10-year experience. Laryngoscope 2004;114:2–19.
29. de Bree R, Pouw B, Heuveling DA, Castelijns JA. Fusion of Freehand SPECT and Ultrasound to Perform Ultrasound-Guided Fine-Needle Aspiration Cytology of Sentinel Nodes in Head and Neck Cancer. AJNR Am J Neuroradiol 2015;36:2153–8.
30. Giammarile F, Schilling C, Gnanasegaran G, Bal C, Oyen WJ, Rubello D, *et al.* The EANM practical guidelines for sentinel lymph node localisation in oral cavity squamous cell carcinoma. Eur J Nucl Med Mol Imaging 2019;46:623–37.
31. Heuveling DA, van Weert S, Karagozoglu KH, de Bree R. Evaluation of the use of freehand SPECT for sentinel node biopsy in early stage oral carcinoma. Oral Oncol 2015;51:287–90.
32. KleinJan GH. Karakullukçu B, Klop WMC, Engelen T, van den Berg NS, van Leeuwen FWB. Introducing navigation during melanoma-related sentinel lymph node procedures in the head-and-neck region. EJNMMI Res 2017;7:65.

33. Meershoek P, van den Berg NS, Brouwer OR, Teertstra HJ, Lange CA, Valdés-Olmos RA, *et al.* Three-Dimensional Tumor Margin Demarcation Using the Hybrid Tracer Indocyanine Green-99mTc-Nanocolloid: A Proof-of-Concept Study in Tongue Cancer Patients Scheduled for Sentinel Node Biopsy. J Nucl Med 2019;60:764–9.
34. Bluemel C, Matthies P, Herrmann K, Povoski SP. 3D scintigraphic imaging and navigation in radioguided surgery: freehand SPECT technology and its clinical applications. Expert Rev Med Devices 2016;13:339–51.
35. Tsuchimochi M, Hayama K. Intraoperative gamma cameras for radioguided surgery: technical characteristics, performance parameters, and clinical applications. Phys Med 2013;29:126–38.
36. van Leeuwen FW, Schottelius M, Brouwer OR, Vidal-Sicart S, Achilefu S, Klode J, *et al.* Trending: Radioactive and Fluorescent Bimodal/Hybrid Tracers as Multiplexing Solutions for Surgical Guidance. J Nucl Med 2020;61:13–9.
37. Van Oosterom MN, Rietbergen DD, Welling MM, Van Der Poel HG, Maurer T, Van Leeuwen FW. Recent advances in nuclear and hybrid detection modalities for image-guided surgery. Expert Rev Med Devices 2019;16:711–34.
38. van Leeuwen FW, Winter A, van Der Poel HG, Eiber M, Suardi N, Graefen M, *et al.* Technologies for image-guided surgery for managing lymphatic metastases in prostate cancer. Nat Rev Urol 2019;16:159–71.
39. Hoogendam JP, Hobbelink MG, Veldhuis WB, Verheijen RH, van Diest PJ, Zweemer RP. Preoperative sentinel node mapping with (99m)Tc-nanocolloid SPECT-CT significantly reduces the intraoperative sentinel node retrieval time in robot assisted laparoscopic cervical cancer surgery. Gynecol Oncol 2013;129:389–94.
40. Jeschke S, Lusuardi L, Myatt A, Hruby S, Pirich C, Janetschek G. Visualisation of the lymph node pathway in real time by laparoscopic radioisotope- and fluorescence-guided sentinel lymph node dissection in prostate cancer staging. Urology 2012;80:1080–6.
41. Leong SP, Kim J, Ross M, Faries M, Scoggins CR, Metz WL, *et al.* A phase 2 study of (99m) Tc-tilmanocept in the detection of sentinel lymph nodes in melanoma and breast cancer. Ann Surg Oncol 2011;18:961–9.
42. Marcinow AM, Hall N, Byrum E, Teknos TN, Old MO, Agrawal A. Use of a novel receptor-targeted (CD206) radiotracer, 99mTc-tilmanocept, and SPECT/CT for sentinel lymph node detection in oral cavity squamous cell carcinoma: initial institutional report in an ongoing phase 3 study. JAMA Otolaryngol Head Neck Surg 2013;139:895–902.
43. Mariani G, Moresco L, Viale G, Villa G, Bagnasco M, Canavese G, *et al.* Radioguided sentinel lymph node biopsy in breast cancer surgery. J Nucl Med 2001;42:1198–215.
44. Saikawa Y, Otani Y, Kitagawa Y, Yoshida M, Wada N, Kubota T, *et al.* Interim results of sentinel node biopsy during laparoscopic gastrectomy: possible role in function-preserving surgery for early cancer. World J Surg 2006;30:1962–8.
45. Satoh M, Ito A, Kaiho Y, Nakagawa H, Saito S, Endo M, *et al.* Intraoperative, radio-guided sentinel lymph node mapping in laparoscopic lymph node dissection for Stage I testicular carcinoma. Cancer 2005;103:2067–72.
46. Sondak VK, King DW, Zager JS, Schneebaum S, Kim J, Leong SP, *et al.* Combined analysis of phase III trials evaluating [99mTc]tilmanocept and vital blue dye for identification of sentinel lymph nodes in clinically node-negative cutaneous melanoma. Ann Surg Oncol 2013;20:680–8.

47. Surasi DS, O'Malley J, Bhambhvani P. 99mTc-Tilmanocept: A Novel Molecular Agent for Lymphatic Mapping and Sentinel Lymph Node Localization. J Nucl Med Technol 2015;43:87–91.
48. Takeuchi H, Goto O, Yahagi N, Kitagawa Y. Function-preserving gastrectomy based on the sentinel node concept in early gastric cancer. Gastric Cancer 2017;20:53–9.
49. Tokin CA, Cope FO, Metz WL, Blue MS, Potter BM, Abbruzzese BC, *et al.* The efficacy of Tilmanocept in sentinel lymph mode mapping and identification in breast cancer patients: a comparative review and meta-analysis of the 99mTc-labeled nanocolloid human serum albumin standard of care. Clin Exp Metastasis 2012;29:681–6.
50. Valdés Olmos RA, Rietbergen DD, Vidal-Sicart S, Manca G, Giammarile F, Mariani G. Contribution of SPECT/CT imaging to radioguided sentinel lymph node biopsy in breast cancer, melanoma, and other solid cancers: from "open and see" to "see and open". Q J Nucl Med Mol Imaging 2014;58:127–39.
51. van den Berg NS, Buckle T, KleinJan GH, van der Poel HG, van Leeuwen FW. Multispectral Fluorescence Imaging During Robot-assisted Laparoscopic Sentinel Node Biopsy: A First Step Towards a Fluorescence-based Anatomic Roadmap. Eur Urol 2017;72:110–7.
52. Wallace AM, Han LK, Povoski SP, Deck K, Schneebaum S, Hall NC, *et al.* Comparative evaluation of [(99m)tc]tilmanocept for sentinel lymph node mapping in breast cancer patients: results of two phase 3 trials. Ann Surg Oncol 2013;20:2590–9.
53. Weckermann D, Thalgott M, Holl G, Wagner T, Harzmann R. Radioguided surgery in urological malignancies. Indian J Urol 2008;24:4–9.
54. Engelen T, Winkel BM, Rietbergen DD, KleinJan GH, Vidal-Sicart S, Olmos RA, *et al.* The next evolution in radioguided surgery: breast cancer related sentinel node localization using a freehandSPECT-mobile gamma camera combination. Am J Nucl Med Mol Imaging 2015;5:233–45.
55. Freesmeyer M, Winkens T, Opfermann T, Elsner P, Runnebaum I, Darr A. Real-time ultrasound and freehand-SPECT. Experiences with sentinel lymph node mapping. Nucl Med (Stuttg) 2014;53:259–64.
56. Hellingman D, de Wit-van der Veen LJ, Klop WM, Olmos RA. Detecting near-the-injection-site sentinel nodes in head and neck melanomas with a high-resolution portable gamma camera. Clin Nucl Med 2015;40:e11–6.
57. Hellingman D, Vidal-Sicart S, de Wit-van der Veen LJ, Paredes P, Valdés Olmos RA. A New Portable Hybrid Camera for Fused Optical and Scintigraphic Imaging: First Clinical Experiences. Clin Nucl Med 2016;41:e39–43.
58. KleinJan GH, van den Berg NS, Brouwer OR, de Jong J, Acar C, Wit EM, *et al.* Optimisation of fluorescence guidance during robot-assisted laparoscopic sentinel node biopsy for prostate cancer. Eur Urol 2014;66:991–8.
59. KleinJan GH, van Werkhoven E, van den Berg NS, Karakullukcu MB, Zijlmans HJ, van der Hage JA, *et al.*; KleinJan. The best of both worlds: a hybrid approach for optimal pre- and intraoperative identification of sentinel lymph nodes. Eur J Nucl Med Mol Imaging 2018;45:1915–25.
60. Ohyama C, Chiba Y, Yamazaki T, Endoh M, Hoshi S, Arai Y. Lymphatic mapping and gamma probe guided laparoscopic biopsy of sentinel lymph node in patients with clinical stage I testicular tumor. J Urol 2002;168:1390–5.
61. Valdés Olmos RA, Vidal-Sicart S, Manca G, Mariani G, León-Ramírez LF, Rubello D, *et al.* Advances in radioguided surgery in oncology. Q J Nucl Med Mol Imaging 2017;61:247–70.

62. van den Berg NS, Simon H, Kleinjan GH, Engelen T, Bunschoten A, Welling MM, *et al.* First-in-human evaluation of a hybrid modality that allows combined radio- and (near-infrared) fluorescence tracing during surgery. Eur J Nucl Med Mol Imaging 2015;42:1639–47.

63. van Oosterom MN, Meershoek P, KleinJan GH, Hendricksen K, Navab N, van de Velde CJ, *et al.* Navigation of Fluorescence Cameras during Soft Tissue Surgery-Is it Possible to Use a Single Navigation Setup for Various Open and Laparoscopic Urological Surgery Applications? J Urol 2018;199:1061–8.

64. Vermeeren L, Valdés Olmos RA, Meinhardt W, Bex A, van der Poel HG, Vogel WV, *et al.* Intraoperative radioguidance with a portable gamma camera: a novel technique for laparoscopic sentinel node localisation in urological malignancies. Eur J Nucl Med Mol Imaging 2009;36:1029–36.

65. de Korne CM, Wit EM, de Jong J, Valdés Olmos RA, Buckle T, van Leeuwen FW, *et al.* Anatomical localization of radiocolloid tracer deposition affects outcome of sentinel node procedures in prostate cancer. Eur J Nucl Med Mol Imaging 2019;46:2558–68.

66. Folli S, Wagnières G, Pèlegrin A, Calmes JM, Braichotte D, Buchegger F, *et al.* Immunophotodiagnosis of colon carcinomas in patients injected with fluoresceinated chimeric antibodies against carcinoembryonic antigen. Proc Natl Acad Sci USA 1992;89:7973–7.

67. Pollard J, Zaidi B, Graham M. Comparative analysis of 99mTc-Tilmanocept (Lymphoseek) vs. 99mTc-Sulfur Colloid Sentinel Node Lymphoscintigraphy and Biopsy. J Nucl Med 2016;57:411

68. Betancourt Hernández JA, Vera Donoso C, Martinez-Sarmiento M, Monserrat JJ, Bello Jarque P, Boronat Tormo F. Application of the Radio-Guided Occult Lesion Localization Technique for Renal Lumpectomy: From the Laboratory to the Patient. Clin Nucl Med 2017;42:e467–8

69. Bowles H, Sánchez N, Tapias A, Paredes P, Campos F, Bluemel C, *et al.* Radioguided surgery and the GOSTT concept: from pre-operative image and intraoperative navigation to image-assisted excision. Rev Esp Med Nucl Imagen Mol 2017;36:175–84

70. Cerit ET, Yalçin MM, Özkan Ç, Aktürk M, Altinova AE, Akdemir ÜÖ, *et al.* Guided intraoperative scintigraphic tumor targeting of metastatic cervical lymph nodes in patients with differentiated thyroid cancer: a single-center report. Arch Endocrinol Metab 2018;62:495–500

71. Galetta D, Bellomi M, Grana C, Spaggiari L. Radio-Guided Localization and Resection of Small or Ill-Defined Pulmonary Lesions. Ann Thorac Surg 2015;100:1175–80

72. García JR, Fraile M, Soler M, Bechini J, Ayuso JR, Lomeña F. [PET/CT-guided salvage surgery protocol. Results with ROLL Technique and PET probe]. Rev Esp Med Nucl 2011;30:217-22

73. KleinJan GH, Brouwer OR, Mathéron HM, Rietbergen DD, Valdés Olmos RA, Wouters MW, *et al.*; KleinJan. Hybrid radioguided occult lesion localization (hybrid ROLL) of (18) F-FDG-avid lesions using the hybrid tracer indocyanine green-(99m)Tc-nanocolloid. Rev Esp Med Nucl Imagen Mol 2016;35:292–7

74. Lavoué V, Nos C, Clough KB, Baghaie F, Zerbib E, Poulet B, *et al.* Simplified technique of radioguided occult lesion localization (ROLL) plus sentinel lymph node biopsy (SNOLL) in breast carcinoma. Ann Surg Oncol 2008;15:2556–61

75. Lombardi A, Nigri G, Scopinaro F, Maggi S, Mattei M, Bonifacino A, *et al.* High-resolution, handheld camera use for occult breast lesion localization plus sentinel node biopsy (SNOLL): a single-institution experience with 186 patients. Surgeon 2015;13:69–72.
76. Monti S, Galimberti V, Trifiro G, De Cicco C, Peradze N, Brenelli F, *et al.* Occult breast lesion localization plus sentinel node biopsy (SNOLL): experience with 959 patients at the European Institute of Oncology. Ann Surg Oncol 2007;14:2928–31.
77. Müller J, Putora PM, Schneider T, Zeisel C, Brutsche M, Baty F, *et al.* Handheld single photon emission computed tomography (handheld SPECT) navigated video-assisted thoracoscopic surgery of computer tomography-guided radioactively marked pulmonary lesions. Interact Cardiovasc Thorac Surg 2016;23:345–50.
78. Paredes P, Vidal-Sicart S, Zanón G, Roé N, Rubí S, Lafuente S, *et al.* Radioguided occult lesion localisation in breast cancer using an intraoperative portable gamma camera: first results. Eur J Nucl Med Mol Imaging 2008;35:230–5.
79. Vitral GS, Salgado HC, Rangel JM. Use of radioguided surgery in abdominal wall endometriosis: an innovative approach. World J Nucl Med 2018;17:204–6.
80. Grogan EL, Jones DR, Kozower BD, Simmons WD, Daniel TM. Identification of small lung nodules: technique of radiotracer-guided thoracoscopic biopsy. Ann Thorac Surg 2008;85:S772–7.
81. Manca G, Mazzarri S, Rubello D, Tardelli E, Delgado-Bolton RC, Giammarile F, *et al.* Radioguided Occult Lesion Localization: Technical Procedures and Clinical Applications. Clin Nucl Med 2017;42:e498–503.
82. Thind CR, Tan S, Desmond S, Harris O, Ramesh HS, Chagla L, *et al.* SNOLL. Sentinel node and occult (impalpable) lesion localization in breast cancer. Clin Radiol 2011;66:833–9.
83. Donker M, Straver ME, Wesseling J, Loo CE, Schot M, Drukker CA, *et al.* Marking axillary lymph nodes with radioactive iodine seeds for axillary staging after neoadjuvant systemic treatment in breast cancer patients: the MARI procedure. Ann Surg 2015;261:378–82.
84. Pouw B, de Wit-van der Veen LJ, Stokkel MP, Loo CE, Vrancken Peeters MJ, Valdés Olmos RA. Heading toward radioactive seed localization in non-palpable breast cancer surgery? A meta-analysis. J Surg Oncol 2015;111:185–91.
85. Pouw B, de Wit-van der Veen LJ, van Duijnhoven F, Rutgers EJ, Stokkel MP, Valdés Olmos RA, *et al.* Intraoperative 3D Navigation for Single or Multiple 125I-Seed Localization in Breast-Preserving Cancer Surgery. Clin Nucl Med 2016;41:e216–20.
86. van der Noordaa ME, Pengel KE, Groen E, van Werkhoven E, Rutgers EJ, Loo CE, *et al.* The use of radioactive iodine-125 seed localization in patients with non-palpable breast cancer: a comparison with the radioguided occult lesion localization with 99m technetium. Eur J Surg Oncol 2015;41:553–8.
87. Koolen BB, Donker M, Straver ME, van der Noordaa ME, Rutgers EJ, Valdés Olmos RA, *et al.* Combined PET-CT and axillary lymph node marking with radioactive iodine seeds (MARI procedure) for tailored axillary treatment in node-positive breast cancer after neoadjuvant therapy. Br J Surg 2017;104:1188–96.
88. van der Noordaa ME, van Duijnhoven FH, Straver ME, Groen EJ, Stokkel M, Loo CE, *et al.* Major Reduction in Axillary Lymph Node Dissections After Neoadjuvant Systemic Therapy for Node-Positive Breast Cancer by combining PET/CT and the MARI Procedure. Ann Surg Oncol 2018;25:1512–20.

89. Essner R, Hsueh EC, Haigh PI, Glass EC, Huynh Y, Daghighian F. Application of an [(18) F]fluorodeoxyglucose-sensitive probe for the intraoperative detection of malignancy. J Surg Res 2001;96:120–6.

90. Gulec SA, Daghighian F, Essner R. PET-Probe: Evaluation of Technical Performance and Clinical Utility of a Handheld High-Energy Gamma Probe in Oncologic Surgery. Ann Surg Oncol 2016;23:9020–7.

91. Kim WW, Kim JS, Hur SM, Kim SH, Lee SK, Choi JH, *et al.* Radioguided surgery using an intraoperative PET probe for tumor localization and verification of complete resection in differentiated thyroid cancer: a pilot study. Surgery 2011;149:416–24.

92. Kraeber-Bodéré F, Cariou B, Curtet C, Bridji B, Rousseau C, Dravet F, *et al.* Feasibility and benefit of fluorine 18-fluoro-2-deoxyglucose-guided surgery in the management of radioiodine-negative differentiated thyroid carcinoma metastases. Surgery 2005;138:1176–82, discussion 1182.

93. Lee A, Chang J, Lim W, Kim BS, Lee JE, Cha ES, *et al.* Effectiveness of breast-specific gamma imaging (BSGI) for breast cancer in Korea: a comparative study. Breast J 2012;18:453–8.

94. Povoski SP, Neff RL, Mojzisik CM, O'Malley DM, Hinkle GH, Hall NC, *et al.* A comprehensive overview of radioguided surgery using gamma detection probe technology. World J Surg Oncol 2009;7:11.

95. Zervos EE, Desai DC, DePalatis LR, Soble D, Martin EW. 18F-labeled fluorodeoxyglucose positron emission tomography-guided surgery for recurrent colorectal cancer: a feasibility study. J Surg Res 2001;97:9–13.

96. Fei B, Schuster DM. PET Molecular Imaging-Directed Biopsy: A Review. AJR Am J Roentgenol 2017;209:255–69.

97. Huppe AI, Mehta AK, Brem RF. Molecular Breast Imaging: A Comprehensive Review. Semin Ultrasound CT MR 2018;39:60–9.

98. Arbizu J, Rodriguez-Fraile M, Dominguez-Prado I, Garrastachu P, Rotellar F, Sangro B, *et al.* Whole body 18fluoro-L-dopa PET-CT: a useful tool for location and surgical guidance in primary carcinoid tumours. Eur J Nucl Med Mol Imaging 2008;35:1577.

99. Aras G, Gültekin SS, Küçük NO, Demirer S, Tuğ T. Intraoperative gamma probe guidance with 99mTc-pertechnetate in the completion thyroidectomy. Ann Nucl Med 2009;23:421–6.

100. Selverstone B, Sweet WH, Robinson CV. The Clinical Use of Radioactive Phosphorus in the Surgery of Brain Tumors. Ann Surg 1949;130:643–50.

101. Adams S, Acker P, Lorenz M, Staib-Sebler E, Hör G. Radioisotope-guided surgery in patients with pheochromocytoma and recurrent medullary thyroid carcinoma: a comparison of preoperative and intraoperative tumor localization with histopathologic findings. Cancer 2001;92:263–70.

102. Axelsson CK, Nielsen BP, Graff J. Radioisotope-guided surgical biopsy of costal metastases in breast cancer patients. Scand J Surg 2002;91:333–5.

103. Isgoren S, Demir H, Daglioz-Gorur G, Selek O. Gamma probe guided surgery for osteoid osteoma: is there any additive value of quantitative bone scintigraphy? Rev Esp Med Nucl Imagen Mol 2013;32:234–9.

104. Krag DN, Ford PV, Patel M, Schneider PD, Goodnight JE Jr. A simplified technique to resect abnormal bony radiolocalizations using a gamma counter. Surg Oncol 1992;1:371–7.

105. Rietbergen DD, Meershoek P, van Oosterom MN, Roestenberg M, van Erkel AR, Smit F, *et al.* [Freehand-SPECT with 99mTc-HDP as tool to guide percutaneous biopsy of skeletal lesions detected on bone scintigraphy]. Rev Esp Med Nucl Imagen Mol 2019;38:218–23.

106. Robinson LA, Preksto D, Muro-Cacho C, Hubbell DS. Intraoperative gamma probe-directed biopsy of asymptomatic suspected bone metastases. Ann Thorac Surg 1998;65:1426–32.

107. von Meyenfeldt EM, Siebenga J, van der Pol HA, Schreurs WM, Hulsewe KW. Radionuclide-guided biopsy of bone lesions in cancer patients; a reliable, well-tolerated technique. Eur J Surg Oncol 2014;40:193–6.

108. Duarte GM, Cabello C, Torresan RZ, Alvarenga M, Telles GH, Bianchessi ST, *et al.* Radioguided Intraoperative Margins Evaluation (RIME): preliminary results of a new technique to aid breast cancer resection. Eur J Surg Oncol 2007;33:1150–7.

109. Ikeda Y, Takayama J, Takami H. Minimally invasive radioguided parathyroidectomy for hyperparathyroidism. Ann Nucl Med 2010;24:233–40.

110. Mariani G, Gulec SA, Rubello D, Boni G, Puccini M, Pelizzo MR, *et al.* Preoperative localization and radioguided parathyroid surgery. J Nucl Med 2003;44:1443–58.

111. Martinez DA, King DR, Romshe C, Lozano RA, Morris JD, O'Dorisio MS, *et al.* Intraoperative identification of parathyroid gland pathology: a new approach. J Pediatr Surg 1995;30:1306–9.

112. Placzkowski K, Christian R, Chen H. Radioguided parathyroidectomy for recurrent parathyroid cancer. Clin Nucl Med 2007;32:358–60.

113. Rahbar K, Colombo-Benkmann M, Haane C, Wenning C, Vrachimis A, Weckesser M, *et al.* Intraoperative 3-D mapping of parathyroid adenoma using freehand SPECT. EJNMMI Res 2012;2:51.

114. Vilela Filho O, Carneiro Filho O. Gamma probe-assisted brain tumor microsurgical resection: a new technique. Arq Neuropsiquiatr 2002;60:1042–7.

115. Yu X, Hu G, Zhang Z, Qiu F, Shao X, Wang X, *et al.* Retrospective and comparative analysis of (99m)Tc-Sestamibi breast specific gamma imaging versus mammography, ultrasound, and magnetic resonance imaging for the detection of breast cancer in Chinese women. BMC Cancer 2016;16:450.

116. Schattner A, Cohen A, Wolfson L, Melloul M. Unexplained systemic symptoms and Gallium-67—guided decisions. Am J Med Sci 2001;321:198–200.

117. Vos CG, Hartemink KJ, Muller S, Oosterhuis JW, Meijer S, van den Tol MP, *et al.* Clinical applications of FDG-probe guided surgery. Acta Chir Belg 2012;112:414–8.

118. Kumar R, Mittal BR, Bhattacharya A, Singh H, Bal A, Prakash G, *et al.* 18F-FDG PET/CT-Guided Real-Time Automated Robotic Arm-Assisted Needle Navigation for Percutaneous Biopsy of Hypermetabolic Bone Lesions: Diagnostic Performance and Clinical Impact. AJR Am J Roentgenol 2019;212:W10–8.

119. Radhakrishnan RK, Mittal BR, Gorla AK, Basher RK, Sood A, Bal A, *et al.* Real-time intraprocedural 18F-FDG PET/CT-guided biopsy using automated robopsy arm (ARA) in the diagnostic evaluation of thoracic lesions with prior inconclusive biopsy results: initial experience from a tertiary health care centre. Br J Radiol 2017;90:20170258.

120. Wiegmann AL, Broucek JR, Fletcher RN, Luu MB, Deziel DJ, Myers JA. Image-Guided Navigation in Lymph Node Biopsy. JSLS 2018;22:22.

121. Ashkenazy M, Davis L, Martin J. An evaluation of the technic and results of the radioactive di-iodo-fluorescein test for the localization of intracranial lesions. J Neurosurg 1951;8:300–14.

122. Berland TL, Smith SL, Metzger PP, Nelson KL, Fakhre GP, Chua HK, *et al.* Intraoperative gamma probe localization of the ureters: a novel concept. J Am Coll Surg 2007;205:608–11.

123. Donker M, Drukker CA, Valdés Olmos RA, Rutgers EJ, Loo CE, Sonke GS, *et al.* Guiding breast-conserving surgery in patients after neoadjuvant systemic therapy for breast cancer: a comparison of radioactive seed localization with the ROLL technique. Ann Surg Oncol 2013;20:2569–75.

124. Bluemel C, Safak G, Cramer A, Wöckel A, Gesierich A, Hartmann E, *et al.* Fusion of freehand SPECT and ultrasound: first experience in preoperative localization of sentinel lymph nodes. Eur J Nucl Med Mol Imaging 2016;43:2304–12.

125. Hartl A, Shakir DI, Lasser T, Ziegler SI, Navab N. Detection models for freehand SPECT reconstruction. Phys Med Biol 2015;60:1031–46.

126. Anderson RS, Eifert B, Tartt S, King P. Radioimmunoguided surgery using indium-111 capromab pendetide (PROSTASCINT) to diagnose supraclavicular metastasis from prostate cancer. Urology 2000;56:669.

127. Badalament RA, Burgers JK, Petty LR, Mojzisik CM, Berens A, Marsh W, *et al.* Radioimmunoguided radical prostatectomy and lymphadenectomy. Cancer 1993;71:2268–75.

128. Maurer T, Eiber M, Schwaiger M, Gschwend JE. Current use of PSMA-PET in prostate cancer management. Nat Rev Urol 2016;13:226–35.

129. Maurer T, Robu S, Schottelius M, Schwamborn K, Rauscher I, van den Berg NS, *et al.* 99mTechnetium-based Prostate-specific Membrane Antigen-radioguided Surgery in Recurrent Prostate Cancer. Eur Urol 2019;75:659–66.

130. Rauscher I, Düwel C, Wirtz M, Schottelius M, Wester HJ, Schwamborn K, *et al.* Value of 111 In-prostate-specific membrane antigen (PSMA)-radioguided surgery for salvage lymphadenectomy in recurrent prostate cancer: correlation with histopathology and clinical follow-up. BJU Int 2017;120:40–7.

131. Rauscher I, Horn T, Eiber M, Gschwend JE, Maurer T. Novel technology of molecular radio-guidance for lymph node dissection in recurrent prostate cancer by PSMA-ligands. World J Urol 2018;36:603–8.

132. Povoski SP, Hall NC, Murrey DA Jr, Sharp DS, Hitchcock CL, Mojzisik CM, *et al.* Multimodal imaging and detection strategy with 124 I-labeled chimeric monoclonal antibody cG250 for accurate localization and confirmation of extent of disease during laparoscopic and open surgical resection of clear cell renal cell carcinoma. Surg Innov 2013;20:59–69.

133. Strong VE, Humm J, Russo P, Jungbluth A, Wong WD, Daghighian F, *et al.* A novel method to localize antibody-targeted cancer deposits intraoperatively using handheld PET beta and gamma probes. Surg Endosc 2008;22:386–91.

134. Dawson PM, Blair SD, Begent RH, Kelly AM, Boxer GM, Theodorou NA. The value of radioimmunoguided surgery in first and second look laparotomy for colorectal cancer. Dis Colon Rectum 1991;34:217–22.

135. Gu J, Zhao J, Li Z, Yang Z, Zhang J, Gao Z, *et al.* Clinical application of radioimmunoguided surgery in colorectal cancer using 125I-labeled carcinoembryonic antigen-specific monoclonal antibody submucosally. Dis Colon Rectum 2003;46:1659–66.

136. Hladik P, Vizda J, Bedrna J, Simkovic D, Strnad L, Smejkal K, *et al.* Immunoscintigraphy and intra-operative radioimmunodetection in the treatment of colorectal carcinoma. Colorectal Dis 2001;3:380–6.

137. Martin EW Jr, Tuttle SE, Rousseau M, Mojzisik CM, O'Dwyer PJ, Hinkle GH, *et al.* Radioimmunoguided surgery: intraoperative use of monoclonal antibody 17-1A in colorectal cancer. Hybridoma 1986;5:S97–108.

138. Muxi A, Pons F, Vidal-Sicart S, Setoain FJ, Herranz R, Novell F, *et al.* Radioimmunoguided surgery of colorectal carcinoma with an 111In-labelled anti-TAG72 monoclonal antibody. Nucl Med Commun 1999;20:123–30.

139. Nieroda CA, Mojzisik C, Hinkle G, Thurston MO, Martin EW Jr. Radioimmunoguided surgery (RIGS) in recurrent colorectal cancer. Cancer Detect Prev 1991;15:225–9.

140. O'Dwyer PJ, Mojzisik CM, Hinkle GH, Rousseau M, Olsen J, Tuttle SE, *et al.* Intraoperative probe-directed immunodetection using a monoclonal antibody. Arch Surg 1986;121:1391–4.

141. Russomando A, Bellini F, Bocci V, Collamati F, Lucia ED, Faccini R, *et al.* An Intraoperative $\beta ^{-}$ Detecting Probe for Radio-Guided Surgery in Tumour Resection. IEEE Trans Nucl Sci 2016;63:2533–9.

142. Wang C, Wang Y, Su X, Lin B, Xu X, Zhang M, *et al.* [Iodine-125 labeled monoclonal antibody 3H11: in radioimmunoguided surgery for primary gastric cancer]. Zhonghua Wai Ke Za Zhi 2000;38:507–9.

143. Xu G, Zhang M, Liu B, Li Z, Lin B, Xu X, *et al.* Radioimmunoguided surgery in gastric cancer using 131-I labeled monoclonal antibody 3H11. Semin Surg Oncol 1994;10:88–94.

144. Ind TE, Granowska M, Britton KE, Morris G, Lowe DG, Hudson CN, *et al.* Peroperative radioimmunodetection of ovarian carcinoma using a hand-held gamma detection probe. Br J Cancer 1994;70:1263–6.

145. Krag DN, Haseman MK, Ford P, Smith L, Taylor MH, Schneider P, *et al.* Gamma probe location of 111indium-labeled B72.3: an extension of immunoscintigraphy. J Surg Oncol 1992;51:226–30.

146. Adams S, Baum RP, Hertel A, Wenisch HJ, Staib-Sebler E, Herrmann G, *et al.* Intraoperative gamma probe detection of neuroendocrine tumors. J Nucl Med 1998;39:1155–60.

147. Cuccurullo V, Di Stasio GD, Mansi L. Radioguided surgery with radiolabeled somatostatin analogs: not only in GEP-NETs. Nucl Med Rev Cent East Eur 2017;20:49–56.

148. Cuntz MC, Levine EA, O'Dorisio TM, Watson JC, Wray DA, Espenan GD, *et al.* Intraoperative gamma detection of 125I-lanreotide in women with primary breast cancer. Ann Surg Oncol 1999;6:367–72.

149. Einspieler I, Novotny A, Okur A, Essler M, Martignoni ME. First experience with image-guided resection of paraganglioma. Clin Nucl Med 2014;39:e379–81.

150. Freesmeyer M, Wurst C, Uberrueck T, Scholz T, Knösel T, Schulz S, *et al.* Intraoperative identification of a neuroendocrine tumour diagnosed by 68Ga-DOTATOC PET but undetectable by surgical palpation or conventional imaging. Nucl Med (Stuttg) 2009;48:N50–1.

151. Gay E, Vuillez JP, Palombi O, Brard PY, Bessou P, Passagia JG. Intraoperative and postoperative gamma detection of somatostatin receptors in bone-invasive en plaque meningiomas. Neurosurgery 2005;57:107–13, discussion 107–13.

152. Grossrubatscher E, Vignati F, Dalino P, Possa M, Belloni PA, Vanzulli A, *et al.* Use of radioguided surgery with [111In]-pentetreotide in the management of an ACTH-secreting bronchial carcinoid causing ectopic Cushing's syndrome. J Endocrinol Invest 2005;28:72–8.

153. Gulec SA, Baum R. Radio-guided surgery in neuroendocrine tumors. J Surg Oncol 2007;96:309–15.

154. Hubalewska-Dydejczyk A, Kulig J, Szybinski P, Mikolajczak R, Pach D, Sowa-Staszczak A, *et al.* Radio-guided surgery with the use of [99mTc-EDDA/HYNIC]octreotate in intra-operative detection of neuroendocrine tumours of the gastrointestinal tract. Eur J Nucl Med Mol Imaging 2007;34:1545–55.

155. Kaemmerer D, Prasad V, Daffner W, Haugvik SP, Senftleben S, Baum RP, *et al.* Radioguided surgery in neuroendocrine tumors using Ga-68-labeled somatostatin analogs: a pilot study. Clin Nucl Med 2012;37:142–7.

156. Mansi L, Rambaldi PF, Panza N, Esposito D, Esposito V, Pastore V. Diagnosis and radioguided surgery with 111In-pentetreotide in a patient with paraneoplastic Cushing's syndrome due to a bronchial carcinoid. Eur J Endocrinol 1997;137:688–90.

157. Martelli H, Ricard M, Larroquet M, Wioland M, Paraf F, Fabre M, *et al.* Intraoperative localization of neuroblastoma in children with 123I- or 125I-radiolabeled metaiodobenzylguanidine. Surgery 1998;123:51–7.

158. Öhrvall U, Westlin JE, Nilsson S, Juhlin C, Rastad J, Lundqvist H, *et al.* Intraoperative gamma detection reveals abdominal endocrine tumors more efficiently than somatostatin receptor scintigraphy. Cancer 1997;80:2490–4.

159. Panareo S, Carcoforo P, Lanzara S, Corcione S, Bagatin E, Casali M, *et al.* Radiolabelled somatostatin analogs for diagnosis and radio-guided surgery of neuroendocrine breast cancer undetectable with conventional imaging procedures. Breast 2008;17:111–4.

160. Ricard M, Tenenbaum F, Schlumberger M, Travagli JP, Lumbroso J, Revillon Y, *et al.* Intraoperative detection of pheochromocytoma with iodine-125 labelled meta-iodobenzylguanidine: a feasibility study. Eur J Nucl Med 1993;20:426–30.

161. Sadowski SM, Millo C, Neychev V, Aufforth R, Keutgen X, Glanville J, *et al.* Feasibility of Radio-Guided Surgery with 68Gallium-DOTATATE in Patients with Gastro-Entero-Pancreatic Neuroendocrine Tumors. Ann Surg Oncol 2015;22:S676–82.

162. Sánchez N, Tapias A, Bowles H, Delgado E, Almenara R, Fuster D, *et al.* [Multimodal approach in radioguided surgery in a case of multiple paraganglioma]. Rev Esp Med Nucl Imagen Mol 2018;37:41–5.

163. Schirmer WJ, O'Dorisio TM, Schirmer TP, Mojzisik CM, Hinkle GH, Martin EW. Intraoperative localization of neuroendocrine tumors with 125I-TYR(3)-octreotide and a hand-held gamma-detecting probe. Surgery 1993;114:745–51, discussion 751–2.

164. van Hulsteijn LT, Corssmit EP, van der Hiel B, Smit JW, Stokkel MP. Is there a role for radioguided surgery with iodine-labeled metaiodobenzylguanidine in resection of neuroendocrine tumors? Clin Nucl Med 2012;37:1083–8.

165. El Lakis M, Gianakou A, Nockel P, Wiseman D, Tirosh A, Quezado MA, *et al.* Radioguided Surgery With Gallium 68 Dotatate for Patients With Neuroendocrine Tumors. JAMA Surg 2019;154:40–5.

166. Lastoria S, Maurea S, Vergara E, Acampa W, Varrella P, Klain M, *et al.* Comparison of labeled MIBG and somatostatin analogs in imaging neuroendocrine tumors. Q J Nucl Med 1995;39:145–9.

167. Kluijfhout WP, Pasternak JD, Gosnell JE, Shen WT, Duh QY, Vriens MR, *et al.* 18F Fluorocholine PET/MR Imaging in Patients with Primary Hyperparathyroidism and Inconclusive Conventional Imaging: A Prospective Pilot Study. Radiology 2017;284:460–7.

168. Quak E, Blanchard D, Houdu B, Le Roux Y, Ciappuccini R, Lireux B, *et al.* F18-choline PET/CT guided surgery in primary hyperparathyroidism when ultrasound and MIBI SPECT/CT are negative or inconclusive: the APACH1 study. Eur J Nucl Med Mol Imaging 2018;45:658–66.

169. Rubello D, Casara D, Giannini S, Piotto A, De Carlo E, Muzzio PC, *et al.* Importance of radio-guided minimally invasive parathyroidectomy using hand-held gamma probe and low (99m)Tc-MIBI dose. Technical considerations and long-term clinical results. Q J Nucl Med 2003;47:129–38.

170. Udelsman R, Lin Z, Donovan P. The superiority of minimally invasive parathyroidectomy based on 1650 consecutive patients with primary hyperparathyroidism. Ann Surg 2011;253:585–91.

171. Wang S, Yang W, Deng J, Zhang J, Ma F, Wang J. Reduction in the recurrence of meningiomas by combining somatostatin receptor scintigraphy of (99m)Tc-HYNIC-octreotide SPECT/CT and radio guidance with a hand-held γ-probe during surgery. Nucl Med Commun 2013;34:249–53.

172. Mueller JJ, Dauer LT, Murali R, Iasonos A, Pandit-Taskar N, Abu-Rustum NR, *et al.* Positron Lymphography via Intracervical 18F-FDG Injection for Presurgical Lymphatic Mapping in Cervical and Endometrial Malignancies. J Nucl Med 2020;61:1123–30.

173. Povoski SP, Sarikaya I, White WC, Marsh SG, Hall NC, Hinkle GH, *et al.* Comprehensive evaluation of occupational radiation exposure to intraoperative and perioperative personnel from 18F-FDG radioguided surgical procedures. Eur J Nucl Med Mol Imaging 2008;35:2026–34.

174. Spinelli AE, Ferdeghini M, Cavedon C, Zivelonghi E, Calandrino R, Fenzi A, *et al.* First human Cerenkography. J Biomed Opt 2013;18:20502.

175. Heckathorne E, Dimock C, Dahlbom M. Radiation dose to surgical staff from positron-emitter-based localization and radiosurgery of tumors. Health Phys 2008;95:220–6.

176. Ballinger JR. The use of protein-based radiocolloids in sentinel node localisation. Clin Transl Imaging 2015;3:179–86.

177. KleinJan GH, Bunschoten A, van den Berg NS, Olmos RA, Klop WM, Horenblas S, *et al.*; KleinJan. Fluorescence guided surgery and tracer-dose, fact or fiction? Eur J Nucl Med Mol Imaging 2016;43:1857–67.

178. Cundiff JD, Wang YZ, Espenan G, Maloney T, Camp A, Lazarus L, *et al.* A phase I/II trial of 125I methylene blue for one-stage sentinel lymph node biopsy. Ann Surg 2007;245:290–6.

179. Meershoek P, KleinJan GH, van Oosterom MN, Wit EM, van Willigen DM, Bauwens KP, *et al.* Multispectral-Fluorescence Imaging as a Tool to Separate Healthy from Disease-Related Lymphatic Anatomy During Robot-Assisted Laparoscopy. J Nucl Med 2018;59:1757–60.

185. International Atomic Energy Agency. Radiopharmaceuticals for Sentinel Lymph Node Detection: Status and Trends. Vienna: IAEA; 2015.

186. Golay J, Semenzato G, Rambaldi A, Foà R, Gaidano G, Gamba E, *et al.* Lessons for the clinic from rituximab pharmacokinetics and pharmacodynamics. MAbs 2013;5:826–37.

187. Brouwer OR, Buckle T, Vermeeren L, Klop WM, Balm AJ, van der Poel HG, *et al.* Comparing the hybrid fluorescent-radioactive tracer indocyanine green-99mTc-nanocolloid with 99mTc-nanocolloid for sentinel node identification: a validation study using lymphoscintigraphy and SPECT/CT. J Nucl Med 2012;53:1034–40.

188. Bugby SL, Lees JE, Perkins AC. Hybrid intraoperative imaging techniques in radioguided surgery: present clinical applications and future outlook. Clin Transl Imaging 2017;5:323–41.

189. Baranski AC, Schäfer M, Bauder-Wüst U, Roscher M, Schmidt J, Stenau E, *et al.* PSMA-11-Derived Dual-Labeled PSMA Inhibitors for Preoperative PET Imaging and Precise Fluorescence-Guided Surgery of Prostate Cancer. J Nucl Med 2018;59:639–45.

190. Buckle T, van Willigen DM, Spa SJ, Hensbergen AW, van der Wal S, de Korne CM, *et al.* Tracers for Fluorescence-Guided Surgery: How Elongation of the Polymethine Chain in Cyanine Dyes Alters the Pharmacokinetics of a Dual-Modality c[RGDyK] Tracer. J Nucl Med 2018;59:986–92.

191. Bunschoten A, van Willigen DM, Buckle T, van den Berg NS, Welling MM, Spa SJ, *et al.* Tailoring Fluorescent Dyes To Optimize a Hybrid RGD-Tracer. Bioconjug Chem 2016;27:1253–8.

192. Hensbergen AW, Buckle T, van Willigen DM, Schottelius M, Welling MM, van der Wijk FA, *et al.* Hybrid Tracers Based on Cyanine Backbones Targeting Prostate-Specific Membrane Antigen: Tuning Pharmacokinetic Properties and Exploring Dye-Protein Interaction. J Nucl Med 2020;61:234–41.

193. Ahmadzadehfar H, Muckle M, Sabet A, Wilhelm K, Kuhl C, Biermann K, *et al.* The significance of bremsstrahlung SPECT/CT after yttrium-90 radioembolization treatment in the prediction of extrahepatic side effects. Eur J Nucl Med Mol Imaging 2012;39:309–15.

194. van Oosterom MN, Simon H, Mengus L, Welling MM, van der Poel HG, van den Berg NS, *et al.* Revolutionizing (robot-assisted) laparoscopic gamma tracing using a drop-in gamma probe technology. Am J Nucl Med Mol Imaging 2016;6:1–17.

195. Brouwer OR, Valdés Olmos RA, Vermeeren L, Hoefnagel CA, Nieweg OE, Horenblas S. SPECT/CT and a portable gamma-camera for image-guided laparoscopic sentinel node biopsy in testicular cancer. J Nucl Med 2011;52:551–4.

196. Wendler T, Herrmann K, Schnelzer A, Lasser T, Traub J, Kutter O, *et al.* First demonstration of 3-D lymphatic mapping in breast cancer using freehand SPECT. Eur J Nucl Med Mol Imaging 2010;37:1452–61.

197. Markus A, Ray AS, Bolla D, Müller J, Diener PA, Wendler T, *et al.* Sentinel lymph node biopsy in endometrial and cervical cancers using freehand SPECT—first experiences. Gynecol Surg 2016;13:499–506.

198. Mandapathil M, Teymoortash A, Heinis J, Wiegand S, Güldner C, Hoch S, *et al.* Freehand SPECT for sentinel lymph node detection in patients with head and neck cancer: first experiences. Acta Otolaryngol 2014;134:100–4.

199. Schilling C, Gnansegaran G, Thavaraj S, McGurk M. Intraoperative sentinel node imaging versus SPECT/CT in oral cancer - A blinded comparison. Eur J Surg Oncol 2018;44:1901–7.

200. Mihaljevic AL, Rieger A, Belloni B, Hein R, Okur A, Scheidhauer K, *et al.* Transferring innovative freehand SPECT to the operating room: first experiences with sentinel lymph node biopsy in malignant melanoma. Eur J Surg Oncol 2014;40:42–8.

201. Sulzbacher L, Klinger M, Scheurecker C, Wacha M, Shamiyeh A, Malek M, *et al.* Clinical Usefulness of a Novel Freehand 3D Imaging Device for Radio-Guided Intraoperative Sentinel Lymph Node Detection in Malignant Melanoma. Clin Nucl Med 2015;40:e436–40.

202. Castillo VT, Rioja ME, Diaz-Laugart E, *et al.* Intraoperative demonstration of 3D tumor localization using freehand SPECT in a duodenum NET patient. J Nucl Med 2012;53:1252.

203. Maurer T, Weirich G, Schottelius M, Weineisen M, Frisch B, Okur A, *et al.* Prostate-specific membrane antigen-radioguided surgery for metastatic lymph nodes in prostate cancer. Eur Urol 2015;68:530–4.

204. Brouwer OR, van den Berg NS, Mathéron HM, Wendler T, van der Poel HG, Horenblas S, *et al.* Feasibility of intraoperative navigation to the sentinel node in the groin using preoperatively acquired single photon emission computerized tomography data: transferring functional imaging to the operating room. J Urol 2014;192:1810–6.

205. van den Berg NS, Engelen T, Brouwer OR, Mathéron HM, Valdés-Olmos RA, Nieweg OE, *et al.* A pilot study of SPECT/CT-based mixed-reality navigation towards the sentinel node in patients with melanoma or Merkel cell carcinoma of a lower extremity. Nucl Med Commun 2016;37:812–7.

206. van Oosterom MN, van der Poel HG, Navab N, van de Velde CJ, van Leeuwen FW. Computer-assisted surgery: virtual- and augmented-reality displays for navigation during urological interventions. Curr Opin Urol 2018;28:205–13.

207. Brouwer OR, Buckle T, Bunschoten A, Kuil J, Vahrmeijer AL, Wendler T, *et al.* Image navigation as a means to expand the boundaries of fluorescence-guided surgery. Phys Med Biol 2012;57:3123–36.

208. Freesmeyer M, Opfermann T, Winkens T. Hybrid integration of real-time US and freehand SPECT: proof of concept in patients with thyroid diseases. Radiology 2014;271:856–61.

209. KleinJan GH, van den Berg NS, van Oosterom MN, Wendler T, Miwa M, Bex A, *et al.*; KleinJan. Toward (Hybrid) Navigation of a Fluorescence Camera in an Open Surgery Setting. J Nucl Med 2016;57:1650–3.

210. Heller S, Zanzonico P. Nuclear probes and intraoperative gamma cameras. Semin Nucl Med 2011;41:166–81.

211. Camillocci ES, Baroni G, Bellini F, Bocci V, Collamati F, Cremonesi M, *et al.* A novel radioguided surgery technique exploiting β(-) decays. Sci Rep 2014;4:4401.

212. Solfaroli Camillocci E, Schiariti M, Bocci V, Carollo A, Chiodi G, Colandrea M, *et al.* First ex vivo validation of a radioguided surgery technique with β-radiation. Phys Med 2016;32:1139–44.

213. Collamati F, Moretti R, Alunni-Solestizi L, Bocci V, Cartoni A, Collarino A, *et al.* Characterisation of a β detector on positron emitters for medical applications. Phys Med 2019;67:85–90.

214. Mester C, Bruschini C, Magro P, Demartines N, Dunet V, Grigoriev E, *et al.* A handheld β+ probe for intra-operative detection of radiotracers. Procedia Engineering 2011;1812-4.

215. Sabet H, Stack BC, Nagarkar VV. Hand-Held, Intra-Operative Positron Imaging Probe for Surgical Applications. IEEE Trans Nucl Sci 2015;62:1927–34.

216. Singh B, Stack BC Jr, Thacker S, Gaysinskiy V, Bartel T, Lowe V, *et al.* A hand-held beta imaging probe for FDG. Ann Nucl Med 2013;27:203–8.

217. Monge F, Shakir DI, Lejeune F, Morandi X, Navab N, Jannin P. Acquisition models in intraoperative positron surface imaging. Int J CARS 2017;12:691–703.

218. Wendler T, Traub J, Ziegler SI, Navab N. Navigated three dimensional beta probe for optimal cancer resection. Med Image Comput Comput Assist Interv. 2006; 9:561-9.

219. Lees JE, Bugby SL, Alqahtani MS, Jambi LK, Dawood NS, McKnight WR, *et al.* A Multimodality Hybrid Gamma-Optical Camera for Intraoperative Imaging. Sensors (Basel) 2017;17:554.

220. Poumellec MA, Dejode M, Figl A, Darcourt J, Haudebourg J, Sabah Y, *et al.* [Sentinel node detection using optonuclear probe (gamma and fluorescence) after green indocyanine and radio-isotope injections]. Gynécol Obstét Fertil 2016;44:207–10.

221. Vidal-Sicart S, Seva A, Campos F, Sánchez N, Alonso I, Pahisa J, *et al.* Clinical use of an opto-nuclear probe for hybrid sentinel node biopsy guidance: first results. Int J CARS 2019;14:409–16.

222. van Oosterom MN, Meershoek P, Welling MM, Pinto F, Matthies P, Simon H, *et al.* Extending the Hybrid Surgical Guidance Concept With Freehand Fluorescence Tomography. IEEE Trans Med Imaging 2020;39:226–35.

223. KleinJan GH, Hellingman D, van den Berg NS, van Oosterom MN, Hendricksen K, Horenblas S, *et al.*; KleinJan; Hellingman; van den Berg; van Oosterom; Hendricksen; Horenblas. Hybrid Surgical Guidance: Does Hardware Integration of γ- and Fluorescence Imaging Modalities Make Sense? J Nucl Med 2017;58:646–50.

3

Head-to-head comparison of the hybrid tracer indocyanine green-^{99m}Tc-nanocolloid with ^{99m}Tc-Senti-Scint using sentinel node lymphoscintigraphy and single-photon emission computed tomography combined with computer tomography in melanoma

Adapted from:
Rietbergen DDD, Meershoek P, KleinJan GH, Donswijk M, Valdés Olmos RA, van Leeuwen FWB, Klop MWMC, van der Hage JA.

Nucl Med Commun. 2020 Oct;41(10):1010-1017

Abstract

Introduction and objectives: The hybrid tracer ICG-^{99m}Tc-Nanocolloid has been introduced for sentinel node imaging. However, until now comparison of this tracer with other radiocolloids with a larger particle size has not been effectuated. Based on a head-to-head evaluation in patients with melanoma we have compared ICG-^{99m}Tc-nanocolloid (particle size 5-80nm) with ^{99m}Tc-Senti-Scint (particle size 100-600nm) in order to establish differences in drainage pattern and sentinel node (SN) localization using lymphoscintigraphy and SPECT-CT in melanoma patients scheduled for SN biopsy.

Materials and methods: Twenty-five patients (mean age: 56.9y, range: 25-79y) with a melanoma scheduled for SLN biopsy prior to (re)excision of the primary lesion (scar) were prospectively included following a two-day procedure. The first day, after ^{99m}Tc-SentiScint injection in 4 intradermal depots around the primary lesion or scar, early/delayed lymphoscintigraphy and SPECT-CT images were acquired. The injection sites were marked. The second day, after assessing lymph node radioactivity using planar scintigraphy, ICG-^{99m}Tc-nanocolloid was injected at the previously marked skin points and imaging was performed. The paired planar and SPECT-CT images of both tracers were evaluated with respect to drainage patterns, SLN visualization and nonSLN appearing.

Results: Twenty-four out of 25 patients were evaluable. SLN visualization on a patient basis was 100% for ICG-^{99m}Tc-nanocolloid and 96% for ^{99m}Tc-Senti-Scint, whereas uptake in non-SLNs was found in respectively 71% (17/24) and 61% (14/23). Concordance in drainage to 45 lymph node basins was 91%. Discordant drainage was found for two melanomas in the head-and-neck and one in the clavicular area. Unique lymph node basins were seen in 44/45 (98%) for ICG-^{99m}Tc-nanocolloid and 42/45 (93%) for ^{99m}Tc-Senti-Scint. Concerning identified SLNs the number was similar 3 for both tracers (n=58); however, more non-SLNs (65 vs 50) were visualized with ICG-^{99m}Tc-nanocolloid than with ^{99m}Tc-Senti-Scint.

Conclusion: A slightly higher SLN visualization accompanied by a tendency to depict more non-SLNs was found for ICG-^{99m}Tc-nanocolloid. Excepting the head and neck area, an overall high concordance in drainage was found for both radiotracers. With an additional value for the hybrid tracer due to the combination of preoperative imaging and the additional visual signal in the operation room, added by the fluorescent component of the hybrid tracer, there was a preference for ICG-^{99m}Tc-nanocolloid.

Introduction

A unique aspect of lymphatic mapping procedures is that they are able to minimally invasively target the lymphatic drainage pathways of primary tumors. This procedure helps to accurately identify sentinel lymph nodes (SLNs) that can harbor micro-metastases in node-negative patients following biopsy.[1] While there are discussions ongoing with regard to the clinical value of subsequent lymph node dissections in these patients, there is consensus that identification of early lymphatic micro-metastases holds prognostic value by increasing the rate of regional disease control. Furthermore, positive node(s) indicates which patients are eligible for adjuvant treatment with immunotherapy. Extensive lymph node dissection increases the rate of regional disease control and provides prognostic information but does not increase melanoma-specific survival among patients with melanoma and sentinel-node metastases.[2] Following the introduction of the approach by Cabañas, the modernization of the sentinel concept by Morton et al led to personalized nodal identification and biopsy with minimal chance of side effects in breast cancer and melanoma care.[3-6] The same approach, complemented by Single Photon Emission Computed Tomography combined with Computer Tomography (SPECT-CT), has been incorporated for the SN procedure in head-and-neck surgery, gynecology and urology.[7-11]

Despite the success of the hybrid tracer Indocyanine Green (ICG)-^{99m}Tc-nanocolloid in targeting of the SLNs, overflow to higher echelon nodes (non-SLNs) is still observed.[12-13] One reason for this is could be a discrepancy between drainage speed and the volume/quantity of contrast administered. Such discrepancy occurs especially in areas of complex anatomy like the head-and-neck, parts of the trunk 5 and pelvis.[14,15] Preoperative imaging based on a combination of sequential scintigraphy and SPECT-CT allows for an accurate discrimination of the true SLNs from non-SLNs.[16,17] With the addition of ICG to ^{99m}Tc-nanocolloid the intraoperative search of SLNs in complex anatomic areas has been simplified thanks to the use of a fluorescence camera in combination with gamma-devices.[12] This hybrid approach with preoperative SLN mapping using lymphoscintigraphy and SPECT-CT as a roadmap to identify SLNs in the operation room may obviate the application of surrogate markers such as the 10% rule by surgeons.[18-20] In the future, the development of tracers that only accumulate in SLNs would significantly simplify the procedures by transforming the prevailing imaging paradigm "not all radioactive nodes are sentinel nodes" to an alternative one resting on "all radioactive lymph nodes are sentinel nodes".[21]

It is well known that radiocolloids like with a particle size varying from 5 to 80 nm have an enhanced SLN specificity compared to small molecule dyes (e.g., patent blue diameter +1nm) and dyes such as ICG that interact with native human serum

albumin (HSA; + 7nm).[22,23] On the other hand, since lymphatic distribution and nodal filtration is influenced by particle size, there is a tendency to reduce the number of non-SLNs by using radiocolloids with a larger size.[24] This rationale has provided the basis for the development of radiocolloids with a larger particle size such as ^{99m}Tc-Senti-Scint (diameter 100-600 nm). However, until now it has not been documented if in fact radiocolloids with a larger particle size yield superior performance.

Given all the above-mentioned variables that can influence lymphatic flow of a radiocolloid, in analogy to the set-up previously used to validate the similarity of lymphatic drainage for ^{99m}Tc-nanocolloid and ICG-^{99m}Tc-nanocolloid, we have 6 now compared the differences in drainage patterns of ^{99m}Tc-Senti-Scint and ICG-^{99m}Tc-nanocolloid.[25]We decided to perform this comparison on the basis of a head-to-head evaluation using lymphoscintigraphy and SPECT-CT in melanoma patients scheduled for SLN biopsy. Further, we studied whether the increased particle size could reduce the amount of non-SLNs, while preserving the SLN identification.

Materials and methods

Patient demographics

The trial was initially registered as the prospective study N13ICG (^{99m}Tc-SentiScint vs ICG^{99m}Tc-nanocolloid for sentinel node biopsy of malignant melanoma of the trunk, of an extremity or in the head and neck) at the Netherlands Cancer Institute – Antoni van Leeuwenhoek Hospital. Following approval of the Protocol Review Board of the institution the study was activated on June 16, 2014 as the trial NL4568 in the Netherlands Trial Register, and closed on November 30, 2017. Twenty-five patients (mean age: 56.9y, range: 25-79y) with a melanoma scheduled for SLN biopsy prior to (re)excision of the primary lesion (scar) were prospectively included after informed consent. One patient with a nose melanoma was excluded since the SPECT-CT data were not completed, meaning twenty-four patients were evaluated. The localization of the primary lesion was as follows: head-and-neck region (n=5), the trunk (n=11) and extremities (n=8).

Imaging procedure

All patients followed a two-day procedure. On the first day, 90 MBq (±10%; 2.43 mCi) ^{99m}Tc-Senti-Scint was injected in 4 intradermal depots around the primary 7 lesion or scar. Injection points were marked on skin with indelible ink to facilitate reproducibility in the administration of the second tracer. Lymphatic drainage was mapped using dynamic lymphoscintigraphy (0-10 minutes), static lymphoscintigraphy (15 minutes and 2 h post injection) and SPECT-CT (2h post injection). The second day, after planar images to control resting lymph node radioactivity, 90 MBq (±10%; 2.43 mCi) ICG-^{99m}Tc-nanocolloid was injected and similar images were acquired. The paired planar and SPECT-CT images of both tracers were evaluated with respect

to drainage to lymph node basins, SLN visualization and non-SLN uptake. Both lymphoscintigraphy and SPECT-CT were acquired using a hybrid system (Symbia T6, Siemens, Erlangen, Germany). Flow chart of the study setup is presented in more detail in figure 1.

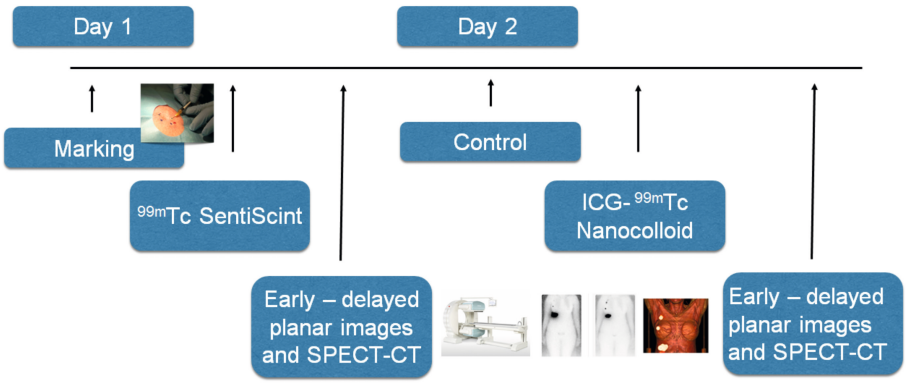

Figure 1. flowchart of the study design. The first day, 4 intradermal depots ^{99m}Tc-Senti-Scint ware injected around the primary lesion or scar after marking the skin points. Early and delayed planar lymphoscintigraphy and SPECT-CT were acquired. The second day, after planar images to control resting lymph node radioactivity, ICG-^{99m}Tc-nanocolloid was injected at the previously marked skin points. The same image acquisitions were acquired for both tracers and reviewed by two experienced nuclear medicine physicians.

Comparison imaging findings ICG-^{99m} TC-nanocolloid and ^{99m}Tc-Senti-Scint and scoring

The derived early, delayed planar and SPECT-CT data of both the tracers were reviewed by two experienced nuclear medicine physicians. The number of drainage basins, numbers of SLNs, non-SLNs and their anatomical localization were scored. The first lymph node on which a tumor drains is considered to be the sentinel node. The early, delayed planar and SPECT-CT images of both tracers were compared to each other and scored on concordant or discordant findings.

Surgical guidance

Planar images were used to mark the location of identified SLNs on the skin, while SPECT-CT images were used to indicate the anatomical SLN location in relation to muscles and vessels in the draining lymph node basin. Figure 1 shows the flow 8 chart of the study. For the intraoperative procedure only the findings of the ICG-^{99m}Tc-nanocolloid study were used. Following gamma-probe (Neoprobe, Johnson&Johnson Medical, Hamburg, Germany) localization at the indicated SLN site, SLNs were further prepared and removed under guidance of a fluorescent

camera (PhotoDynamic Eye, Hamamatsu Photonics, Hamamatsu, Japan) as previously described.[12]

Results

The SLN visualization rate on a patient basis was 100% for ICG-^{99m}Tc-nanocolloid and 96% for ^{99m}Tc-Senti-Scint due to a non-visualization in one patient in the latter group. Drainage to 45 unique lymph node basins were seen with a concordant rate of 91% between both the tracers. Uptake in non-SLNs was found in respectively 71% (17/24) and 61% (14/23) of patients (table 1 and figure 2). The concordance of drainage basins was 100% for melanomas located in extremities.

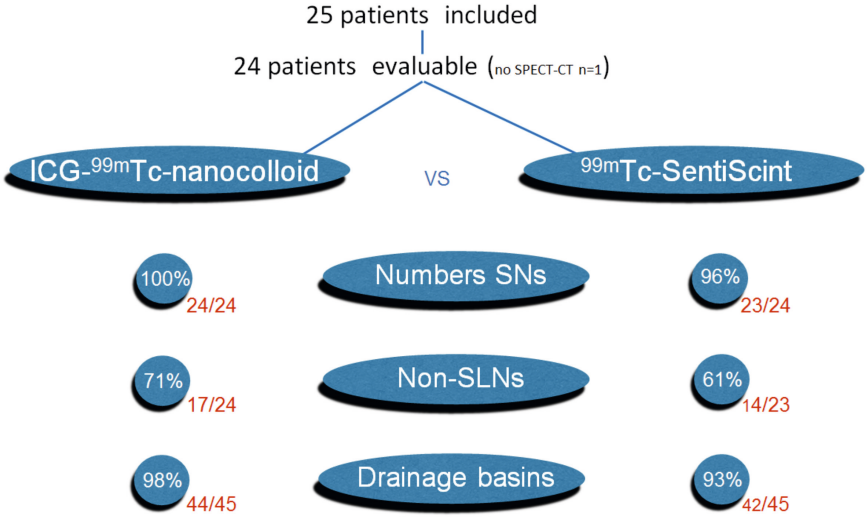

Figure 2. Schematic overview of the results. Of the 25 patients which were included, 24 patients could be evaluated. SLN visualization rate on a patient basis was 100% for ICG-^{99m}Tc -nanocolloid and 96% for ^{99m}Tc -Senti-Scint due to one non-visualization. Concerning the overall number of SLNs identified, this was 56 with ICG-^{99m}Tc-nanocolloid and 54 (96%) with ^{99m}Tc-Senti-Scint. Uptake in non-SLNs was found in respectively 71% and 61% of the patients. Drainage to 45 unique lymph node basins were seen with a concordant rate of 91%.

Table 1. Schematic overview of the results of the 24 which could be evaluated.

		Basin(s) (number)		SN(s) (number)		Non-SN	
Patient (gender, age)	**Primary Lesion Site**	**^{99m}Tc-Senti-Scint**	**ICG-^{99m}Tc-nanocolloid**	**^{99m}Tc-Senti-Scint**	**ICG-^{99m}Tc-nanocolloid**	**^{99m}Tc-Senti-Scint**	**ICG-^{99m}Tc-nanocolloid**
Head and Neck							
1 (M, 68y)	cheek	2	2	2	2	-	-
2 (F, 42y)	preauricular	1	2	1	2	-	-
3 (F, 57y)	occipital	3	3	3	3	+	+
4 (M, 72y)	nose	3	3	3	3	+	+
5 (M, 55y)	nose	3	2	5	4	-	-
Extrimities							
1 (F, 79y)	hand	2	2	4	4	+	+
2 (F, 35y)	upper leg	1	1	1	1	+	+
3 (F, 51y)	upper arm	1	1	1	1	+	+
4 (F, 51y)	upper leg	1	1	1	1	+	+
5 (M, 64y)	lower leg	1	1	1	1	+	+
6 (M, 58y)	upper leg	1	1	2	2	+	+
7 (M, 68y)	upper leg	1	1	2	2	+	+
8 (M, 54y)	upper leg	1	1	2	2	+	+

Table 1. Continued

Patient (gender, age)	Primary Lesion Site	Basin(s) (number)		SN(s) (number)t		Non-SN	
		^{99m}Tc-Senti-Scint	ICG-^{99m}Tc-nanocolloid	^{99m}Tc-Senti-Scint	ICG-^{99m}Tc-nanocolloid	^{99m}Tc-Senti-Scint	ICG-^{99m}Tc-nanocolloid
Trunk							
1 (F, 58y)	shoulder	1	1	2	2	-	-
2 (F, 36y)	back	1	1	1	1	-	+
3(M, 74y)	back	2	2	2	2	-	+
4 (M, 67y)	upper back	4	4	4	4	-	-
5 (M, 50y)	back	2	2	3	3	+	+
6 (M, 66y)	upper back	4	4	4	4	-	-
7 (M, 68y)	upper back	1	1	1	1	+	+
8 (M, 55y)	upper back	3	3	6	6	+	+
9 (F, 56y)	trunk	2	2	2	2	-	-
10 (M, 25y)	gluteal	1	1	1	1	+	+
11 (M, 47y)	clavicular area	0	2	0	2	-	+
N=24 Mean age= 56y Range=25-79y		N=42 basins 42/45 = 93% HN=12 Ext=9 Trunk=21	N=44 basins 44/45 = 98% HN=12 Ext=9 Trunk=23	N=54 SN 23/24= 96% HN=14 Ext=14 Trunk=26	N=56 SN 24/24 = 100% HN=14 Ext=14 Trunk=28	14/23=61%	17/24=71%

Ext, extrimities; F, female; HN, head and neck; ICG, indocyanine green; M, male; +, Non-SN present; -, Non-SN absent.

Discordant findings were mainly seen in the head-and-neck area whereas two out of 5 patients showed discrepancy between the images of both tracers (figure 3). In one patient with a midline nose melanoma, the images showed bilateral neck drainage with tracer concordance for the right side but discordant findings on the left side with an extra submandibular sentinel lymph node visualized only with ^{99m}Tc-Senti-Scint (figure 4). In the other case, a patient with a melanoma of the skin (parietotemporal region), the images of both tracers showed a lymph node in region 2 of the neck, with an additional lymph node (in the parotic area) between the injection site and the previously mentioned concordant SLN only seen on the ICG-^{99m}Tc-nanocolloid (figure 5).

Moreover, the only patient with a non-concordant study in the trunk was a patient with a melanoma in the clavicular area (figure 6), which is an area adjacent to the neck also characterized by a high degree of unpredictable drainage. In the 3 patients where discordance was seen between the two radiotracers, the pathologic exam did not reveal any micro- or macro-metastasis.

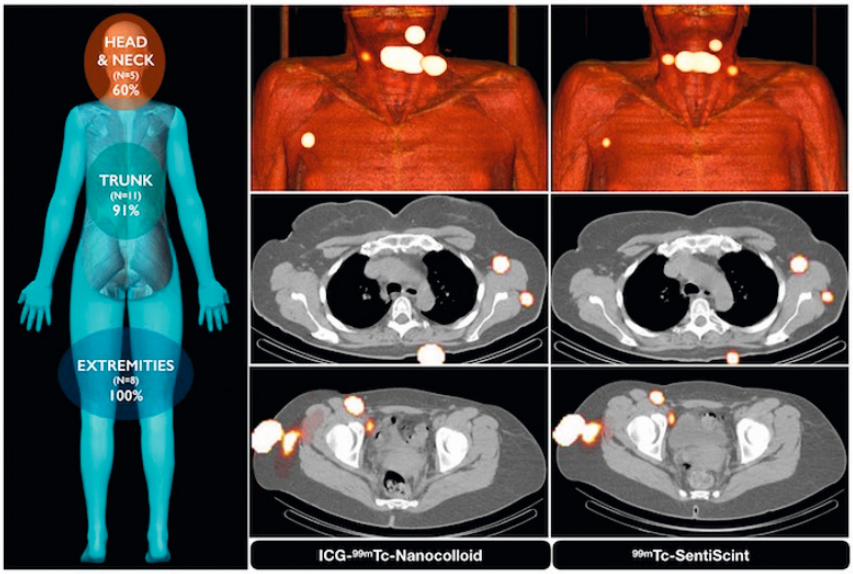

Figure 3. On the left, lymphatic drainage concordance rate between ICG-^{99m}Tc- Nanocolloid and ^{99m}Tc-Senti-Scint related to the primary melanoma location varying from 100% for extremities to 60% for head/neck. Discordant findings were seen in two out of 5 patients with melanomas in the head and neck area. In one patient, there was a non-visualization in a Senti-Scint patient in trunk melanoma (clavicular region). On the right, SPECT-CT based examples of concordance for melanomas of the midline of the neck showing drainage to 3 cervical lymph node stations and the right axilla (upper row), left medial upper back with drainage to sentinel nodes in the left scapular area and left axilla (middle row) and lateral right upper leg with drainage to an inguinal sentinel node and an iliac second-tier node on the right (lower row).

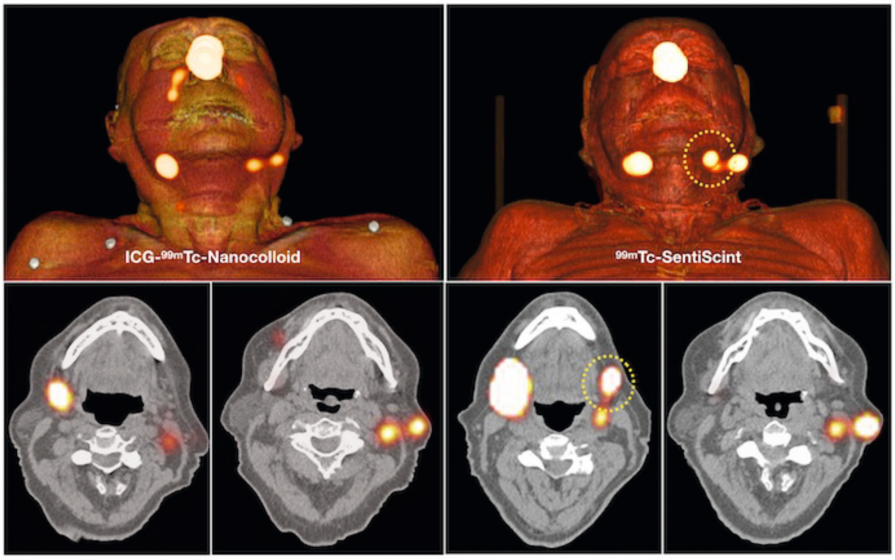

Figure 4. Volume rendered (top) and transaxial (below) SPECT-CT of a patient with a midline nose melanoma showing bilateral neck drainage with tracer concordance for the right side but discordant findings in the left side with a submandibular sentinel lymph node visualized only with ^{99m}Tc-Senti-Scint (dotted circles). There is some lymph duct visualization lateral from the ICG-^{99m}Tc-nanocolloid injection nasal site.

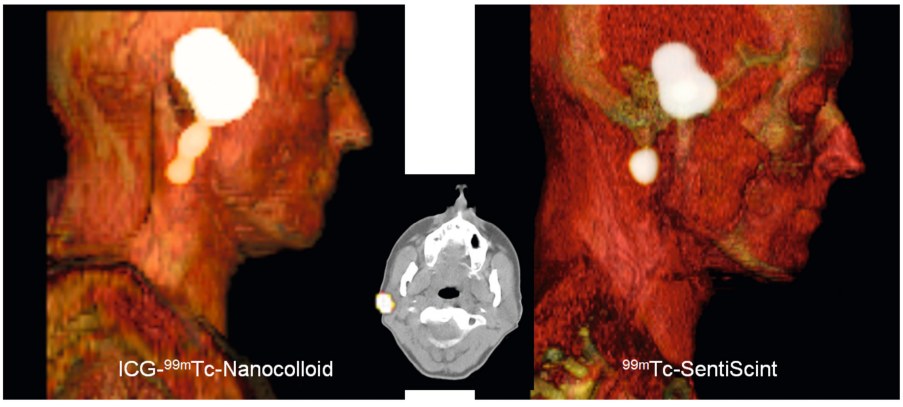

Figure 5. Volume rendered image of a patient with a melanoma of the skin (parietotemporal region). On both images a lymph node is seen region 2 of the neck. The left image (nanocolloid) also shows a SLN between the injection site and the concordant SLN, a SLN in the parotic area.

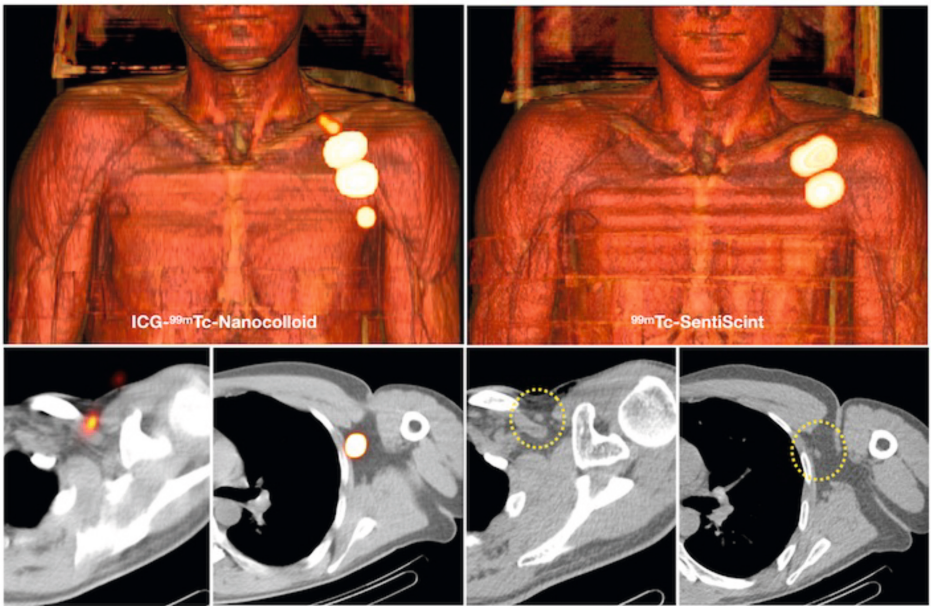

Figure 6. Volume rendered (top) and transaxial (below) SPECT-CT of a patient with a melanoma in the left subclavicular area showing (on the left) drainage to sentinel lymph nodes in the left periclavicular and axillar area on the study performed with ICG-^{99m}Tc-nanocolloid. By contrast (on the right) no migration of ^{99m}Tc-Senti-Scint from the injection site to the above-mentioned nodes (dotted circles) is observed.

Discussion

In this study two different radiocolloids for SLN imaging were compared to document lymphatic drainage in relation to particle size in a head-to-head designed approach in patients with melanoma scheduled for SLN biopsy. Related to lymph node basin, an overall 91% drainage concordance was found. The concordance of drainage basins was 100% for melanomas located in extremities.

The SN visualization rate was 100% for ICG-^{99m}Tc-nanocolloid and 96% for ^{99m}Tc-Senti-Scint with slightly higher non-SLNs for ICG-^{99m}Tc-nanocolloid group. Based on these findings and the high overall concordance rate, it is possible to conclude that in melanoma in areas with predictable lymphatic drainage, like the extremities and part of the trunk, the particle size of radiotracers for SLN imaging does not play a critical role. However, in complex anatomical regions with multidirectional lymphatic drainage, like head-and-neck area and the upper part of the trunk, SLN imaging using larger colloid particles tends to reduce the detection accuracy. Apparently here the increased size impairs the drainage, meaning it is not able to optimally cover all lymph node basins draining from the primary melanoma.[14] The discordance appears

to increase with a favor for ICG-^{99m}Tc-nanocolloid. The 100% concordance observed in a previous head-to-head evaluation of ICG-^{99m}Tc-nanocolloid with ^{99m}Tc-nanocolloid (25 patients including head-and-neck melanoma), underlines that particle size does influence drainage as observed in the present study.[25] The current data seems to indicate a larger particle size can mean SLNs can be missed in areas of more complex lymphatic drainage, which would result in false negatives of the SLN procedure. This conclusion should, however, be confirmed in a larger series of patients.

Alternative to the use of radiocolloids with a larger particle size it has been proposed to use radiotracers that have an affinity for CD206 receptors expressed in on the surface of macrophages and dendritic cells in lymph nodes and expressed along lymphatic ducts.[26] ^{99m}Tc-Tilmanocept with a particle size of +7nm is a dextran particle containing mannosyl units.[27] A trial similar to the one performed in the present study comparing this new generation tracer with the standard radiocolloids for SN work is necessary.

The quest for improvement of SLN targeting with new radiocolloids, simply stated, aims to simplify the role of nuclear medicine imaging in the SLN procedures. While one can argue whether this is desirable or not, there is a tendency among some surgeons to perform the procedure without the involvement of nuclear medicine. The current data suggests that preoperative mapping using lymphoscintigraphy and SPECT-CT, remains today the only imaging modality providing an effective roadmap able to personalize lymphatic imaging. At the up side, the inclusion of fluorescence guidance via ICG-^{99m}Tc-nanocolloid makes surgeons prefer use of this tracer (in combination with SPECT-CT) in areas of complex drainage.[12] Hence is seems that future tracer developments for lymphatic mapping 11 should also aim to address the desire for integrated fluorescence imaging capabilities.

Conclusion

The hybrid tracer ICG-^{99m}Tc-nanocolloid showed a high concordance in lymphatic mapping in comparison to a tracer with significant larger particle size like ^{99m}Tc-Senti-Scint. Discordant findings were exclusively seen in a minority of patients with complex multidirectional lymphatic drainage, like head and neck, where the hybrid tracer can be of added value. The slightly higher SN visualization found for ICG-^{99m}Tc-nanocolloid was accompanied by depiction of more non-SLNs in some patients. However, the combination of preoperative imaging with the hybrid intraoperative approach adding the fluorescent component to the procedure can help surgeons to effectively identify SNs at the operation room.

References

1. Moncayo VM, Alazraki AL, Alazraki NP, Aarsvold JN. Sentinel Lymph Node Biopsy Procedures. Semin Nucl Med. 2017;47(6):595-617.
2. Faries MB, Thompson JF, Cochran, et al. Completion Dissection or Observation for Sentinel-Node Metastasis in Melanoma. N Engl J Med. 2017;376(23):2211- 2222.
3. Cabanas RM. An approach for the treatment of penile carcinoma. Cancer. 1977 Feb;39(2):456-66.
4. Morton DL, Wen DR, Wong JH, et al. Technicals details of intraoperative lymphatic mapping for early stage melanoma. Arch Surg. 1992;127(4):392-9.
5. Giammarile F, Alazraki N, Aarsvold JN, et al. The EANM and SNMMI practice guideline for lymphoscintigraphy and sentinel node localization in breast cancer. Eur J Nucl Med Mol Imaging. 2013;40(12):1932-47.
6. Bluemel C, Herrmann K, Giammarile F, et al. EANM practice guidelines for lymphoscintigraphy and sentinel lymph node biopsy in melanoma. Eur J Nucl Med Mol Imaging. 2015;42(11):1750-1766.
7. Giammarile F, Schilling C, Gnanasegaran G, et al. The EANM practical guidelines for sentinel lymph node localisation in oral cavity squamous cell carcinoma. Eur J Nucl Med Mol Imaging. 2019;46(3):623-637.
8. Sharma D, Koshy G, Grover S, Sharma B. Sentinel Lymph Node Biopsy: A new approach in the management of head and neck cancers. Sultan Qaboos Univ Med J. 2017;17(1):e3-e10.
9. Giammarile F, Bozkurt MF, Cibula D, et al. The EANM clinical and technical guidelines for lymphoscintigraphy and sentinel node localization in gynaecological cancers. Eur J Nucl Med Mol Imaging. 2014;41:1463–1477.
10. van der Poel HG, Wit EM, Acar C, et al. Sentinel Node Prostate Cancer Consensus Panel Group members. Sentinel node biopsy for prostate cancer: report from a consensus panel meeting. BJU Int. 2017;120(2):204-211.
11. Mehralivand S, van der Poel H, Winter A, Choyke PL, Pinto PA, Turkbey B. Sentinel lymph node imaging in urologic oncology. Transl Androl Urol. 2018;7(5):887-902.
12. KleinJan GH, van Werkhoven E, van den Berg NS, et al. The best of both worlds: a hybrid approach for optimal pre- and intraoperative identification of sentinel lymph nodes. Eur J Nucl Med Mol Imaging. 2018;45(11):1915-1925
13. van den Berg NS, Brouwer OR, Klop WM, et al. Concomitant radio- and fluorescence-guided sentinel lymph node biopsy in squamous cell carcinoma of the oral cavity using ICG-(99m)Tc-nanocolloid. Eur J Nucl Med Mol Imaging. 2012;39(7):1128-36.
14. Statius Muller MG, Hennipman FA, van Leeuwen PAM, Pijpers R, Vuylsteke RJ, Meijer S. Unpredictability of lymphatic drainage patterns in melanoma patients. Eur J Nucl Med Mol Imaging. 2002;29:255-61.
15. Ballinger JR. The use of protein-based radiocolloids in sentinel node localization. Clin Transl Imaging. 2015;3:179-86.
16. Doepker MP, Yamamoto M, Applebaum MA, et al. Comparison of Single-Photon Emission Computed Tomography-Computed Tomography (SPECT/CT) and Conventional Planar Lymphoscintigraphy for Sentinel Node Localization in Patients with Cutaneous Malignancies. Ann Surg Oncol. 2017;24(2):355-361.

17. Valdés Olmos RA, Rietbergen DD, Vidal-Sicart S, Manca G, Giammarile F, Mariani G. Contribution of SPECT/CT imaging to radioguided sentinel lymph node 14 biopsy in breast cancer, melanoma, and other solid cancers: from “open and see” to “see and open”. Q J Nucl Med Mol Imaging. 2014;58(2):127-39.
18. McMasters KM, Reintgen DS, Ross MI, er al. Sentinel lymph node biopsy for melanoma: how many radioactive nodes should be removed? Ann Surg Oncol. 2001;8(3):192-7.
19. Liu LC, Parrett BM, Jenkins T, et al. Selective sentinel lymph node dissection for melanoma: importance of harvesting nodes with lower radioactive counts without the need for blue dye. Ann Surg Oncol. 2011;18(10):2919-24.
20. Kroon HM, Lowe L, Wong S, et al. What is a sentinel node? Re-evaluating the 10% rule for sentinel lymph node biopsy in melanoma. J Surg Oncol. 2007;95(8):623-8.
21. Vidal-Sicart S, Vera DR, Valdés Olmos RA. Next generation of radiotracers for sentinel lymph node biopsy: What is still necessary to establish new imaging paradigms? Revista Esp Med Nucl Im Molecular. 2018;37:373-9.
22. Van Den Berg NS, Buckle T, Kleinjan GI, et al. Hybrid tracers for sentinel node biopsy. Q J Nucl Med Mol Imaging. 2014;58(2):193-206.
23. Boxen I, McCready D, Ballinger JR. Sentinel node detection and definition may depend on the imaging agent and timing. Clin Nucl Med. 1999;24(6):390-4.
24. De Cicco C, Cremonesi M, Luini A, et al. Lymphoscintigraphy and radioguided biopsy of the sentinel axillary node in breast cancer. J Nucl Med. 1998;39(12):2080-4.
25. Brouwer OR, Buckle T, Vermeeren L, et al. Comparing the hybrid fluorescentradioactive tracer indocyanine green-99mTc-nanocolloid with 99mTc-nanocolloid for sentinel node identification: a validation study using lymphoscintigraphy and SPECT/CT. J Nucl Med. 2012;53(7):1034-40.
26. Engering AJ, Cella M, Fluitsma D, et al. The mannose receptor functions as a high capacity and broad specificity antigen receptor in human dendritic cells. Eur J Immunol. 1997;27(9):2417–25.
27. Sondak VK, King DW, Zager JS, et al. Combined analysis of phase III trials evaluating [99mTc]tilmanocept and vital blue dye for identification of sentinel lymph nodes in clinically node-negative cutaneous melanoma. Ann Surg Oncol. 2013;20:680–8.

4

Does ^{99m}Tc-tilmanocept, as next generation radiotracer, meet with the requirements for improved sentinel node imaging?

Adapted from:
Rietbergen DD, Pereira Arias-Bouda LM, van der Hage J, Valdés Olmos RA.

Rev Esp Med Nucl Imagen Mol. 2021; 40:275-280

Abstract

Introduction and objectives: To evaluate the migration of ^{99m}Tc-tilmanocept from the injection site (IS) as well as the uptake in sentinel nodes (SNs) and non-SNs for lymphatic mapping in patients with breast cancer and melanoma, scheduled for SN biopsy after interstitial tracer administration.

Materials and methods: For 29 primary tumours in 28 patients (mean age: 62y, range: 45–81y) scheduled for SN biopsy planar images were acquired 10 and 120 min after administration of 74 MBq ^{99m}Tc-tilmanocept, in order to evaluate lymphatic drainage as well as uptake ratios between injection site (IS), SN and non-SN. SPECT-CT was performed immediately after delayed planar images to enable anatomical lymph node localization.

Results: SNs were visualized in all patients (100%) with drainage to 34 basins. Uptake in non-SNs was perceived in 16 basins (47%). Number of SNs was concordant between early and delayed images in all basins excepting five (86%). In 24 patients tracer migrated to one lymph node basin (LNB), in three to 2 and in one to 4. When IS was included (N = 29) on image, IS/SN ratio could be measured per LNB. The IS/SN ratio at 2 h compared to 15 min decreased with an average of 66% (range: 15–96%). SN/non-SN 2 h ratio in LNBs with visible non-SNs averaged 6.6 (range: 2.3–15.6). In 9 patients with two SNs SN1/SN2 ratio averaged 1.9 on delayed images. At histopathology, SNs were found to be tumour positive in 7 basins (20%).

Conclusion: ^{99m}Tc-tilmanocept appears to meet the requirements for improved SN imaging in breast cancer and melanoma on the basis of early and persistent SN visualization frequently accompanied by no or markedly less non-SN uptake. This is associated to rapid migration from the injection site together with increasing SN uptake and retention as expressed by decreasing IS/SN and persistently high SN/non-SN ratios. Further head-to-head comparison of ^{99m}Tc-tilmanocept with standard SN radiotracers in larger series of patients is necessary.

Introduction

Radiotracers with small particle size have been associated with a successful sentinel node (SN) visualization; however, in many cases concomitant non-SN lymph node uptake may difficult image interpretation and radioguided procedures at the operating room leading to an overestimation of the number of SNs.[1]

Recently, ^{99m}Tc-tilmanocept, with an average molecular size of 7 nm, has become available in Europe; due to the improved receptor affinity of its mannose component in surface macrophages this tracer is aimed to combine increased uptake in SN with a rapid clearance from the site of injection.[2] In recent literature, the use of ^{99m}Tc-tilmanocept has been found to be effective for SN localization in melanoma,[3] breast cancer [4] and oral cavity malignancies.[5] However, in these publications as well as in earlier literature [6] the evaluation of ^{99m}Tc-tilmanocept has been based on the assessment of its efficacy for lymphatic mapping and sentinel node identification, but not on the evaluation of the aspects related to tracer migration and SN uptake and retention, which are important to characterize the additional value of a small-particle radiotracer with specific SN affinity.

The introduction of ^{99m}Tc-tilmanocept has renewed the discussion about the potential of next generation radiotracers to meet the requirements for improved SN imaging.[2] The current paradigm for SN identification is based on the observation that not all depicted radioactive nodes are SNs. This is principally due to the overflow of colloid particles from first to second echelon lymph nodes frequently seen for current tracers routinely used for the SN procedure in Europe.[1] In order to compensate this shortcoming related to the first generation of SN tracers, since the initial validation of the SN procedure, protocols for preoperative imaging have been designed to acquire sequential images on the basis of the combination of an initial dynamic study with subsequent planar images at different points of time. Directly from the injection site draining lymph nodes in each basin are identified as SN and marked on skin by nuclear physicians to enable subsequent resection at the operating room. A switch to a paradigm associating all radioactive nodes with sentinel nodes is not possible with first generation radiocolloids. It would be only feasible if radioactive tracers are highly retained at first echelon lymph nodes after injection as it is postulated for ^{99m}Tc-tilmanocept and the next generation of radiotracers.

In order to analyze the pattern of migration of ^{99m}Tc-tilmanocept following interstitial tracer administration we evaluated the relationships between radioactivity at the site of injection and uptake in SNs and non-SNs in a group of patients scheduled for SN biopsy because of breast cancer and melanoma.

Materials and methods

Patients
A total of 28 patients (mean age: 62 years, range: 45–81years) was included in the study; 13 breast cancer patients (N=14 tumours; with N=10 lobular carcinoma, N=2 DCIS and N=2 NST; mean size 20.9 mm, range 3–90 mm) and 15 melanoma patients (Breslow depth; mean 2.06, range 0.5–7.0). All patients (22 female, 6 male) had no clinical evidence for regional lymph node involvement and were referred for lymphatic mapping using ^{99m}Tc-tilmanocept in the context of their regular procedure for SN biopsy related to breast cancer or melanoma.

Patients consented to publication of data corresponding to the evaluation of lymphatic mapping in accordance with the Declaration of Helsinki. The local institutional review board approved retrospective analysis of the imaging data as non-WMO research obligation.

Image acquisition
All patients were scheduled for a two-day procedure with pre- operative SN mapping the first day and intraoperative SN resection the second day. For melanoma patients (N = 15), 41 MBq (mean 40.7 MBq, range 38–44 MBq) ^{99m}Tc-tilmanocept was injected in 4 intradermal depots around the primary lesion or scar. Lymphatic mapping was effectuated at the Alrijne Hospital in Leiderdorp using dynamic lymphoscintigraphy (0–10 min), static lymphoscintigraphy (15 min and 2 h post injection) and SPECT-CT (2 h postinjection) using a hybrid system (Discovery NM/CT 670 Pro, GE Healthcare, Milwaukee, USA). For breast cancer patients (N = 13), 107 MBq (±38%; 2.89 mCi) (mean 107 MBq, 75–148 MBq) ^{99m}Tc-tilmanocept was injected periareolar in the involved quadrant. Lymphatic mapping were acquired at the Leiden University Medical Centre using a hybrid system (Symbia T6, Siemens, Erlangen, Germany). One patient had bilateral breast cancer and SN biopsy was effectuated for both sides the same day using 2 injections of 136 and 141 MBq ^{99m}Tc-tilmanocept. If possible, the site of injection was included in the gamma camera field of view. SPECT-CT was performed immediately after delayed planar images to enable anatomical lymph node localization.

Image evaluation
The derived dynamic, early, delayed planar and SPECT-CT data were reviewed by two experienced nuclear medicine physicians. The SN is the first lymph node in which a tumour drains on, seen as the first focus on the images, due to migration of the radioactivity from the injection site. Non-SNs are nodes that are located in the same lymph node basin, behind the SN and further away from the injection site and in most cases less radioactive. The number of SNs was correlated between early and delayed images. Radioactive lymph nodes identified as SNs were topographically

related to the draining lymph node basin (LNB). Regions of interest (ROIs) were drawn for injection site (IS), SN and non-SN on static planar images. Subsequently IS/SN, SN/non-SN and SN1/SN2 ratios on the base of mean counts per ROI were calculated on both early and delayed images.

Surgical guidance
Planar images were used to mark the location of identified SLNs on the skin, while SPECT-CT images were used to indicate the anatomical SLN location in relation to muscles and vessels in the draining lymph node basin. For the intraoperative procedure only a gamma-probe (Europrobe) was used for localization at the indicated SLN site.

Results

SNs were visualized in all patients (100%), with lymphatic drainage to 34 basins. In 11 of them (39%), there was no visible non-SLN uptake on both planar and SPECT-CT. Uptake in non-SN was perceived in 18 basins (52%) with 7/15 (47%) for breast cancer and 11/20 (55%) for melanoma.

A total of 49 SNs was identified and the number of SNs was concordant between early and delayed images in all basins except five (85%). In 24 patients tracer migrated to one LNB (Figure 1), in three to 2 (Figures 2 and 3) and in one to 4 LNBs.

When IS was included in the field of view, IS/SN ratio per LNB (N=29) at 2 h decreased with an average of 66% (range: 15–96%) in comparison to the ratio at 15 min with increasing in SN uptake and retention. SN/non-SN 2-h ratio in LNB with visible non-SNs averaged 6.6 (range: 2.3–15.6). In 12 patients with at least two SNs in a LNB, SN1/SN2 ratio averaged 1.9 (range: 0.8–4.1) on delayed images, whereas for 7 of these patients with evaluable uptake SN1/SN2 ratio averaged 1.6 (range: 0.65–5) on early images. At histopathology, SNs were found to be tumour positive in 7 basins (20%) concerning 6 patients. Results are summarized in Table 1.

In this study the migration of ^{99m}Tc-tilmanocept from the injection site (IS) as well as the uptake in sentinel nodes (SNs) and non-SNs was evaluated for SN imaging in melanoma and breast cancer patients. According to the results of the present study ^{99m}Tc-tilmanocept appears to meet the requirements for improved SN imaging. This can be concluded on the basis of an early and persistent SN visualization in all patients frequently accompanied with no (46%) or markedly less non-SN lymph uptake in the draining LNB. This is associated with rapid migration from the injection site together with an increasing SN uptake, as expressed by decreasing IS/SN ratios.

Small particle size molecules like colloid-based SN tracers could give a high number of non-SNs. A study of Lamichhane et al. evaluated the overnight migration of radiolabelled sulfur colloid in 70 patients. The SN was successfully identified in 95.71% of the patients and showed a high range of non-SN (5–22; mean 13.3) in regard of the number of SN (1–5; mean 1.5).[7] The decreased overflow from first to second echelon lymph nodes as observed on delayed images of many patients of the present study may be explained by the high level of extraction of ^{99m}Tc-tilmanocept in the SN. This appears to match with the described specific receptor high affinity for CD206 receptors expressed in on the surface of macrophages and dendritic cells in lymph nodes and expressed along lymphatic ducts.[2] In complex anatomical regions with multidirectional lymphatic drainage, like head-and-neck area and the upper part of the trunk, small particle size molecules give a lot of SNs and non-SNs and Tilmanocept could be of added value.[8]

The rapid and persistent SN visualization with rapid migration from the injection site and increasing SN uptake over time, found in this study, suggests that early imaging could be dropped, which is cost effective and more patient friendly, but further study need to be done. Another interesting observation is that the decrease in IS/SN ratios was not associated with a further increase in non-SN uptake in the majority of LNB.

The rapid migration from the IS demonstrated in the current study appears to reinforce the possibility to use ^{99m}Tc-tilmanocept in primary lesions draining to lymph nodes located in their vicinity as observed in some melanomas of head/neck and trunk. Also, for oral cavity malignancies draining to submandibular lymph node basins, it is necessary to obtain a clear differentiation for SNs in the proximity of IS. [9]

The question rises if ^{99m}Tc-tilmanocept has an added value in breast cancer patients in perspective of number of non-SNs. Unkart et al. compared ^{99m}Tc-sulfur colloid with ^{99m}Tc-tilmanocept in two arms in breast cancer patients and did not found a significant difference in the number of identified SNs between both groups (1.96 vs. 2.04).[10] Khandekar et al. found the same results; there was no significant difference in the detection of radioactive SNs in breast lymphatic mapping procedures using ^{99m}Tc-sulfur colloid and ^{99m}Tc-tilmanocept. They did found that the injection site clearance of ^{99m}Tc-tilmanocept was statistical significant greater than sulfur colloid.[11]

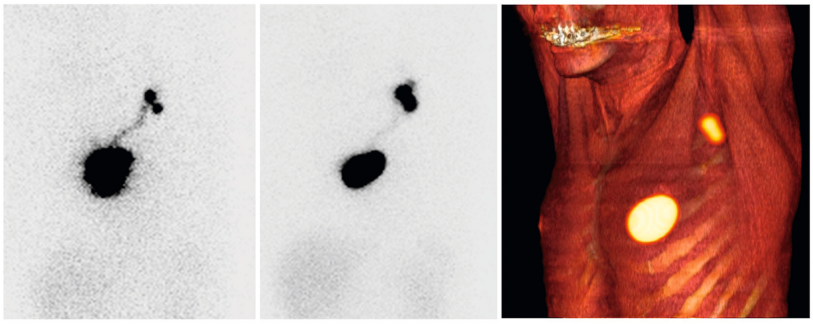

Figure 1. Planar left oblique images acquired 10 min (on the left) and 2 h (middle) after ^{99m}Tc-tilmanocept injection in a breast cancer patient. Note that the rapid migration from the injection site in the left breast is accompanied by an increasing uptake in two sentinel nodes located in level 1 of the axilla as seen on volume rendering SPECT-CT (on the right). At surgery, two sentinel nodes were removed. Histopathology was negative.

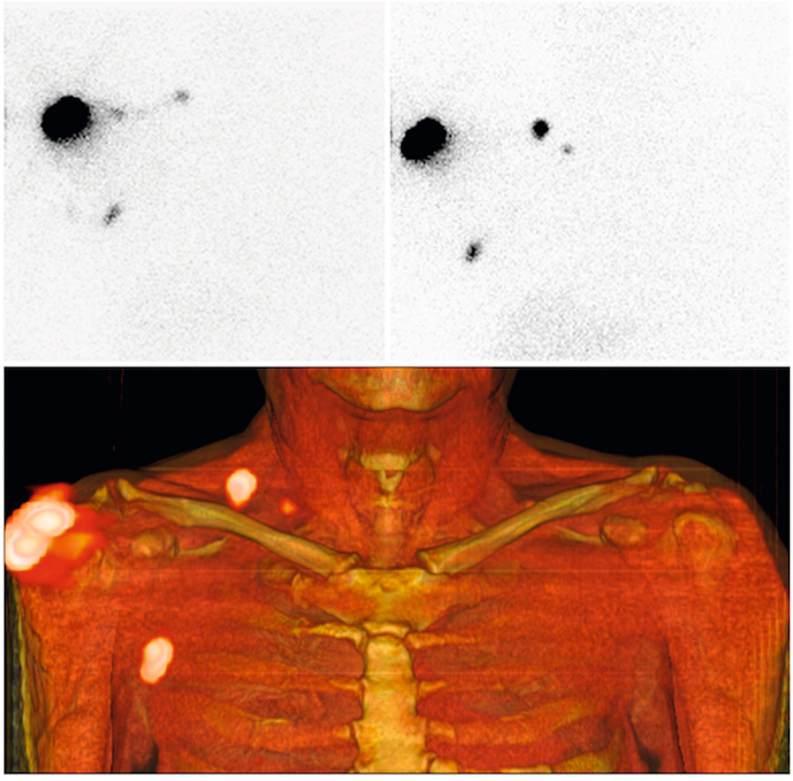

Figure 2. (Above) Anterior planar static images acquired 10 min (on the left) and 2 h (on the right) after injection of ^{99m}Tc-tilmanocept in a patient with a melanoma in the right shoulder showing rapid drainage to two sentinel nodes. Volume rendered SPECT-CT (bottom) shows the sentinel nodes respectively in the right axilla and supraclavicular area. A second echelon node with markedly less uptake accompanies this latter node. At histopathology, isolated tumour cells were found in the supraclavicular SN. The axillary SN resulted tumour negative.

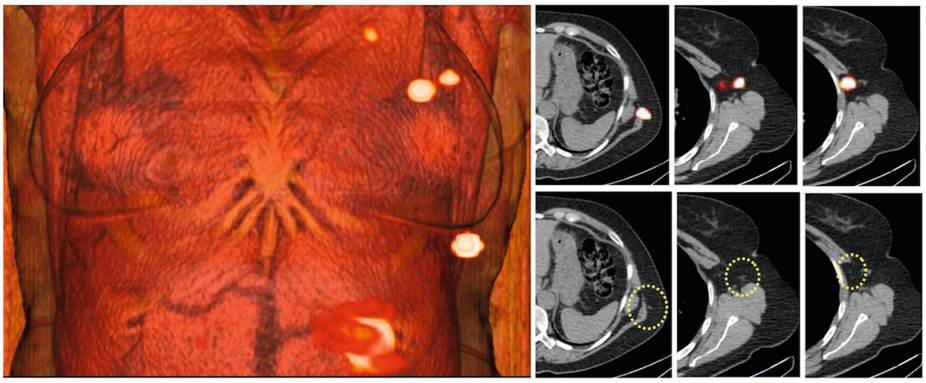

Figure 3. SPECT-CT acquired 2 h after injection of ^{99m}Tc-tilmanocept in a patient with a melanoma in the left side of the trunk. Volume rendered (on the left) shows one sentinel node in the left side of the trunk and two sentinel nodes in left axilla. Cross-sectional fused SPECT-CT slices (upper row) show the lower sentinel node in the subcutaneous space of the left side whereas both axillary sentinel nodes are located in level I. Note on CT (lower row) that none of the sentinel nodes (circles) is enlarged. At histopathology, sentinel node micrometastases were found in both basins.

However, further head-to-head comparison of ^{99m}Tc-tilmanocept with standard SN radiotracers in larger series of patients is necessary to definitively assess the potential superiority of this next generation radiotracer. This is particularly relevant for malignancies with complex lymphatic drainage and/or draining first-tier lymph nodes located in the proximity of primary lesions.

Table 1. Clinical characteristics and imaging findings. SN = sentinel node; IS = injection site; np = not possible; mi = micrometastases; itc = isolated tumour cells.

Patient (gender, age)	Primary Lesion Site	Basin	SN	Non-SN	2-hour IS/SN	Δ IS/SN	SN/non-SN at 2 hours	SNs at pathology
1 (F, 57y)	R-breast	R-axilla	1	3	13.4	-82%	4.8	Negative
	L-breast	L-axilla	2	1	5.4	-57%	7.1	Negative
2 (F, 50y)	L-breast	L-axilla	3	0	44.3	-62%	n.p.	Negative
3 (F, 61y)	R-breast	R-axilla	1	0	141	-41%	n.p	Negative
4 (F, 69y)	L-breast	L-axilla	1	1	9.5	-67%	15.6	Negative
5 (F, 69y)	R-breast	R-axilla	1	1	17.7	-96%	5.9	Negative
6 (F, 45y)	R-breast	R-axilla	1	0	10.3	-50%	5.9	Positive (mi)
7 (F, 58y)	L-breast	L-axilla	1	0	116	-75%	4.3	Negative
8 (F, 74y)	L-breast	L-axilla	1	0	29.3	-82%	n.p.	Negative
9 (F, 47y)	R-breast	R-axilla	1	0	81	-69%	n.p.	Negative
10 (F, 49y)	R-breast	R-axilla	1	1	28	-82%	2.3	Positive (mi)
11 (F, 66y)	L-breast	L-axilla	1	0	72.6	-87%	n.p.	Negative
12 (F, 74y)	L-breast	L-axilla	2	0	14.1	-87%	n.p.	Negative
13 (F, 49y)	R-breast	R-axilla	1	0	1.9	n.p.	n.p.	Negative
14 (F, 58y)	L-leg	L-groin	2	3	n.p.	n.p.	15.1	Negative
15 (M, 62y)	R-side back	R-axilla	1	0	2.6	-48%	n.p.	Negative
16 (F, 56y)	L-side trunk	L-trunk	1	0	12.1	-68%	n.p.	Positive (mi)
		L-axilla	2	1	34.8	-87%	15.4	Positive (mi)

Table 1. Continued

Patient (gender, age)	Primary Lesion Site	Basin	SN	Non-SN	2-hour IS/SN	Δ IS/SN	SN/non-SN at 2 hours	SNs at pathology
17 (F, 74y)	R-leg	R-groin	2	2	n.p.	n.p.	4.2	Negative
18 (F, 81y)	L-leg	L-groin	1	4	67.2	-19%	3	Negative
19 (M, 48y)	R-side back	R-axilla	1	1	35.2	-84%	4.5	Negative
20 (M, 67y)	R-upper abdomen	R-axilla	1	2	23.7	-68%	4.4	Negative
		R-aureolar	1	0	24.6	-15%	n.p.	Negative
		L-axilla	1	0	197.8	-80%	n.p.	Negative
		R-groin	1	0	32.3	-92%	n.p	Negative
21 (F, 78y)	L-side trunk	L-axilla	2	0	14	-47%	n.p.	Positive (mi)
22 (M, 63y)	L-leg	L-groin	3	2	7.2	-89%	5.9	Negative
23 (F, 62y)	L-leg	L-groin	3	2	n.p.	n.p.	4.7	Negative
24 (M, 65y)	R-shoulder	R-clavicular	1	1	31.7	-76%	3.6	Positive (itc)
		R-axilla	1	0	n.p.	n.p.	n.p.	Negative
25 (F, 71y)	R-leg	R-groin	2	3	n.p.	n.p.	4.4	Negative
26 (F, 71y)	L-arm	L-axilla	2	0	276	n.p.	n.p.	Negative
27 (M, 57y)	R-arm	R-axilla	2	1	31.2	-41%	8	Negative
28 (F, 56y)	L-back	L-axilla	1	0	29.9	-44%	n.p.	Positive (mi)
N=28	N=29	N=34 basins	N=49 SN	N=16 basins	N=29 basins	N=29 basins	N=18	SN Positive = 7/34 basins
Mean age=62y				N=29 non-SN	Max 276	Max -96	Max=15.6	(20%)
Range=45-81y					Min 1.9	Min -15	Min=2.3	
					Mean 48,4	Mean-66	Mean=6.6	

Conclusion

^{99m}Tc-tilmanocept appears to meet the requirements for improved SN imaging in breast cancer and melanoma on the basis of early and persistent SN visualization frequently accompanied by no or markedly less non-SN uptake. This is associated to rapid migration from the injection site together with increasing SN uptake and retention as expressed by decreasing IS/SN and persistently high SN/non-SN ratios. Further head-to-head comparison of ^{99m}Tc-tilmanocept with standard SN radiotracers in larger series of patients is necessary.

Acknowledgement

Tilmanocept was provided by SpePharm A.G. - part of the Norgine Group of companies, Amsterdam, The Netherlands. The tracer was provided free of charge and this support came without restrictions.

References

1. JR. The use of protein-based radiocolloids in sentinel node localization. Clin Transl Imaging. 2015;3:179–86.
2. Vidal-Sicart S, Vera DR, Valdés Olmos RA. Next generation of radiotracers for sentinel lymph node biopsy: what is still necessary to establish new imaging paradigms? Rev Esp Med Nucl Imagen Mol. 2018;37:373–9.
3. Silvestri C, Christopher A, Intenzo C, Kairys JC, Kim S, Willis A, et al. Consecutive series of melanoma sentinel node biopsy for Lymphoseek compared to sulfur colloids. J Surg Res. 2019;233:149–53.
4. Unkart JT, Proudfoot J, Wallace AM. Outcomes of "one-day" vs "two-day" injec- tion protocols using Tc-99m tilmanocept for sentinel lymph node biopsy in breast cancer. Breast J. 2018;24:526–30.
5. Agrawal A, Civantos FJ, Brumund KT, Chepeha DB, Hall NC, Carrol WR, et al. (99m) Tilmanocept accurately detects sentinel lymph nodes and predicts node pathology status in patients with oral squamous cell carcinoma of the head and neck: results of a phase III multi-institutional trial. Ann Surg Oncol. 2015;22:3708–15.
6. Tokin CA, Cope FO, Metz WL, Blue MS, Potter BM, Abbruzzese BC, et al. The efficacy of Tilmanocept in sentinel lymph node mapping and identification in breast cancer patients: a comparative review and meta-analysis of the 99m Tc- labeled nanocolloid human serum albumin standard of care. Clin Exp Metastasis. 2012;29:681–6.
7. Lamichhane N, Shen KW, Li CL, Han QX, Zhang YJ, Shao ZM, et al. Sentinel lymph node biopsy in breast cancer patients after overnight migration of radiolabelled sulphur colloid. Postgrad Med J. 2004;80:546–50.
8. Engering AJ, Cella M, Fluitsma D, Brockhaus M, Hoefsmit EC, Lanzavecchia A, et al. The mannose receptor functions as a high capacity and broad speci-ficity antigen receptor in human dendritic cells. Eur J Immunol. 1997;27: 2417–25.
9. Giammarile F, Schilling C, Gnanasegaran G, Bal C, Oyen WJG, Rubello D, et al. The EANM practical guidelines for sentinel lymph node localisation in oral cavity squamous cell carcinoma. Eur J Nucl Med Mol Imaging. 2019;46:623–37.
10. Unkart JT, Hosseini A, Wallace AM. Tc-99m Tilmanocept versus Tc-99m sul- fur colloid in breast cancer sentinel lymph node identification: results from a randomized, blinded clinical trial. Randomized Controlled Trial J Surg Oncol. 2017;116:819–23.
11. Khandekar S, Neumann D, Amin K, DiFilippo F. Comparison of Tc 99m- tilmanocept and filtered Tc 99m-sulfur colloid for breast lymphatic mapping.J Nucl Med. 2014;55:2522.

5

Evaluation of the Hybrid Tracer Indocyanine Green–^{99m}Tc-Nanocolloid for Sentinel Node Biopsy in Bladder Cancer

A Prospective Pilot Study

Adapted from:
Daphne D.D. Rietbergen, Erik J. van Gennep, Gijs H. KleinJan, Maarten Donswijk, Renato A. Valdés Olmos, Bas W. van Rhijn, Henk G. van der Poel, Fijs W.B. van Leeuwen.

Clin Nucl Med. 2022; 47: 774–780

Abstract

Introduction and objectives: In muscle-invasive bladder cancer (MIBC), lymph node invasion has proven to be an independent predictor of disease recurrence and cancer-specific survival. We evaluated the feasibility of targeting the sentinel node (SN) for biopsy in MIBC patients using the hybrid tracer indocyanine green (ICG)–^{99m}Tc-nanocolloid for simultaneous radioguidance and fluorescence guidance.

Materials and methods: Twenty histologically confirmed cN0M0 MIBC patients (mean age, 63.3 years; range, 30–82 years), scheduled for radical cystectomy with SN biopsy and extended pelvic lymph node dissection (ePLND), were prospectively included. Twelve patients were operated on following neoadjuvant chemo- therapy. The patients received lymphoscintigraphy as well as SPECT/CT after 4 transurethral injections of ICG-^{99m}Tc-nanocolloid (mean, 208 MBq; range, 172–229 MBq) around the tumor/scar in the detrusor muscle of the bladder on the day before radical cystectomy. Sentinel node resection was performed un- der radioguidance and fluorescence guidance.

Results: Nineteen patients could be analyzed. On preoperative imaging, SNs could be identified in 10 patients (53%; mean, 1.6 SN/patient), which revealed drainage pathways outside the ePLND in 20% of the patients. Interesting to note is that 2 patients (10%) with preoperative nonvisualization displayed fluorescent and radioactive SNs during surgery. Location of the primary tumor near the left lateral side of the bladder seemed to be a factor for nonvisualization. Nodal harvesting with ePLND varied among patients (mean, 23.3). Histopathology confirmed tumor-positive nodes in 4 (21%) of all patients. In the 2 patients where an SN could be identified, the ePLND specimens were tumor-negative. All patients with tumor-positive nodes had advanced disease (stage III).

Conclusion: Sentinel node biopsy in bladder cancer using the hybrid tracer ICG-^{99m}Tc-nanocolloid is feasible, and preoperative imaging is predictive for the ability to perform SN biopsy in 83% of the patients who displayed an SN. In patients with a successful preoperative SN mapping using lymphoscintigraphy and SPECT/CT, the intraoperative SN guidance and detection were effective, even outside the ePLND area. As such, this study underscores the critical role that preoperative imaging plays in challenging image-guided surgery applications.

Introduction

Bladder cancer is the seventh most diagnosed cancer in the male population worldwide and the 11th considering both sexes.[1] In the Netherlands, almost 5000 patients are diagnosed with bladder cancer each year, which leads to more than 1200 deaths per year.[2] Because of risk factors (e.g., smoking, exposure to toxins, chronic irritation of the bladder), diagnostic strategies, and available treatment options, the incidence and treatment outcomes vary worldwide.[3] For bladder cancer, lymph node invasion is an independent predictor and prognostic factor for disease recurrence and cancer-specific survival.[4] Radical cystectomy (RC) is the treatment of choice for many patients with muscle-invasive bladder cancer (MIBC). This includes, according to the guidelines, a bilateral extended pelvic lymph node dissection (ePLND).[5–7] Surgical planning for MIBC is mostly based on contrast-enhanced CT (CeCT) images of the abdominal and pelvic area. Unfortunately, this radiologic form of diagnostic imaging is limited in its capability to identify microscopic lymphatic spread. Because of the surrogate rule of the short axis on CeCT, CeCT can result in very low sensitivities (5%–54%) for the detection of nodal metastases.[8,9] Approximately 25% of the cN0M0 MIBC patients who underwent an RC combined with ePLND have histopathologically proven metastatic lymph nodes,[10] whereas preoperative CeCT fails to detect these nodal metastases in one-third of the patients. This suggests there is a discrepancy between the nodal status at presurgical staging and the metastatic lymph node burden seen in surgical samples. The molecular imaging modality ^{18}F-FDG PET is becoming of more incremental value relevant in staging and recurrence disease because of the higher sensitivity compared with CeCT.[11]

An ePLND can increase the regional disease control but comes with increased comorbidities (e.g., vascular, ureteral and nerve injury, lymphocele, thromboembolic events) and will miss nodal metastases outside the resection template. Sentinel node (SN) biopsy can provide a less invasive and more personalized lymph node (LN) dissection. The SNs that usually are the first site of tumor seeding, preceding systemic spreading,[12–17] can be preoperatively identified by mapping-via lymphoscintigraphy and SPECT/CT-the drainage profile of a radiocolloid. This procedure was initially described for bladder cancer by Sherif et al.[12] Intraoperative SN identification was realized by complementing the preoperative imaging roadmap with the use of gamma probe to identify the radiocolloids. Alternative means for intraoperative SN identification have been pursued using blue dye and/or the fluorescence dye indocyanine green (ICG).[12–24]

In the present study, we have used the hybrid tracer ICG-^{99m}Tc-nanocolloid in patients with MIBC who underwent RC with or without neoadjuvant chemotherapy (NAC). This hybrid tracer has successfully been used for SN biopsy in various malignancies[25] but, so far, remained undocumented in bladder cancer. To establish its feasibility,

we compared the results of the preoperative SPECT/CT-based SN mapping with the intraoperative SN identification using complementary radioguidance and fluorescence guidance.

Materials and Methods

Patient Demographics

This prospective trial was registered at the Netherlands Trial Register as NL48901.031.14 and was executed at the Netherlands Cancer Institute–Antoni van Leeuwenhoek Hospital after approval of the Medical Ethical Review Board of the institution (M14HSN). Patients with histologically confirmed MIBC or high-risk patients (carcinoma in situ) were scheduled for SN biopsy before RC combined with ePLND. Patients were preoperatively staged using CT– intravenous urogram and ^{18}F-FDG PET for imaging and underwent transurethral tumor resection. Half of these patients received NAC. All patients were prospectively included after informed consent. The main exclusion criteria were suspected nodal disease on imaging and prior pelvic radiation and/or surgery.

SN Imaging Procedure

All patients followed a 2-day SN procedure. On the day before surgery, a volume of 2 mL containing 208 MBq (SD, 15.8; 5.6 mCi) ICG-^{99m}Tc-nanocolloid (GE Healthcare, Leiderdorp, the Netherlands) was injected in 4 transurethral injections into the detrusor muscle of the bladder, around the tumor or transurethral re- section scar, under cystoscopic guidance using an endoscopic needle (Injetak; Laborie) with a 5-mm tip length. Lymphatic drainage was mapped based on early and delayed static lymphoscintigraphy (15 minutes and 2 hours postinjection) as well as SPECT/CT (2 hours postinjection) using a dual-head SPECT/CT gamma camera (Symbia T6; Siemens, Erlangen, Germany) equipped with a 6-row CT scanner. SPECT parameters were as follows: 128 x 128 matrix, zoom of 1.0, and 180-degree rotation with 20 views per head (30 sec- onds per view). CT (130 keV, 40 mAs, B30s kernel, 2-mm axial re- construction) was used for attenuation correction and anatomical localization. Multiplanar reconstruction, image fusion, and 3D image reconstruction of the SPECT/CT images were done using an Osirix software program (Pixmeo SARL, Bernex, Switzerland). Planar and SPECT/CT images were evaluated with respect to drainage to lymph node basins, SN visualization, and non-SN uptake and their corresponding anatomical localizations. Nodes were considered as SN when visualized as intense focal uptake on the early, delayed images and/or SPECT, with increase in uptake in time. When SNs were visualized, SPECT/CT images were used to indicate their anatomical location in relation to muscles and vessels in the draining lymph node basins. A flowchart of the study setup and a graphic image of the bladder with its corresponding anatomical zones are presented in Figure 1 and Figure 2, respectively.

Surgical Guidance

The day following tracer administration and imaging, the patient was operated on using DaVinci Surgical Robotic System (Intuitive Surgical, Sunnyvale, Calif) or underwent an open RC. The SNs were intraoperatively identified under combined radioguidance and fluorescence guidance using a laparoscopic gamma probe (Neoprobe; Johnson & Johnson Medical, Hamburg, Germany) and an integrated fluorescence camera (Firefly) in robotic surgery; a traditional gamma probe (Europrobe; Eurorad, Strasbourg, France) and FIS-00 Hamamatsu camera (Hamamatsu Photonics K.K., Hamamatsu, Japan) were used in open setting. Excised samples were also examined ex vivo by using the FIS-00 Hamamatsu camera.

Pathology

All surgically removed nodes (SNs and non-SNs in separate packages) were histopathologically examined for tumor cells by the pathologist. Micrometastases were defined as lesions smaller than 2 mm and macrometastases as lesions larger than 2 mm, whereas conglomerates of isolated tumor cells smaller than 0.2 mm were denoted as submicrometastases.

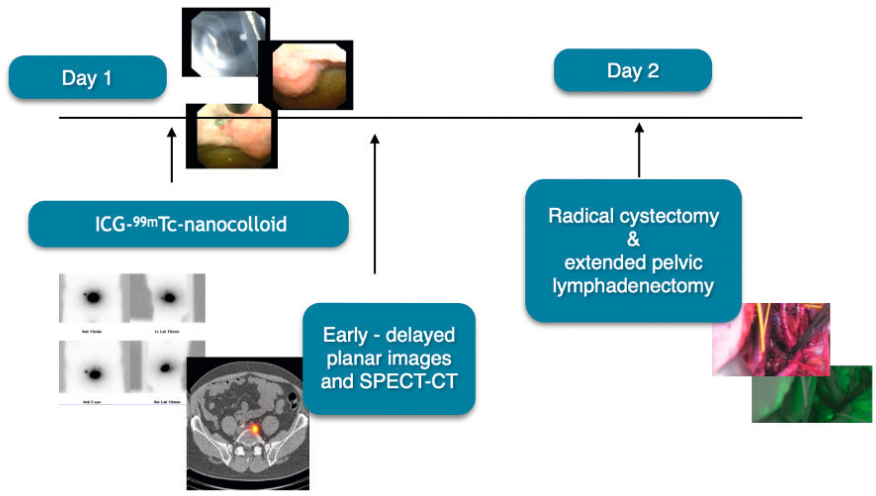

Figure 1. Flowchart of the study design. On the first day, 208 MBq (SD, 15.8; 5.6 mCi) ICG-^{99m}Tc-nanocolloid was injected in 4 to 6 transurethral injections into the detrusor muscle of the bladder; around the tumor, divided over the bladder. The procedure took place under cystoscopic guidance using an endoscopic needle. Lymphatic drainage was mapped using early and delayed static lymphoscintigraphy (15 minutes and 2 hours postinjection) and SPECT/CT (2 hours postinjection). On the second day, the patient was operated during open or robotic (DaVinci) procedure. The SNs were intraoperatively identified under combined radioguidance and fluorescence guidance using a (laparoscopic) gamma probe and fluorescence camera (Firefly or Hamamatsu for robotic and open surgery, respectively).

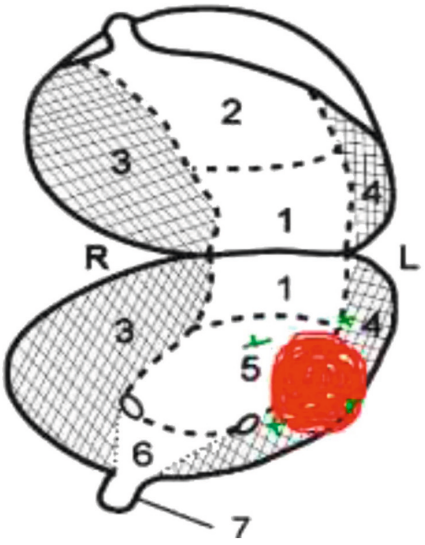

Figure 2. Graphic image of the bladder with its corresponding zones (1. dorsal part, 2. apex vesicae, 3. base, 4. left lateral border, 5. right lateral border, 6. trigonum vesicae). Red dot corresponds with the location of the tumor in this particular case; the surrounding green crosses correspond with the tracer injection site.

Table 1. Schematic overview of the results. Of the 20 patients which were included, 19 patients could be evaluated. In 52,6% (N=10 patients) lymphoscintigraphy (SPECT/CT) reveals at least 1 SLN. Of those patients (visualized SLN), six patients revealed one SLN (60%), in 3 patients two SLN were seen (30%) and in one patient 4 SLN were seen. During surgery all except one marked SLNs were seen. Histopathology positive nodes containing metastases were seen in four patients (21%), and in 8 patients, these nodes were without metastases. In 9 patients (47,4%), a non-visualization was seen on preoperative imaging, in some cases (3/9) the surgeon could find a lymph node during surgery and in six out of nine patients the surgeon did find a lymph node either. Pathology of the lymph nodes did not reveal any metastasized disease. Primary side R = right, L = left; 1= dorsal, 2 = apex vesicae, 3 = base, 4 = left lateral border, 5 = right lateral border.

Patient (Gender, age)	Primary lesion site and region	Surgery	NAC/ NAC-naive	SLN SPECT/ CT	Side	Non-SN	Basin	lymph node OR	ePLND number nodes	T at pathology	Nodes at pathology
1 (F, 82y)	R, 3	O	no-NAC	1	R	0	obt	1	39	3b	Positive
2 (M, 55y)	L, 5	R	NAC	1 1	R L	0	obt ext	3	13	3a	Positive
3 (M, 77y)	L, 4	R	no-NAC	0	-	0	-	0	16	2	Negative
4 (M, 47y)	R, 3	R	NAC	1	R	0	obt	8	40	0	Negative
5 (M, 56y)	L, 5	O	NAC	0	-	0	-	6	15	3b	Positive
6 (M, 74y)	L, 4	O	NAC	1	L	0	obt	0	10	CIS	Negative
7 (F, 72y)	L, 2-4	R	no-NAC	0	-	0	-	0	9	CIS	Negative
8 M, 42y)	L, 4	R	NAC	0	-	0	-	0	19	0	Negative
9 (M, 64y)	R, 1-3	R	NAC	1 1	R L	1	obt ext	7	17	2b	Negative
10 (M, 73y)	L, 1-4	O	NAC	0	-	0	-	0	41	3a	Negative
11 (M, 70y)	L, 4	R	NAC	0	-	0	-	0	29	CIS	Negative

Table 1. Continued

Patient (Gender, age)	Primary lesion site and region	Surgery	NAC/ NAC-naive	SLN SPECT/ CT	Side	Non-SN	Basin	lymph node OR	ePLND number nodes	T at pathology	Nodes at pathology
12 (M, 79y)	L, 4	R	no-NAC	0	-	0	-	1	22	2b	Negative
13 (F, 30y)	R, 2	O	NAC	3 1	R L	3	ext(2x), obt obt	2	31	0	Negative
14 (M, 58y)	L, 4-5	R	NAC	1	L	0	com	1	32	CIS	Negative
15 (M, 62y)	L, 3-5	O	no-NAC	0	-	0	-	1	29	1	Negative
16 (M, 82y)	R, 2-3	O	no-NAC	1	R	0	com/ aor	2	21	1	Negative
18 (F, 49y)	R, 3	R	no-NAC	1	R	0	obt	1	11	CIS	Negative
19 (M, 60y)	L, 4	R	NAC	0	-	0	-	0	33	3b	Positive
20 (M, 71y)	L, 4	R	NAC	1 1	R L	0	com com	3	15	3a	Negative
N=19 Mean age=63y Range=30-82y				N=16 SN		N= 4 non-SN	N=15 basins				SN Positive= 4/19 patients. (21%)

Surgery O = open, R = robotic; NAC = Neo-adjuvant chemotherapy, noNAC = NAC naive patients. CIS = carcinoma in situ. Basin Obt = obturator, com = communic iliac artery, ext = extern iliac artery.

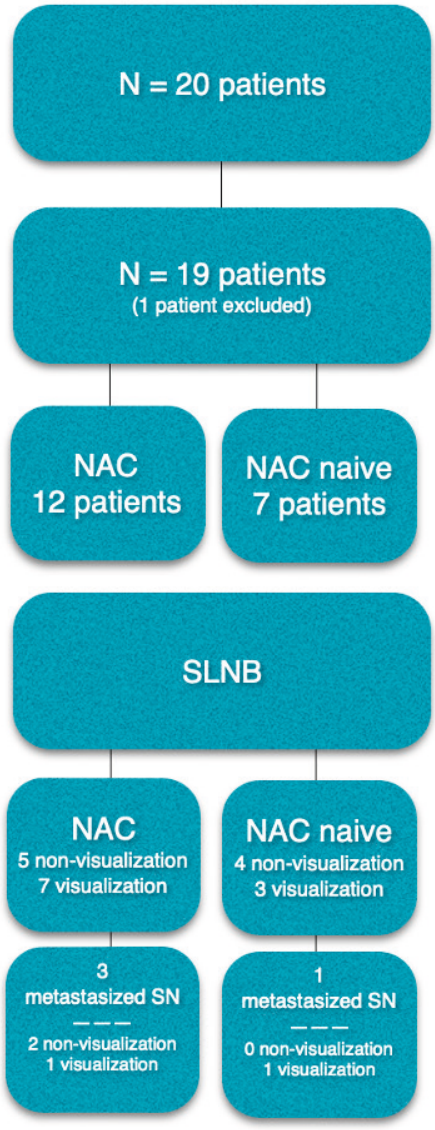

Figure 3. Flowchart of the study, which included 20 patients. One patient was operated in another hospital and had to be excluded from analysis, resulting in a group of 19 patients analyzed. Twelve patients in the NAC group and 7 patients in the NAC-naive group. All patients underwent an SN procedure.

Results

Twenty patients (mean age, 63.3 years; range, 30–82 years) were included for the preoperative SN procedure. One patient was operated on in another hospital and was excluded from analysis. In total, 19 patients were evaluated. Patient characteristics are displayed in Table 1. Twelve patients (63%) were pretreated with NAC, and 7 (37%) patients did not receive treatment before surgery. Seven patients underwent an open RC, and 12 patients were operated on using DaVinci Surgical robot.

Sentinel Nodes

In 53% (n = 10 patients; 7 in the NAC group and 3 in the NAC-naive group), lymphoscintigraphy and SPECT/CT revealed SN(s). A single SN was found in 6 patients (60%), whereas 2 SNs could be identified in 3 patients (30%), and in 1 patient, 4 SNs were observed (10%) in 1 patient. In the remaining 47% of the cases (n = 9 patients; 5 patients in the NAC group and 4 patients in the NAC-naive group, respectively), no SNs could be visualized before surgery. A flowchart of the study setup is presented in Figure 3.

In 9 of the 10 patients with SNs at preoperative imaging, in total 16 SNs could be resected by complementing the preoperative imaging roadmap with intraoperative radioguidance and fluorescence guidance. In 1 robot-operated patient with early-stage tumor of the left lateral border of the bladder, the SN could not be identified during surgery, and ePLND also did not reveal any metastatic disease. The number of additional nodes that were resected during ePLND varied among patients (mean, 23.3; range, 9–41). In the 9 patients without SN visualization on preoperative imaging, 2 radioactive or fluorescent nodes were detected during surgery. This means that overall intraoperative SN guidance was successful in 63% of the patients.

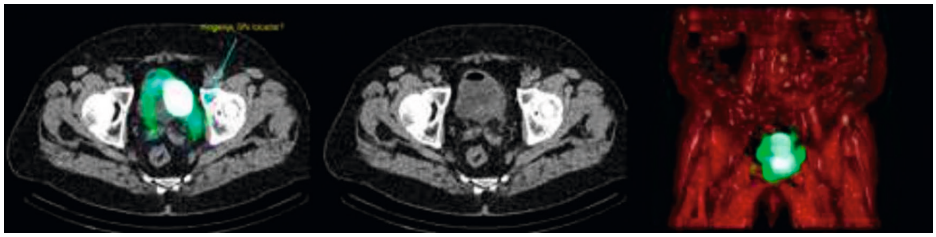

Figure 4. A blurry image is seen without an obvious focus or enlarged lymph node on SPECT/CT images, shine-through phenomena with nonvisualization of the SN, where the injection site shines through and could outshine possible SN nearby. This could lead to false-negative findings.

Relation Between Primary Tumor Location and Preoperative SN Visualization

For tumors located in the base or apex of the bladder, 100% SN visualization was obtained (Figure 4). Of the patients displaying nonvisualization on preoperative lymphoscintigraphy, in 56% the primary tumor was located at the left lateral side (n=5).

The tumors of the 2 patients with preoperative nonvisualization and a positive SN detection during surgery were located at the right side and base/right lateral border, respectively. Other sides with nonvisualization as a result corresponded with apex/left lateral (n = 1), dorsal/left lateral (n = 1), base/right lateral (n = 1), and right lateral border (n = 1).

Location of SNs in Relation to ePLND Template

Of the visualized SNs, 80% were found within the ePLND template, 53% in the obturator fossa and 27% at the external iliac artery (Figures 5-6). In 3 patients (20%), SNs were found outside the ePLND template and 1 aberrant SN localization above the ureteroiliac vessels crossing and the others along the common iliac artery or aorta (Figure 7). Bilateral drainage was seen in 40% of the patients with preoperative imaging. In the remaining 60% of the patients, including the only midline tumor, unilateral draining was observed.

Histopathology

In total, 4 of the 19 patients' (21%) histopathology showed lymph node metastases: 2 in the visualization and 2 in the nonvisualization group, respectively. All tumor-positive nodes, either seen in SN or ePLND material, concerned advanced disease (Figure 3 and Table 1). In all cases with SN visualization on preoperative imaging, the ePLND specimens were tumor-negative, where the SN was the only localization that contained metastatic disease. No additional (micro)metastatic disease was seen in patients with <pT3 tumor(s). In the nonvisualization group, 2 patients (NAC group) had a tumor-positive node in their ePLND specimens, both concerning locally advanced pT3–4 disease.

Neoadjuvant Chemotherapy

Patients pretreated with NAC showed less nonvisualization on preoperative scintigraphy. On the other hand, those patients were more involved in metastasized nodal disease: 3 patients versus 1 patient in the NAC-naive group.

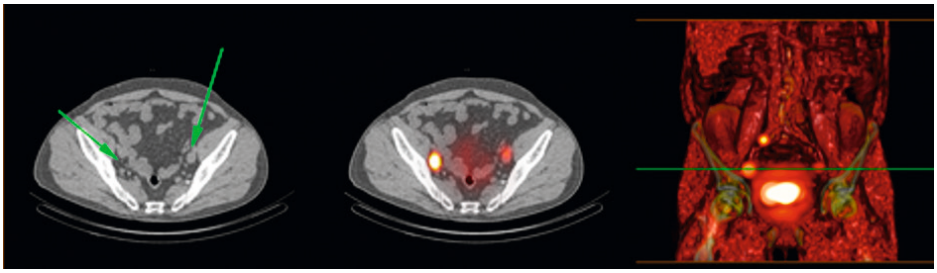

Figure 5. On the left, CT image of the same area revealed no pathologic enlarged lymph node at the right side (arrow right). At the left side, an enlarged lymph node is seen (arrow left). In the middle, transaxial fused SPECT/CT image of lymphatic drainage with SN seen along the iliac artery at both sides. On the right, volume-rendered fusion image of both scintigraphy SPECT and CT is seen with focal uptake in the SN along the right iliac artery. At the left side, a contralateral SLN is seen (crossover phenomenon). At the right side, a higher echelon node is seen along the common iliac artery.

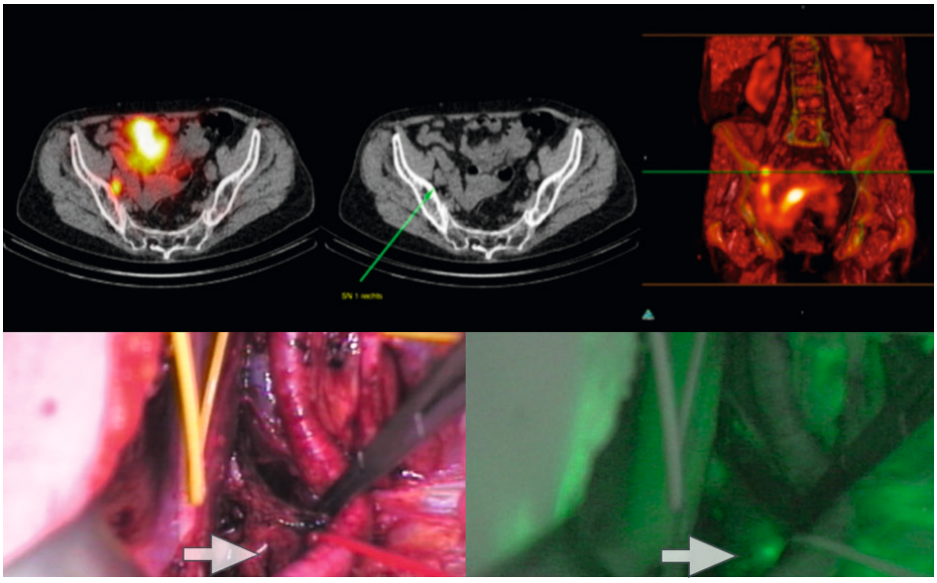

Figure 6. Upper row: Fused SPECT/CT, CT, and volume-rendered fusion image SPECT. Fused images show a focal radioactive signal in the right obturator foramen, marked as the SN. The green arrow on CT shows the corresponding nonenlarged lymph node. Lower row: left: Intraoperative view with white light. Right: view of the fluorescent camera. White arrow shows focal ICG uptake and the corresponding lymph node, the SN.

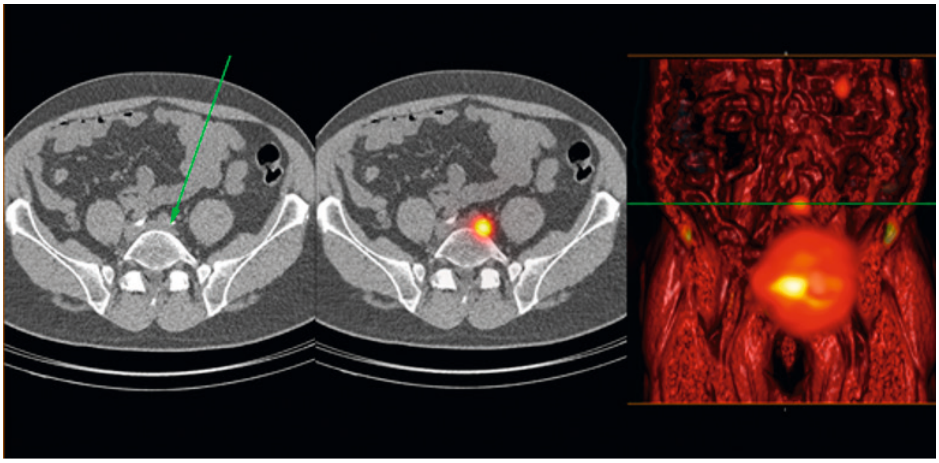

Figure 7. In the middle, transaxial fused SPECT/CT image of lymphatic drainage with SN seen above the normal ePLND area, in the aortic region. On the left, CT image of the same areas revealed a no pathologic enlarged lymph node (arrow). On the right, volume-rendered fusion image of both scintigraphy SPECT and CT.

Discussion

In this pilot study, we demonstrated the feasibility of the hybrid tracer ICG-^{99m}Tc-nanocolloid for SN biopsy in clinical node-negative (cN0) MIBC patients scheduled for RC with ePLND. In 53% of the patients, the preoperative SN procedure was successful. Despite having a preoperative nonvisualization, an additional 10% of the patients displayed an SN during surgery. This means that overall preoperative imaging roadmaps were predictive for the utility of image guidance in 63% of the patients who displayed an SN. The degree of lymphatic drainage of the bladder seemed to be influenced by the location of the primary tumor, and unpredictable drainage and drainage outside the ePLND template were seen in 20%.

Previous studies have explored the feasibility of SN mapping in bladder cancer patients using radioactive colloid, blue, and fluorescent dyes as separated modalities.[13–21] Unfortunately, most studies are based on relatively small patient groups. The studies are also not mutually comparable to ours because of differences in the injection technique and type of tracer that was used. Besides that, there is also a difference in the implementation of preoperative imaging data and the type of intraoperative imaging modalities used. From a surgical perspective, optical SN identification is considered highly desirable. This can be realized using, for example, blue dye or “free” ICG. Relying on such optical agents only for guidance, however, means that the procedure cannot receive guidance via preoperative imaging roadmaps. Also, as a result of their molecular size, these lymphangiographic

agents facilitate more rapid drainage in comparison to radiocolloids, but lack SN specificity.[26,27] In line with this, studies relying solely on free ICG reported higher numbers of SN compared with the 1.6 SN per patient reported by us.[15] This difference in flow rates has also an impact on bilateral drainage patterns. We saw a bilateral drainage in 40% of the patients with preoperative imaging, which is in line with the literature of radiocolloid-based SN localization.[14] However, studies using only free ICG reported a much higher bilateral drainage pattern (90%). Arguing that in pur- suit of precision surgery "less is more," one can argue that use of lymphangiographic rather than SN-specific agents means the procedure drifts away from its original minimally invasive concept. Using hybrid tracers such as ICG-^{99m}Tc-nanocolloid intraoperative optical imaging can be combined with SN specificity and preoperative imaging.[25,28–31]

In our study, the preoperative SN visualization rate on a per-patient basis was 53%, although lower than other SN applications, this value is in line with the 23% to 94% range described in the literature.[12–17] As seen in the study by Liedberg et al,[18] omitting the preoperative imaging, the percentage of SN identification dropped to 23%. We found that preoperative nonvisualization was highly related to the chance of intraoperative SN identification. Intraoperative detection rate of preoperatively defined SN using the gamma probe in our study was 90%, which was in line with the reported 81% to 100% in the literature.[13,14,16,18–21] Using fluorescence imaging only, we could detect 58%, which was in the high end if compared with the detection percentages reported for use of ICG only (0%–90%).[22–24]

Histopathology-confirmed tumor-positive SNs were seen in 21% of the total population, which is in line with earlier findings in the literature, although Polom et al[14] reported 34% nodal metastases in their resected SNs. In the study by Polom et al,[14] 6.4% of the SNs were seen outside the PLND area. The radiotracer study by Liedberg et al[18] found more than 40% outside the obturator foramen. In our study, unexpected localizations were found in 20% and concerned mostly patients from the NAC group (66%), independent of tumor stage, indicating that the neoadjuvant treatment could alter lymphatic drainage.

The current study is limited by the sample size, heterogeneity between patients, and lack of outcome data. Also, the SN nonvisualization rate of 47% reported by us and others represents a serious limitation concerning the added value of SN in MIBC. This suggests that there is room for improvement concerning the ability to induce lymphatic tracer drainage from primary bladder cancer. Hence, a more extensive research based on a more homogenous group of patients is needed to show whether SN biopsy adds clinical value by staging the pelvis in bladder cancer. Interestingly, correlating the location of the primary tumor and injection side and the ability of successful SN procedure revealed a higher nonvisualization in the

tumors located at the left lateral border compared with other localizations. Future studies need to focus on methodological aspects related to bladder pressure,[14,22] stimulation of lymphatic flow, and standardization of injection techniques[32] to increase SN visualization rates.

Conclusion

In cN0M0 MIBC patients, the SN procedure using ICG-^{99m}Tc-nanocolloid seems feasible with SN visualization in 63% of the patients (53% preoperative and 58% intraoperative). In patients with a successful preoperative SN mapping using lymphoscintigraphy and SPECT/CT, the intraoperative SN guidance and detection were effective, even outside the ePLND area.

References

1. Witjes JA, Bruins HM, Cathomas R, et al. European Association of Urology guidelines on muscle-invasive and metastatic bladder cancer: summary of the 2020 guidelines. *Eur Urol*. 2021;79:82–104.
2. Nederlandse Kankerregistratie (NKR), IKNL. Received on iknl.nl/nkr- cijfers. September 2021. Available at: https://www.iknl.nl/kankersoorten/ blaaskanker. Accessed April 2022.
3. Wong MCS, Fung FDH, Leung C, et al. The global epidemiology of bladder cancer: a joinpoint regression analysis of its incidence and mortality trends and projection. *Sci Rep*. 2018;8:1129.
4. Leissner J, Koeppen C, Wolf HK. Prognostic significance of vascular and perineural invasion in urothelial bladder cancer treated with radical cystec- tomy. *J Urol*. 2003;169:955–960.
5. Abdollah F, Gandaglia G, Thuret R, et al. Incidence, survival and mortality rates of stage-specific bladder cancer in United States: a trend analysis. *Can- cer Epidemiol*. 2013;37:219–225.
6. Cumberbatch MGK, Jubber I, Black PC, et al. Epidemiology of bladder can- cer: a systematic review and contemporary update of risk factors in 2018. *Eur Urol*. 2018;74:784–795.
7. Fernández MI, Brausi M, Clark PE, et al. Epidemiology, prevention, screen- ing, diagnosis, and evaluation: update of the ICUD-SIU joint consultation on bladder cancer. *World J Urol*. 2019;37:3–13.
8. Paik ML, Scolieri MJ, Brown SL, et al. Limitations of computerized tomog- raphy in staging invasive bladder cancer before radical cystectomy. *J Urol*. 2000;163:1693–1696.
9. Tritschler S, Mosler C, Straub J, et al. Staging of muscle-invasive bladder cancer: can computerized tomography help us to decide on local treatment? *World J Urol*. 2012;30:827–831.
10. Woods ME, Ouwenga M, Quek ML. The role of pelvic lymphadenectomy in the management of prostate and bladder cancer. *ScientificWorldJournal*. 2007;7:789–799.
11. Einerhand SMH, van Gennep EJ, Mertens LS, et al. ^{18}F-fluoro-2-deoxy-D- glucose positron emission tomography/computed tomography in muscle-invasive bladder cancer. *Curr Opin Urol*. 2020;30:654–664.
12. Sherif A, de la Torre M, Malmström PU, et al. Lymphatic mapping and detection of sentinel nodes in patients with bladder cancer. *J Urol*. 2001;166:812–815.
13. Sherif A, Garske U, de la Torre M, et al. Hybrid SPECT-CT: an additional technique for sentinel node detection of patients with invasive bladder can- cer. *Eur Urol*. 2006;50:83–91.
14. Polom W, Markuszewski M, Cytawa W, et al. Radio-guided lymph node mapping in bladder cancer using SPECT/CT and intraoperative γ-probe Methods. *Clin Nucl Med*. 2016;41:e362–e367.
15. Polom W, Markuszewski M, Cytawa W, et al. Fluorescent versus radioguided lymph node mapping in bladder cancer. *Clin Genitourin Cancer*. 2017;15: e405–e409.
16. Marits P, Karlsson M, Sherif A, et al. Detection of immune responses against urinary bladder cancer in sentinel lymph nodes. *Eur Urol*. 2006;49:59–70.
17. Malmström PU, Ren ZP, Sherif A, et al. Early metastatic progression of blad- der carcinoma: molecular profile of primary tumor and sentinel lymph node. *J Urol*. 2002;168:2240–2244.

18. Liedberg F, Chebil G, Davidsson T, et al. Intraoperative sentinel node de- tection improves nodal staging in invasive bladder cancer. *J Urol*. 2006; 175:84–89.
19. Aljabery F, Liedberg F, Häggström C, et al. Management and outcome of muscle-invasive bladder cancer with clinical lymph node metastases. A na- tionwide population-based study in the Bladder Cancer Data Base Sweden (BladderBaSe). *Scand J Urol*. 2019;53:332–338.
20. Rosenblatt R, Johansson M, Alamdari F, et al. Sentinel node detection in muscle-invasive urothelial bladder cancer is feasible after neoadjuvant che- motherapy in all pT stages, a prospective multicenter report. *World J Urol*. 2017;35:921–927.
21. Zarifmahmoudi L, Ghorbani H, Sadeghi R, et al. Sentinel lymph node biopsy in muscle-invasive bladder cancer: single-center experience. *Ann Nucl Med*. 2020;34:718–724.
22. Schaafsma BE, Verbeek FPR, Elzevier HW, et al. Optimization of sentinel lymph node mapping in bladder cancer using near-infrared fluorescence im- aging. *J Surg Oncol*. 2014;110:845–850.
23. Manny TB, Hemal AK. Fluorescence-enhanced robotic radical cystectomy using unconjugated indocyanine green for pelvic lymphangiography, tumor marking, and mesenteric angiography: the initial clinical experience. *Urol- ogy*. 2014;83:824–829.
24. Inoue S, Shiina H, Mitsui Y, et al. Identification of lymphatic pathway in- volved in the spread of bladder cancer: evidence obtained from fluorescence navigation with intraoperatively injected indocyanine green. *Can Urol Assoc. J*. 2013;7:E322–E328.
25. KleinJan GH, van Werkhoven E, van den Berg NS, et al. The best of both worlds: a hybrid approach for optimal pre- and intraoperative identification of sentinel lymph nodes. *Eur J Nucl Med Mol Imaging*. 2018;45:1915–1925.
26. Bunschoten A, Buckle T, Kuil J, et al. Targeted non-covalent self-assembled nanoparticles based on human serum albumin. *Biomaterials*. 2012;33:867–875.
27. Van den Berg NS, Buckle T, Kleinjan GI, et al. Hybrid tracers for sentinel node biopsy. *Q J Nucl Med Mol Imaging*. 2014;58:193–206.
28. Van den Berg NS, Brouwer OR, Klop WM, et al. Concomitant radio- and fluorescence-guided sentinel lymph node biopsy in squamous cell carcinoma of the oral cavity using ICG-(99m)Tc-nanocolloid. *Eur J Nucl Med Mol Im- aging*. 2012;39:1128–1136.
29. Robu S, Schottelius M, Eiber M, et al. Preclinical evaluation and first patient application of ^{99m}Tc-PSMA-I&S for SPECT imaging and radioguided sur- gery in prostate cancer. *J Nucl Med*. 2017;58:235–242.
30. Maurer T, Robu S, Schottelius M, et al. ^{99m}Technetium-based prostate-specific membrane antigen–radioguided surgery in recurrent prostate cancer. *Eur Urol*. 2019;75:659–666.
31. Jeschke S, Lusuardi L, Myatt A, et al. Visualisation of the lymph node path- way in real time by laparoscopic radioisotope- and fluorescence-guided sen- tinel lymph node dissection in prostate cancer staging. *Urology*. 2012;80: 1080–1086.
32. Knapp DW, Adams LG, Degrand AM, et al. Sentinel lymph node mapping of invasive urinary bladder cancer in animal models using invisible light. *Eur Urol*. 2007;52:1700–1708.

Section 2

Innovative approaches in radioguided surgery

6

Freehand-SPECT with ^{99m}Tc-HDP as tool to guide percutaneous biopsy of skeletal lesions detected on bone scintigraphy

Adapted from:
Rietbergen DDD, Meershoek P, van Oosterom MN, Roestenberg M, van Erkel AR, Smit F, van der Hage JA, Valdés Olmos RA, van Leeuwen FWB.

Rev Esp Med Nucl Imagen Mol (Engl Ed). 2019; 38:218-223

Abstract

Introduction and objectives: To assess the feasibility of using freehand Single Photon Emission Computed Tomography (freehandSPECT) for the identification of technetium-99m-hydroxydiphosphonate (^{99m}Tc-HDP) positive bone lesions and to evaluate the possibility of using these imaging data-sets for augmented- and virtual-reality based navigation approaches.

Materials and methods: In 20 consecutive patients referred for scintigraphy with ^{99m}Tc-HDP, 21 three- dimensional freehandSPECT-images were generated using a handheld gamma camera. Concordance of the two different data sets was ranked. Furthermore, feasibility of segmenting the hotspot of tracer accumulation for navigation purposes was assessed.

Results: In 86% of the cases freehandSPECT images showed good concordance with the corresponding part of the scintigraphic images. In lesions with a signal to background ratio (SBR) >1.36, freehandSPECT provided an automatically segmented reference point for navigation purposes. In 14% of the cases (average SBR 1.82, range 1.0–3.4) freehandSPECT images showed intermediate concordance due to difficult anatomical area or negative bone scintigraphy and could not be used as navigation targets.

Conclusion: In this pilot study, in 86% of the cases freehandSPECT demonstrated good concordance with traditional scintigraphy. A lesion with a SBR of 1.36 or more was suitable for navigation. These high-quality freehandSPECT images supported the future exploration navigation strategies, e.g., guided needle biopsies.

Introduction

Technetium-99m-hydroxydiphosphonate (^{99m}Tc-HDP) bone scintigraphy is commonly used for a wide spectrum of bone abnormalities. This rather traditional nuclear medicine technology, which displays increased bone turnover due to high osteoblast activity/bone metabolism, is known for its exquisite sensitivity in detecting bone diseases of different origins. With whole body scintigraphy it is easily identified where the increased bone turnover is situated to determine osseous substrate. The scan is used in benign bone disease like metabolic bone disease, in local pain complains, infection and in (primary and metastatic) malignant bone diseases. Further, it can be used to assess therapeutic responses of both benign and malignant disease. For accurate diagnosis a representative image-guided percutaneous needle biopsy of the lesion is required, which is often guided by CT or ultrasound.[1] A non-diagnostic biopsy, which occurs in 5–31% of the oncological cases and which limits the positive culture results in the case of e.g., osteomyelitis, demands a repeating biopsy or requires the need to convert to an open (surgical) procedure which can delay diagnosis and leads to extra costs, anxiety and pain to the patient.[2,3]

Ideally, an accurate biopsy sample can be obtained from the exact tissue that displays disease related molecular alterations. Against this background it has been reasoned that molecular features identified at nuclear medicine could be used to guide the biopsy process. In such applications mobile radiation detection devices, such as a gamma probes and two-dimensional (2D) hand- held gamma camera's provide an interventional alternative to scintigraphy.[4,5] Uniquely, these technologies can also be used to generate three-dimensional (3D) freehand Single Photon Emission Computed Tomography (freehandSPECT) images in an interventional setting.[6-8] The corresponding declipseSPECT technology allows the freehandSPECT data sets to be converted into a 2D augmented reality overlays and virtual reality displays that support GPS-like navigation of surgical tools towards the target tissue.[8] This concept has been extensively studied for sentinel lymph node (SLN) biopsy procedures in cancer types such as breast cancer, melanoma, head and neck cancer, gynaecologic and prostate cancer.[9] These technologies have also been used to guide minimally invasive parathyroid surgery in patients with parathyroid adenomas.[10] With that a wide range of interventional molecular imaging procedures has become available for a wide range of anatomies.

The goal of this study was to evaluate if the freehandSPECT technology could find applications beyond SLN biopsy and can be used to establish interventional imaging and navigation- guided biopsy concepts for ^{99m}Tc-HDP avid lesions with different origins. Subsequently, we assessed the concordance of freehandSPECT images with traditional scintigraphy and determined what signal to background ratio is required to support automatic target segmentation in the declipse SPECT navigation software.

Materials and Methods

Patient demographics

In this pilot study, twenty-one patients with benign or malignant bone disease, scheduled for whole body bone scintigraphy were included. In one patient, diagnosed with calcinosis cutis, excellent images by freehandSPECT were generated of the hand where the disease was located, but because the area of interest was not properly imaged on whole body bone scintigraphy the patient was excluded from final analysis. Out of the evaluated patients, in one case two areas concerning different anatomical locations were scanned. In total, 21 individual scans were evaluated. Thirteen of these scans (62%) were made in patients suspected for a wide spectrum of benign bone disease such as fracture, infection, degenerative or metabolic bone disease. Four patients (19%) were referred in relation to a primary bone tumour and another four patients (19%) known with prostate cancer were suspected for bone metastasis. Demographics of the study population are presented in more detail in Table 1 and Figure 1. This study received a certificate of no objection by the Institutional Ethics Committee and all patients provided written informed consent.

Imaging procedures

Whole body bone scintigraphy

Whole body bone scintigraphy was performed 3 h after intravenous injection of approximately 550 MBq ^{99m}Tc-HDP. Images were acquired using a two-headed gamma camera (Symbia T6, Siemens, Erlangen, Germany or Toshiba GCA-7200 pi/7200di, Toshiba, Tokyo, Japan), displayed on a 256 × 1024 matrix, zoom factor 1.0. A signal-to-background ratio (SBR) for every lesion was calculated using the counts measured in the regions of interest and the background on the whole body bone scintigraphy using Picture and Archiving Management viewing software system (PACS).

Handheld gamma camera and freehandSPECT

Following bone scintigraphy, a 3D freehandSPECT scan was obtained using a handheld gamma camera (CrystalCam; Crystal Photonics, Berlin, Germany) optimized for detecting ^{99m}Tc (energy range of 40–250 keV and a field of view 40 × 40 mm). Freehand- SPECT images of the area of interest were created with technicians and patients blinded to the results of the scintigraphy. Optical refer- ence trackers (one attached to the gamma camera and one attached to the patient), and an optical tracking device (declipseSPECT, SurgicEye, Munich, Germany), were used to determine the 3D location of the radioactive hot spots. The declipse tracking device also supported the generation of freehandSPECT Images.[8]

To create the freehandSPECT images, the camera had to be moved freely around the region of interest (ROI) in multiple directions and angles. In some cases, the freehandSPECT camera angles were physically limited by the anatomical location of the lesion. After acquisition and processing of the gamma data (2–3 min), the acquired freehandSPECT images could be displayed either as 2D augmented reality or as 3D virtual reality. The total time of the procedure per patient did not exceed 10 min which is comparable to other devices for use in the operation room such as portable gamma-cameras. For 3D virtual reality a gamma probe (SOE 311, Europrobe 3, Eurorad, Eckbolsheim, France), also equipped with a reference tracker, was used to navigate to the lesion of interest enabling both visual and numerical feedback of the distance to the target with continuous depth calculation, which can facilitate biopsy or cytological puncture for instance in deep located suspected vertebral lesions.

Table 1. Indication and number of the different kind of disease of the referred patients which underwent whole body scintigraphy. In the first kind of concordance of the two different data sets was ranked.

Patients (N=20), Measurements (N=21)		**Concordance**			**SBR**	
Indication		**G** (n)	**I** (n)	**P** (n)	**Mean Value**	**Range**
Benign	13					
Sternocostoclavicular hyperostosis	4	3	1	0	1.48	0.89-2.99
Osteomyelitis	1	1	0	0	3.99	3.99
Fibrous Displasia	2	2	0	0	9.78	3.46-16.1
Fracture	2	2	0	0	2.05	1.36-2.73
Degenerative disease	4	2	2	0	2.24	1.05-3.40
Malignant	8					
Primary bone tumor						
Chondrosarcoma	3	3	0	0	5.60	2.41-7.8
Osteosarcoma	1	1	0	0	3.53	3.53
Metastatic disease	4	4	0	0	2.79	2.15-3.58

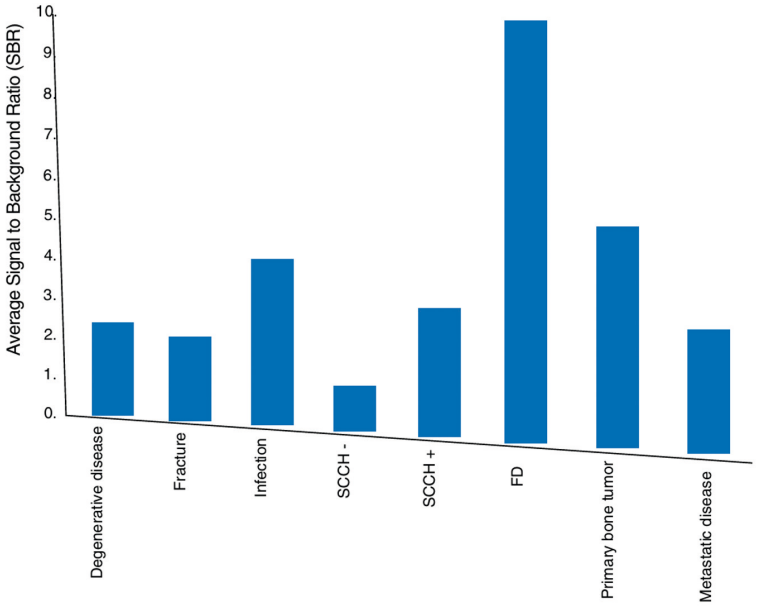

Figure 1. Average SBR in different kind of indications/suspection of disease. SCCH (sternocostochondral hyperostosis). SCCH- (the whole body scintigraphy did not showed any increased bone uptake, the patient was not diagnosed with (metabolic active) SCCH). SCCH + (whole body bone scintigraphy revealed increased uptake at the side of the sternocostochondral junction, the patient was diagnosed with metabolic active SCCH). FD (Fibrous Dysplasia).

Scoring

The derived freehandSPECT data and the bone scintigraphy were reviewed by two experienced nuclear medicine physicians. Derived freehandSPECT images were rated as good, intermediate, poor concordance with respect to whole body bone scintigraphy based on expertise and knowledge of the experienced nuclear medicine physicians. Good concordance was considered when freehand-SPECT showed the same amount and uptake/distribution as the whole body bone scintigraphy, intermediate when there was elevated uptake but more like a blur or, in case of focal uptake, the location was difficult to determine. Poor concordance was ranked when uptake, distribution or location between both scans did not correlate at all.

Tracking of a biopsy drill and navigation in a phantom set-up

The acquired freehandSPECT images were projected on a phantom to create augmented reality overlays and simulated image-guided interventions. The biopsy drill (Arrow OnControl Powered Bone Access System, Teleflex, Wayne, Pennsylvania, USA) was equipped with a reference tracker, and after geometrical calibrations, it was used to navigate to the metabolic active lesion.[11] Using virtual reality visualization, the drill could be virtually escorted to ^{99m}Tc-HDP avid lesions.

Results

Scintigraphic findings

In seventeen cases (81%) whole body bone scintigraphy identified lesions with increased focal or diffuse focal uptake of the radioactive tracer with an average Signal to Background ratio (SBR) of 4.12 (ranging from 1.36 to 16.1), Fig. 2a. These patients were clinically suspect for metastatic disease (N = 4), sternocostoclavicular hyperostosis (SCCH) (N = 1), osteomyelitis (N = 1), primary bone malignancy (N = 4) degenerative disease (N = 3), fracture (N = 2) and fibrous disease (FD) (N = 2). In patients suspected for metabolic active benign bone disease (like FD) and patients with primary bone malignancy, the SBR of the region of interest on scinitigraphy was the highest (average SBR of 9.78 and 5.09, respectively). Infection, fracture, metabolic active SCCH and metastatic disease were visualized with good scan quality and SBR as well. In the remaining four cases (19%; N=3 referred for suspected SCCH and N=1 for degenerative disease/metastatic breast cancer) whole body bone scintigraphy did not reveal any focal abnormalities.

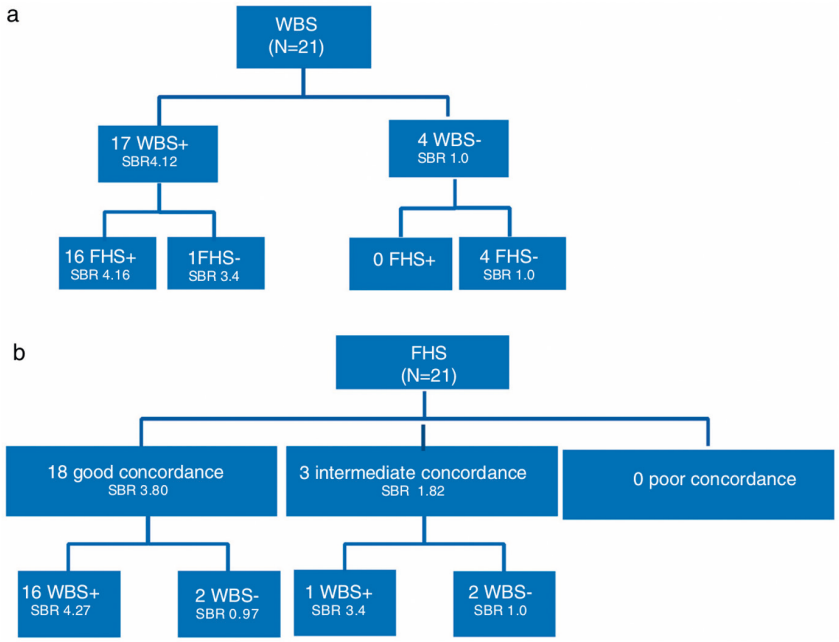

Figure. 2. (a) Results of whole body scintigraphy (WBS) and corresponding freehandSPECT (FHS) outcome with the average signal to background ratio (SBR) of the area of interest measured on whole body scintigraphy. 17 WBS showed increased bone turnover. 16 of them were also positive on the scan made with FHS, 1 scan was metabolic negative on FHS. (b) Results of freehandSPECT (FHS) and its concordance with WBS (whole body bone scintigraphy, metabolic active or not) and corresponding SBR (Signal to Background Ratio) measured on the WBS. Of the 21 freehand SPECT scans which were made, 18 showed similar view in uptake and pattern compared to the WBS, 3 of them showed intermediate concordance with WBS. There were no poor concordances.

FreehandSPECT findings and concordance bone scintigraphy

To allow objective assessment of the freehandSPECT findings, these images were obtained while being blinded for the findings during whole body bone scintigraphy. This meant that the field of view (10×10×10cm) wherein the freehandSPECT scan was obtained was based on the site the patient experienced the most complains.

In 18 cases (86%) freehandSPECT showed a good concordance compared to the scintigraphy. These cases had a clearly higher SBR (average SBR 3.8, range 0.89–16.1) at scintigraphy compared with the three cases which had an intermediate concordance with the bone scintigraphy (average SBR 1.82) In 16 of the 18 cases with good concordance, images had a suitable SBR (average of 4.27, range 1.36–16.1), for automatic target segmentation. Areas that were involved were namely superficial lying bones, such as the sternum and in extremities. In the remaining

two of the 18 cases, scintigraphy showed no increased uptake, in good agreement with freehandSPECT in which a blur was seen (average SBR 0.97).

In the remaining three of the 21 cases (14%), intermediate concordance was observed. In two of these patients, the findings were in line with a low SBR (SBR 1.0) without any focal increase uptake on the whole body bone scintigraphy. In the third patient however, the area of interest had an increased SBR (3.4) which involved a deeper lying structure, the joint in the pelvic area, that was difficult to image with freehandSPECT because of overlying bone structures. Results are displayed in Fig. 2b.

Biopsy needle navigation in a phantom set-up

To underline the potential of using freehandSPECT scans for navigated biopsy procedures, two scans of patients with primary bone malignancy with intense focal uptake on both whole body bone scintigraphy and that yield a good quality freehandSPECT were registered to a skeleton-phantom (Figs. 3 and 4). The augmented reality and virtual reality projections supported effective navigation of the biopsy drill to ^{99m}Tc-HDP avid lesions. Hereby the biopsy tools were guided into the heart of the lesion hotspot.

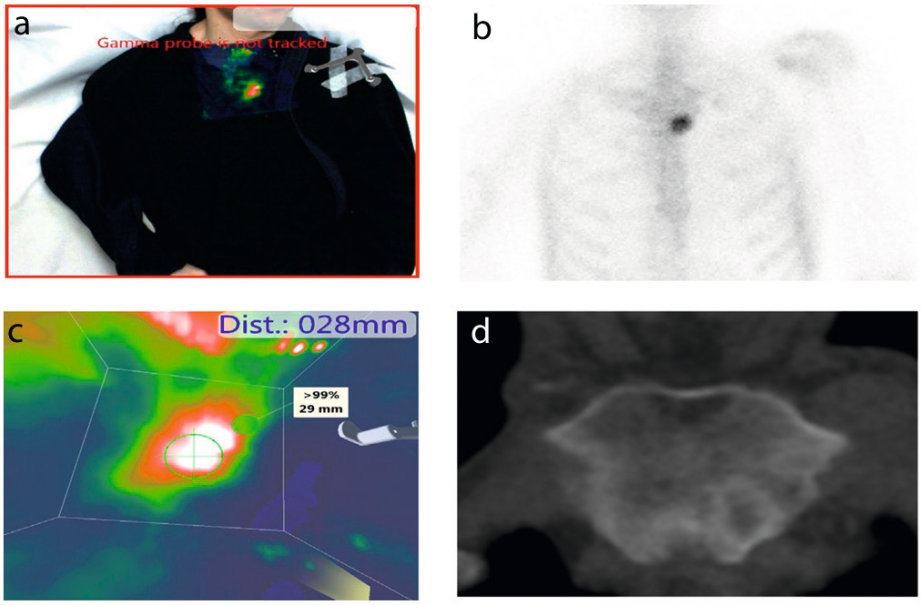

Figure 3. Patient known with malignant primary bone cancer (chondrosarcoma). (a) Overlay view using the video camera of the declipse system after freehandSPECT scanning using mobile gamma camera with high metabolic area in a low background activity. (b) Area of interest of whole body ^{99m}Tc-HDP bone scintigraphy with increased metabolic bone activity in the manubrium sternum at the left side with a high signal to background ratio (SBR 2.41) compared with the surrounding bone tissue. The correlation of the freehandSPECT (a) and bone scintigraphy (b) showed accurate correlation. (c) 3D mode allowing to navigate to the lesion of interest using the handheld gamma detection probe. Green crosshair is the tip of the probe providing measurement distance (28 mm) between the tip of the probe and the area of interest. (d). Reconstructed CT view of the manubrium showing the primary bone malignancy with a small lytic lesion left paramedian with a sclerotic rim.

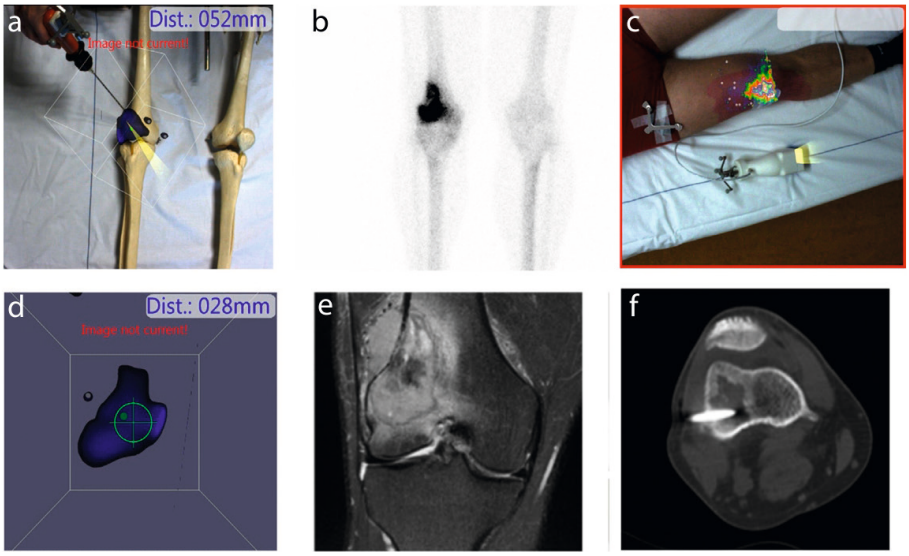

Figure 4. Patient with primary bone disease (chondrosarcoma). (a) Overlay of the acquired freehandSPECT images of one of the patients with the position of the phantom skeleton in our lab, to create augmented reality. The biopsy drill was equipped with the tracking system to allow navigation to the metabolic active lesion. Using virtual reality the drill was escorted to the bone active lesion for a radio-guided bone biopsy. (b) Area of interest of whole body ^{99m}Tc-HDP bone scintigraphy with increased metabolic bone activity in the distal right femur with a high signal to background ratio (SBR 3.53) compared with the surrounding bone tissue. The correlation of the freehandSPECT (a) and bone scintigraphy (b) showed accurate correlation. (c) Overlay view using the video camera of the declipse system after freehandSPECT scanning using mobile gamma camera with high metabolic area in a low background activity. (d) 3D mode allowing to navigate to the lesion of interest using the handheld gamma detection probe. (e) MR showed the corresponding lesion. (f) CT guided biopsy of the primary tumour.

Discussion

In this study we describe the use of freehandSPECT and the thereon based navigation technologies to detect HDP avid lesions. Thereby we extend the utility of the freehandSPECT technology. The concordance between freehandSPECT and ^{99m}Tc-HDP scintigraphy findings underline the potential value of using freehandSPECT to guide percutaneous biopsy of molecularly targeted bone lesions.

The quality of images obtained with freehandSPECT imaging and the ability to use these images for navigation purposes was directly related to the SBR and anatomical location of the ^{99m}Tc-HDP avid lesions. Our findings indicate that a SBR >1.36 is instrumental for obtaining high quality freehandSPECT images. Moreover, the location and depth of the lesion influences the image quality. The last two are mainly the result of the impairment of the rotational freedom of the detector placement during freehandSPECT image acquisition. Most likely, the quality of freehandSPECT imaging will improve when operators expand their experience with the technology.

With the use of a novel tracking and calibration set-up, specifically designed for a bone biopsy needle, we demonstrated that freehandSPECT-guided biopsy was feasible in a phantom. We were able to show that the tip of a biopsy drill can be positioned using 2D augmented reality and 3D virtual reality continuously displaying the distance to the target. This could be validated using the virtual reality feedback. We hypothesize that the use of such navigation guided biopsies will also improve the quality and yield of histopathologic or microbiological diagnosis by positioning the needle exactly in the part of the lesion with the highest disease metabolism. This may reduce the number of non-diagnostic biopsies avoiding subsequent delay, complications and patient anxiety in cases where imaging modalities like CT, MRI or ultrasound lack sensitivity, e.g., in small metastatic disease or in subtle, early or low-grade osteomyelitis.

While this study only evaluated its use with ^{99m}Tc-HDP, it is clear from the literature that the technology works equally well with other ^{99m}Tc-based tracers [9,11,12] or even with other radioisotopes e.g. ^{111}In.[13,14] This can potentially be strengthened by integrating the freehandSPECT technology, with ultrasound, as has previously been used to successfully guide biopsies in breast cancer.[15] Although freehandSPECT can be used as a stand-alone modality, use of whole body bone scintigraphy is essential to map target lesions providing anatomical landmarks and eventually skin marking. This may be particularly useful in lesions with a low SBR or deep located for which stand-alone use of freehandSPECT may be unnecessarily prolonged. As mentioned in the literature also important to emphasize is that scanning with freehandSPECT for radioguided interventions require a specific training period to increase handling

and image reproducibility as well as to enhance its accuracy in the intervention room. [16]

Although freehandSPECT requires a specific operator training to ensure intervention accuracy its application contributes to solve some limitations of other portable devices (e.g., gamma-camera, gamma-probe) for use in the operating room by providing real time depth information and 3D target visualization.

Conclusion

For the first time, freehandSPECT imaging was used to identify benign and malignant bone diseases. This study showed a high degree of concordance in freehandSPECT and scintigraphic findings in cases were ^{99m}Tc-HDP avid lesions displayed a high SBR. Furthermore, we illustrated the possibility of using freehandSPECT technology for future navigated needle biopsies, a concept that can improve future diagnosis of both benign and malignant diseases.

References

1 LeeYJ, SadighS, MankadK,KapseN,RajeswaranG.Theimagingofosteomyelitis. Quant Imaging Med Surg. 2016;6:184–98.

2 Didolkar MM, Anderson ME, Hochman MG, Rissmiller JG, Goldsmith JD, Geb- hardt MG, et al. Image guided core needle biopsy of musculoskeletal lesions: are nondiagnostic results clinically useful? Clin Orthop Relat Res. 2013;471:3601–9.

3 Maciel MJ, Tyng CJ, Barbosa PN, Matushita Junior JP, Zurstrassen CE, et al. Computed tomography-guided percutaneous biopsy of bone lesions: rate of diagnostic success and complications. Radiol Bras. 2014;47:269–74.

4 Infante JR, Lorente R, Rayo JI, Serrano J, Domínguez ML, García L, et al. Use of radioguided surgery in the surgical treatment of osteoid osteoma. Rev Esp Med Nucl Imagen Mol. 2015;34:225–9.

5 Vidal-Sicart S, Vermeeren L, Solà O, Paredes P, Valdés-Olmos RA. The use of a portable gamma camera for preoperative lymphatic mapping: a com- parison with a conventional gamma camera. Eur Nucl Med Mol Imaging. 2011;38:636–41.

6 Wendler T, Hartl A, Lasser T, Traub J, Daghighian F, Ziegler SI, et al. Towards intra- operative 3D nuclear imaging: reconstruction of 3D radioactive distribu- tions using tracked gamma probes. Med Image Comput Comput Assist Interv. 2007;10:909–17.

7 Wendler T, Herrmann K, Schnelzer A, Lasser T, Traub J, Kutter O, et al. First demonstration of 3-D lymphatic mapping in breast cancer using freehand SPECT. Eur J Nucl Med Mol Imaging. 2010;37:1452–61.

8 Engelen T, Winkel BM, Rietbergen DD, KleinJan GH, Vidal-Sicart S, Olmos RA, et al. The next evolution in radioguided surgery: breast cancer related sentinel node localization using a freehandSPECT-mobile gamma camera combination. Am J Nucl Med Mol Imaging. 2015;5:233–45.

9 Bluemel C, Matthies P, Herrmann K, Povoski SP. 3D scintigraphic imaging and navigation in radioguided surgery: freehand SPECT technology and its clinical applications. Expert Rev Med Devices. 2016;13:339–51.

10 Casans-Tormo I, Prado-Wohlwend S, Díaz-Expósito R, Cassinello-Fernández N, Ortega- Serrano J. Initial experience in intraoperative radiolocalization of the parathyroid adenoma with freehand SPECT and comparative assessment with portable gamma- camera. Rev Esp Med Nucl Imagen Mol. 2015;34:116–9.

11 Van Oosterom MN, Engelen MA, van den Berg NS, KleinJan GH, van der Poel HG, vWendler T, et al. Navigation of a robot-integrated fluorescence laparoscope in preoperative SPECT/CT and intraoperative freehand SPECT imaging data: a phantom study. J Biomed Opt. 2016;21:86008.

12 KleinJan GH, van den Berg NS, van Oosterom MN, Wendler T, Miwa M, Bex A, et al. Toward (hybrid) navigation of a fluorescence camera in an open surgery setting. J Nucl Med. 2016;57:1650–3.

13 Rauscher I, Eiber M, Maurer T. PSMA-radioguided surgery for salvage lym- phadenectomy in recurrent prostate cancer. Aktuelle Urol. 2017;48:148–52.

14 Rauscher I, Eiber M, Jilg CA, Gschwend JE, Maurer T. PSMA-radioguided surgery in localized recurrent prostate cancer: Current and future aspects. Urologe A. 2017;56:18–23.

15 Okur A, Hennersperger C, Runyan B, Gardiazaball J, Keicher M, Paepke S, et al. FhSPECT-US guided needle biopsy of sentinel lymph nodes in the axilla: is it feasible? Med Image Comput Comput Assist Interv. 2014;17:577–84.

16 Pouw B, de Wit-van der Veen LJ, Stokkel MP, Valdés Olmos RA. Improved accuracy and reproducibility using a training protocol for freehand-SPECT 3D mapping in radio-guided surgery. Clin Nucl Med. 2015;40:457–60.

7

*h*HEPATO-Cy5, a bi-modal tracer for image-guided hepatobiliary surgery

Adapted from:
Daphne D.D. Rietbergen, Tessa Buckle, Leon J. Slof, Maarten P. van Meerbeek, Clarize M. de Korne, Mick M. Welling, Matthias N. van Oosterom, Kevin Bauwens, Meta Roestenberg, Julia Kloetzl, Fijs W.B. van Leeuwen.

J Nucl Med. 2024;65(8):1301-1306

Abstract

Introduction and objectives: Liver cancer is a leading cause of cancer deaths worldwide. Surgical resection of superficial hepatic lesions is increasingly guided by the disrupted bile excretion of the fluorescent dye indocyanine green (ICG). To extend this approach to deeper-lying lesions a dedicated bi-modal tracer that facilitates both fluorescence- and radio-guidance was developed.

Materials and methods: A tracer comprising a methylated Cy5 fluorescent dye and a mas_3 chelate (*h*HEPATO-Cy5) was synthesized and characterized. Cellular uptake and excretion were evaluated in hepatocyte cultures (2D culture and in vitro lesion model), using a fluorescent bile salt, mitotracker dye and methylated Cy5 as a control. Following radiolabeling, the pharmacokinetics of ^{99m}Tc-*h*HEPATO-Cy5 was assessed in mice over a period of 24hrs (% ID and %ID/g, SPECT/CT imaging and fluorescence imaging). The ability to provide real-time fluorescence guidance during robot-assisted hepatobiliary surgery was evaluated in a porcine model using ICG as reference.

Results: The unique molecular signature of *h*HEPATO-Cy5 promotes hepatobiliary excretion. In vitro studies in hepatocytes showed that where methylated Cy5 remained internalized, *h*HEPATO-Cy5 showed fast clearance (10 minutes) similar to that of fluorescent bile salt. In vivo use of ^{99m}Tc-*h*HEPATO-Cy5 in mice revealed hepatobiliary accumulation and rapid biliary clearance. The effective of bile clearance was best exemplified by the two orders of magnitude reduction in count rate for the gall bladder ($p=0.008$) over time. During hepatobiliary surgery in a porcine model, *h*HEPATO-Cy5 enabled fluorescence-based lesion identification comparable to ICG.

Conclusion: The bi-modal ^{99m}Tc-*h*HEPATO-Cy5 provides effective means to identify liver lesions. Uniquely it helps overcome the shortcomings of fluorescence only approaches by allowing for an extension with in-depth radio-guidance.

Introduction

Annually liver cancer accounts for an estimated 748,300 new cases and 695,900 cancer deaths worldwide. Next to primary liver cancer (e.g., hepatocellular carcinoma), tumorous lesions in the liver are often metastases of cancer with a different origin e.g., colorectal cancer, neuroendocrine tumors, ocular melanoma and breast cancer. [1-5]

For both primary and metastatic liver cancer, surgical resection is considered the primary method to ensure long-term survival and to achieve a potential cure. The improvement in diagnostic imaging, effectiveness of neoadjuvant systemic therapies and development of local treatment strategies has led to a 20-30 % increase in patients that are considered eligible for de novo surgery, or surgery following neoadjuvant treatment.[6] The success of surgery depends on the ability to achieve radical resection and preservation of normal liver tissue function.[7] The high chance of hepatic recurrence (up to 29 %)[8] and complications (60% of cases)[9] indicate substantial improvements can still be made in this line of therapy.

Accurate preoperative lesion identification, procedural planning and intraoperative image guidance are of vital importance for precision surgery. Where preoperative lesion identification generally occurs via MRI, CT, or ^{18}F-FDG-PET, intraoperative identification often relies on the limited sensitivity and resolution of palpation, optical inspection and intraoperative ultrasound.[7,10,11] With the shift from open surgery to minimally-invasive laparoscopic and robotic surgery, the reliance on image guidance technologies has increased.[12] Especially the use of fluorescence-guidance is gaining ground. In 2009 Ishizawa et al. started to exploit the pharmacological clearance profile of the fluorescent dye indocyanine green (ICG) to identify hepatic lesions with a high spatial resolution.[13] Since then, this image guidance approach has been widely adopted, resulting in lower complications (Odds Ratio: 0.523) and shorter hospital stay (Weighted Mean Difference = -1.8).[14] A downside of this fluorescence-based guidance approach is that lesions located > 5 mm below the surface cannot be reliably identified.[11] Conversely, the use of separate techniques for pre- and intraoperative imaging can cause misalignment between the two.[15] The latter not only limits planning and logistics but may also result in excision of additional (false positive) tissue. Ideally nuclear medicine diagnostics and intraoperative fluorescence guidance are integrated. In nuclear medicine there are several radiotracers available that can be used to assess liver function (e.g., iminodiacetic acid)[16],^{99m}Tc-Mebrofenin).[17] However, to support approaches that combine non-invasive nuclear and intraoperative fluorescence imaging, there is a need for new bi-modal/hybrid biliary tracers that contain both a radio- and fluorescent label. Such a combined approach has already demonstrated clinical value during other surgical indications i.e., sentinel node resections.[15]

Although the exact mechanism of ICG accumulation in liver lesions remains unclear, it has been shown that the fluorescence signal accumulates at the transition between healthy and diseased tissue.[11] In particular disruptions in the biliary clearance of the tracer are thought to play an important role in the localization of fluorescence in diseased tissues.[18] With this feature in mind a small-molecule hybrid tracer was designed to support bi-modal imaging of liver lesions. Following tracer synthesis, uptake and excretion were evaluated in vitro in hepatocytes, while in vivo tracer pharmacokinetics were assessed in mice. The surgical utility of the tracer was assessed during robot-assisted fluorescence-based hepatobiliary surgery in a large animal porcine model.

Materials and methods

Synthesis and chemical evaluation of the hybrid tracer hHEPATO-Cy5

Mercaptoacetyltriserine (mas_3), N-Boc-Aminophenol-Merrifield resin and Methyl-Cy5-NH_2 (also used as Cy5 control) were synthesized according to previously described procedures (*19,20*). Methyl-Cy5-mas_3 (*h*HEPATO-Cy5, Figure 1 and Figure SI1-4) was synthesized as followed: mas_3 (27 mg, 68 µmol), HATU (26 mg, 68 µmol) and *N*-methylmorpholine (34 mg, 340 µmol) were dissolved in DMSO (2 mL). Methyl-Cy5-AmineC4 (30 mg, 68 µmol) was added, and the reaction mixture was stirred at RT for 25 min. Hereafter a mixture of H_2O/MeCN (85/15, 8 mL) with 0.1% TFA was added, and the crude product was purified through preparative HPLC. Lyophilisation yielded the product as a vibrant blue solid (30 mg, 54% yield). Compound characterization including absorption/emission (Figure SI2-4), brightness and serum protein binding was performed according to Hensbergen et al.[20]

In vitro tracer metabolism in hepatocytes

HC04 hepatocyte and GEB3 epithelial control cells were cultured in Gibco's Minimum Essential Medium enriched with 10% fetal bovine serum and penicillin/streptomycin (all Life Technologies Inc.).[21,22] Three days prior to fluorescence confocal imaging cells were seeded onto glass bottom culture dishes (MatTek corporation). An in vitro model for hepatic lesions was created by placing a heated metal rod in the center of the culture dish for 1-2 sec, one hour prior to imaging.

Samples were stained with 1 µM *h*HEPATO-Cy5 or 100 nM Cy5 control for 10 or 30 minutes at 37 ^{0}C (N = 6 per tracer and condition). Staining with 1 µM of the bile salt Cholyl-Lys-Fluorescein (CLF) or mitotracker green (2 µL/mL M7514, Thermo Fisher) was used to confirm the staining pattern of *h*HEPATO-Cy5. Hoechst (33342, 1 mg/mL, Thermo Fisher) was added to all samples as nuclear reference.[23] Prior to imaging samples were washed three times with Phosphate buffered saline.

Fluorescence confocal microscopy was performed as previously described.[24] For visualization of in vitro lesions, a tile scan consisting out of a 5 x 5 grid at 20 x magnification was made. Semi-quantitative image analysis and (3D) surface- plot was performed as previously described.[25]

Frozen excised tissue samples that contained a liver lesion were cut at 5 µm and imaged without further pretreatment. Additional sections were cut for standard H&E staining, which was performed as previously described and served as reference for tissue morphology.[26]

Animal experiments

All rodent experiments were granted a licence by the Competent Authority after advice by the Animal Experiments Committee Leiden (AVD1160020173304). Experiments in pigs were approved by ethical board of the University of Ghent (EC2019/79). Experiments were performed in a licensed establishment for the use of experimental animals (LUMC or ORSI Academy, Melle Belgium). Experiments were performed in accordance with the Experiments on Animals Act (Wod, 2014), the applicable legislation in the Netherlands and Belgium in accordance with the European guidelines (EU directive no. 2010/63/EU) regarding the protection of animals used for scientific purposes.

Pigs were housed at the animal facility at ORSI Academy until used for imaging experiments during surgical training (weight per animal approximately 40 kg). Pigs were re-used after surgical training and remained under anesthesia until being euthanized when the examination was completed.

In vivo tracer biodistribution in mice

Radiolabeling of *h*HEPATO-Cy5 (Figure SI5), resulting in ^{99m}Tc-*h*HEPATO-Cy5, and in vivo SPECT imaging (at 1, 2, 4 and 24 hours) was performed according to previously described procedures.[22] For quantitative assessment of the biodistribution of ("hot") ^{99m}Tc-*h*HEPATO-Cy5, 10 MBq (0.5 nmol in 0.1 mL) of the labelled tracer was intravenously administered into female Swiss OF1 mice (6 - 7 weeks old; Charles River). The percentage of the injected dose (%ID) and percentage of the injected dose per gram of tissue (%ID/g) was assessed at 2 and 24 hours post intravenous tracer administration, as previously described (N = 9).[22,27] Semi-quantitative assessment of fluorescence in the liver/gall bladder and intestines was assessed prior to gamma counting, to exemplify the effective hepatobiliary clearance and to complement the quantitative biodistribution, using an IVIS Spectrum preclinical imaging system (Perkin Elmer) and Living Image software (version 3.2).[27] Images were acquired following excitation at 640 nm, and light was collected > 680 nm (acquisition time 5 sec). Fluorescent content was measured in photons/sec/cm^2.

In vivo pharmacokinetic assessments in a porcine model - surgical fluorescence imaging

Since porcine models do not naturally yield liver metastases, (superficial) heat-induced necrotic lesions were created using bi-polar robotic instruments (da Vinci Maryland or Fenestrated forceps). These lesions served as a model for liver metastasis wherein the tumor disrupts the hepatic anatomy.

3.75 mg hHEPATO-Cy5 was dissolved in 150 µL ethanol, whereafter 1350 µL Tween80/Saline was added to achieve a 2.5 mg/mL solution, which was subsequently intravenously injected in individual animals (N = 6). 4 - 6 Hours after tracer administration intraoperative imaging using both white light and Cy5 filtered light was performed using a modified clinical grade IMAGE1 S™ camera system including a D-Light P light source (integrated customized Cy5 filter) and a customized 10 mm 0° laparoscope was used (KARL STORZ SE & Co. KG).[26] The use of radiotracers and a more extended window could not be pursued under the available ethical approval for the surgical training setting.

As a reference, identical experiments were conducted after administration of a similar dye concentration of ICG (3.75 mg, N = 2). In the latter, imaging was performed using the fluorescence setting of a Firefly camera mounted on a Da Vinci surgical robot. After imaging, animals were euthanized, and lesions excised for ex vivo fluorescence imaging and pathological examination. In-house developed image-processing software (C++-programming language using open-source computer vision libraries (OpenCV)) was used to create a color-coded heat-map.[24,26] Differences in fluorescence signal intensity were shown using an intensity-based scale-bar that represents the signal-to-background ratio (SBR).

Statistical analysis

Statistical evaluation to compare uptake values (%ID, %ID/g for radioactive assessment and photons/sec/cm^2 for the fluorescence signal) at different timepoints in the biodistribution was performed using an unpaired two-sided Student's t-test. Values of $p < 0.05$ were considered significant.

Results

Synthesis and characterization

*h*HEPATO-Cy5 was successfully synthesized (Figure 1, Figure SI1-4) and presented favorable chemical (serum protein binding 94%, logP 0.80 ± 0.03) and fluorescent properties (Absorption/emission: 640/665 nm (Figure SI6), brightness: 3445 M^{-1}). After radiolabeling, ^{99m}Tc-*h*HEPATO-Cy5 was obtained with a radiochemical yield of 83 ± 5%.

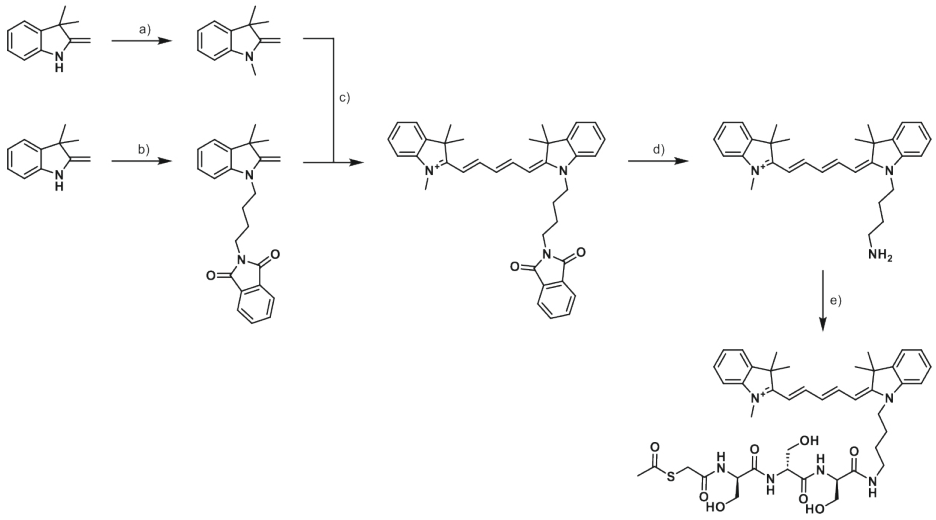

Figure 1. Reaction scheme synthesis *h*HEPATO-Cy5. a) MeI, K_2CO_3, DMF; b) N-(4-bromobutyl)phthalimide, sulfolane; c) first, malonaldehyde dianilide HCl, 1:1 Ac_2O:AcOH, followed by Indole-AmineC4Phth, 3:1 pyridine:Ac_2O, d) 33wt% $MeNH_2$ in EtOH; e) L-mas3, HATU, DiPEA.

In vitro excretion hepatocytes

Using an in vitro lesion model and assessment in hepatocyte cultures, the difference in uptake of *h*HEPATO-Cy5 in damaged and healthy hepatocytes was compared (Figure SI7, Figure 2). In the in vitro lesion model, a high intensity Cy5 fluorescence signal was detected in a ring of damaged hepatocytes (Figure SI7). In these cells uptake was distributed evenly over the whole cell. A change in distribution of the fluorescence signal was seen with increasing distance from the lesion. At approximately 500 µm distance the overall uptake pattern was similar to that in healthy hepatocytes. Here no intracellular uptake was seen but focalized uptake of *h*HEPATO-Cy5 positioned in bile cannulas between cells (Figure 2 and Figure SI7, encircled).[28] As this pattern was shown to be similar to that of (fluorescent) bile salts (Figure 2) this suggests that *h*HEPATO-Cy5 is functionally excreted.

Incubation of epithelial cells with *h*HEPATO-Cy5 resulted in mitochondrial uptake (Figure SI8), which was similar to the uptake of the fluorescent component alone (methylated Cy5 (control)) in both hepatocytes and epithelial cells (Figure 2, Figure SI8). Excretion of *h*HEPATO-Cy5 was underlined by semi-quantitative assessment of the fluorescence signal over time (Figure SI9). In healthy hepatocytes a decrease of *h*HEPATO-Cy5-related fluorescence signal was seen after 30 minutes. In contrast, a substantially higher intracellular signal ($p > 0.0001$) was seen for the Cy5 control that did not decrease over time. Hence, the focal uptake of *h*HEPATO-Cy5 is excusive for hepatocytes and the addition of the mas_3 moiety in *h*HEPATO-Cy5 is crucial for the hepatobiliary excretion driving molecular design.

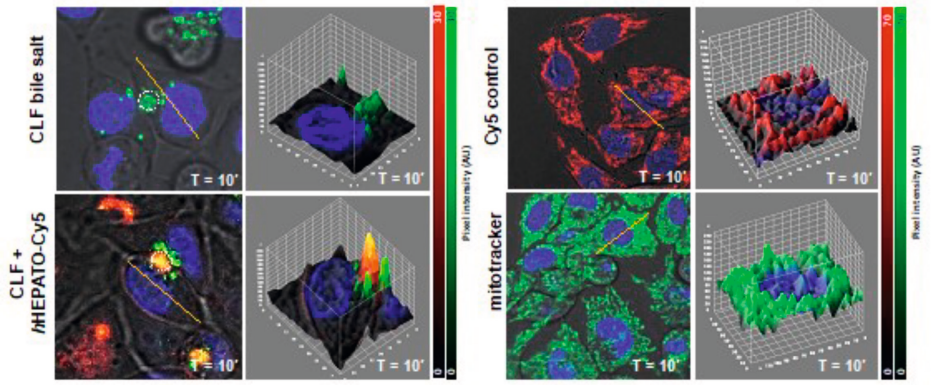

Figure 2. Microscopic assessment of the localization of control stainings in hepatocytes. Fluorescence confocal imaging of HC04 hepatocytes after 10 minutes of incubation with fluorescent bile salt Cholyl-Lys-Fluorescein (CLF), or co-incubation of hHEPATO-Cy5 and CLF), Cy5 control or Mitotracker green. Left image: 2D fluorecence confocal image with nuclear staining in blue, Cy5 in red and mitotracker in green (dashed circle = example of bile canula, yellow line = orientation 3D analysis), right image: 3D representation of tracer distribution throughout the cell. Color bars show pixel intensity (AU).

In vivo biodistribution in mice

As early as 1 hour post intravenous administration, "hot" ^{99m}Tc-*h*HEPATO-Cy5 (0.5 nmol) yielded dominant hepatobiliary excretion, exemplified by the prominent signal seen in the liver, gallbladder, and intestines on SPECT (Figure 3A). Biliary excretion was further substantiated by a significant two orders of magnitude reduction in count rate for the gall bladder (Figure 3B and Table SI1; $p = 0.008$) over time. Instrumental for imaging of liver lesions, a five-fold decrease in count rate was observed in the liver (Table SI1; $p = 0.002$). The latter was further substantiated via ex vivo tissue examination at 2 hours and 24 hours (Figure 3A). At 2 hours post tracer injection high fluorescence intensities were seen in the gall bladder ($2.6*10^8 \pm 5.9*10^7$ photons/sec/cm^2), while intensities in the liver were significantly lower ($3.3*10^7 \pm 7.9*10^6$ photons/sec/cm^2; $p > 0.0001$). After 24 hours fluorescence signal intensities in the liver had further reduced to $1.6*10^7 \pm 2.8*10^6$ photons/sec/cm^2, which correlated to a negligible background staining in this tissue (Figure 3A, insert 24 hours).

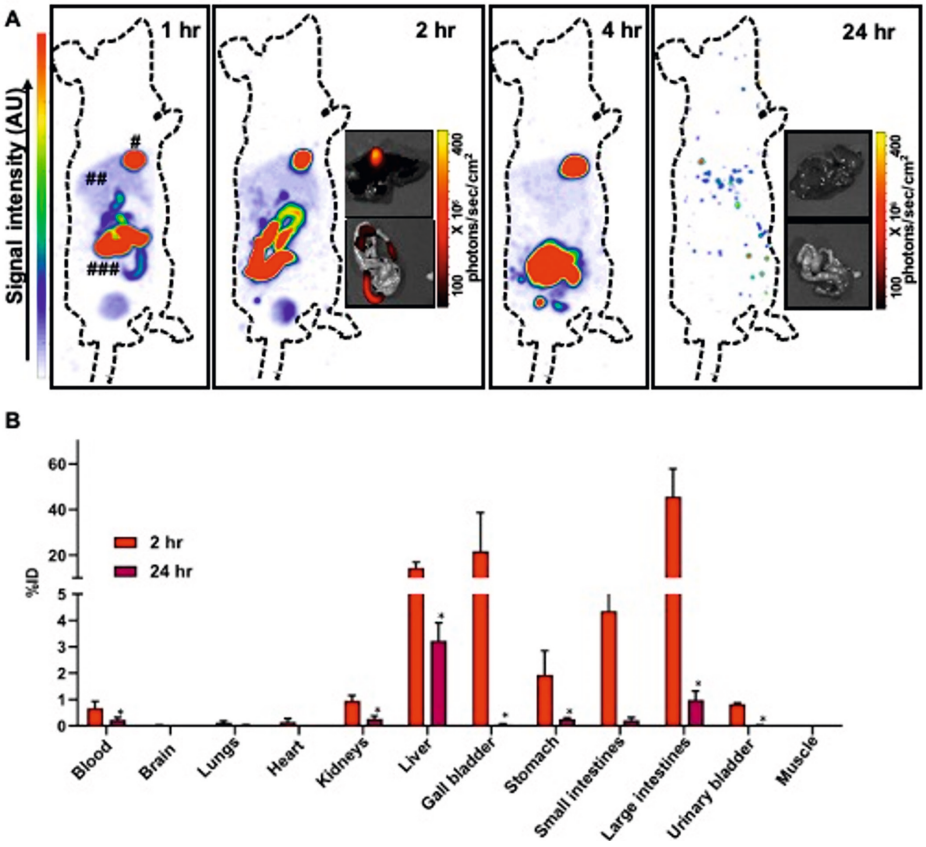

Figure 3. Biodistribution of 99mTc-hHEPATO-Cy5 in mice. A) In vivo SPECT imaging (rainbow scale, AU) at 1, 2, 4 and 24 hours after tracer administration (# = gall bladder, ## = liver and ### = intestines). Inserts at 2 and 24 hours show fluorescence imaging of the liver and gall bladder (top) and intestines (bottom; hotmap, photons/sec/cm^2). *= p>0.01 for 2 vs 24hrs uptake values. Quantitative biodistribution presented as B) percentage of the injected dose (%ID) at 2 hours (red) and 24 hours (purple) after intravenous administration in mice.

In vivo pharmacokinetic assessments in porcine models - surgical fluorescence imaging

In vivo imaging in a porcine model for robot assisted hepatobiliary lesion resection was performed to show the similarities in staining pattern with the current clinical fluorescence only approach (using ICG) and concordance of *h*HEPATO-Cy5 with clinical grade robotic surgery and imaging devices. Fluorescence imaging in this model underscored the hepatobiliary clearance profile for *h*HEPATO-Cy5. A clear fluorescence signal was seen in the gall bladder and intestines. And importantly, already at 4 hours post injection the background uptake in the non-effected liver was neglectable (Figure 4).

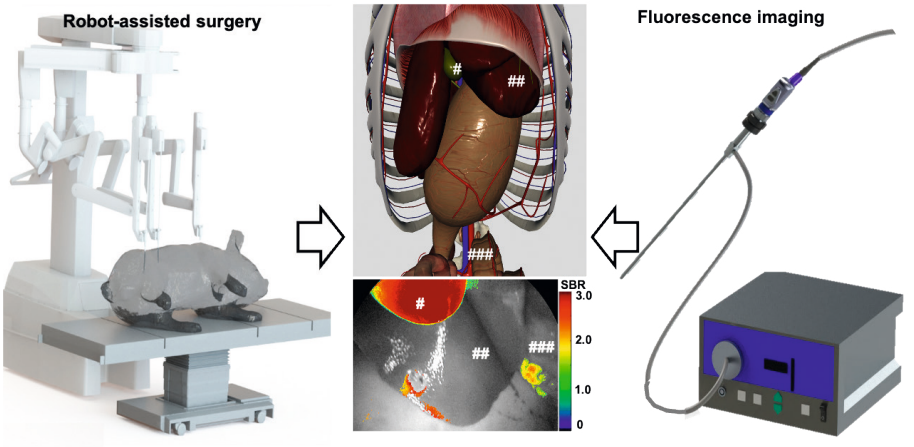

Figure 4. Surgical imaging set-up in a porcine model. Use of **c**linical grade equipment allowed combination of robot assisted surgery (left) laparoscopic fluorescence imaging (right) for the assessment of tracer distribution over the hepatobiliary system (# = gall bladder, ## = liver) and excretion towards the intestines (###) in a porcine model.[29] Top anatomical image: schematic localization of organs of interest, bottom image: heatmap laparoscopic fluorescence image showing *h*HEPATO-Cy5-related fluorescence.

In vivo created liver lesions (Figure 5, Figure SI10) demonstrated a characteristic fluorescent rim located around the border of the lesion (N > 25 lesions tested). Clear discrimination between the liver and surrounding tissue of the abdominal wall could be made, which was especially evident for lesions located on the outer edge of a liver segment. The rim-like staining pattern was in comparable with the accumulation seen in the in vitro model (Figure SI7), and in line with that of ICG in the same model (Figure SI11) but of also of ICG in patients with liver cancer.[18]

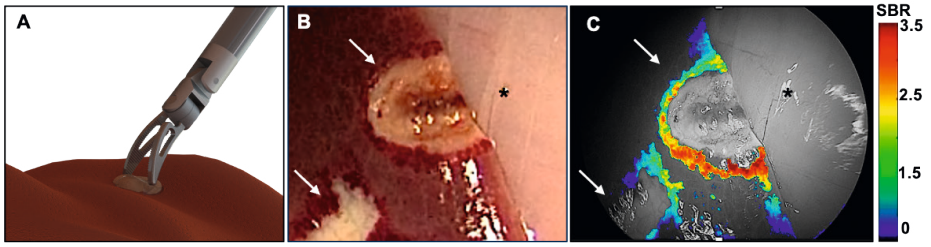

Figure 5. Robot-assisted in vivo imaging of liver lesions in a porcine model. A) Schematic representation of the creation of heat-induced lesions using the coagulation setting of a bipolar robotic forceps. In vivo laparoscopic imaging of a liver lesion (white arrow) and surrounding tissue of the abdominal wall (*) using B) white light imaging and C) Custom image processing algorithms support intensity-based assessment of the fluorescence uptake (SBR = signal-to-background ratio).[26]

Microscopic pathological examination of the excised lesions underscored the difference in morphology between the healthy liver tissue and the lesion (Figure 6A/B). Accumulation of *h*HEPATO-Cy5 (in red) occurred within a transitional rim bridging the lesion (#) and healthy liver tissue (**; Figure 6C). This suggests that damaged hepatocytes in the transitional rim are unable to facilitate bile transport, resulting in local retention of *h*HEPATO-Cy5.

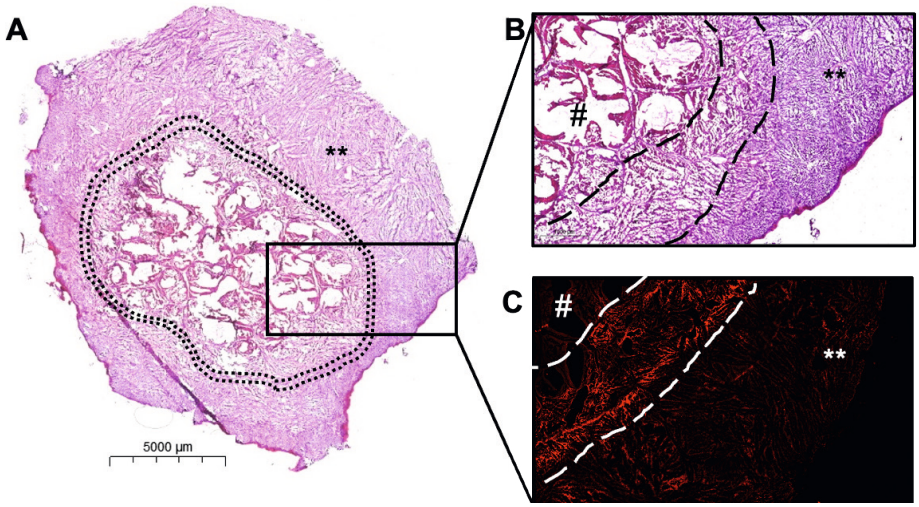

Figure 6. Localization fluorescence signal liver lesions. A) Immunohistochemistry (H&E staining) of an excised liver sample containing healthy liver tissue (**) and a heat-induced liver lesion (encircled). Zoom in of the selected area within the rectangle showing B) a transitional rim (between dashed lines) between necrotic liver tissue (#) and the healthy liver tissue and C) fluorescence confocal imaging in a sequential tissue section with fluorescence uptake (in red) in the transitional rim.

Discussion

By directly conjugating a lipophilic cyanine-5 dye to a mas_3 chelate a hybrid hepatic tracer (*h*HEPATO-Cy5) was generated. This tracer portrays a unique (hepato) biliary excretion profile that could be related to biliary efflux (Figures 1 and 2) in hepatobiliary cultures. In vivo the tracer allowed reliable delineation of liver lesions in real-time using fluorescence-guided robot-assisted surgery in a porcine model (Figure 5).

The hybrid nature of ^{99m}Tc-*h*HEPATO-Cy5 extends fluorescence imaging with the ability to identify preoperative lesions (SPECT). In other oncological surgical applications, this combination has been shown to provide value that is greater than

the sum of the benefit of the individual techniques.[38] Preoperative knowledge of the exact location of the lesion prior to tissue exploration while also providing visual assessment and validation of the excision of the targeted tissue are features that are likely to provide steps towards overcoming existing challenges in hepatobiliary surgery.

While the correlation between nuclear and fluorescence imaging based on *h*HEPATO-Cy5 was provided in mice, constraints within the ethical license prohibited use of radioactivity in the porcine model. As such, the latter only allowed use of the fluorescent readout and subsequent assessment of superficial lesions. Nevertheless, literature indicates that intraoperative extension of fluorescence imaging with in-depth 'drop-in' radioguidance is likely to help facilitate the resection of hepatic lesions that are located deeper below the surface of the liver.[39] This assumption is supported by studies in other clinical indications that clearly provide evidence about the superior in-depth image guidance that can be provided when using a hybrid tracer as compared to a fluorescence only tracer.[38,40]

The mechanism behind ICG uptake in hepatobiliary lesions remains a subject of study. Our work clearly indicates that uptake of *h*HEPATO-Cy5 around a lesion can be contributed to disrupted hepatocytes and is related to the excretion of bile (Figure 1, Figure 2). Further mechanistic studies are needed to help understand how this relates to i.e., multidrug resistance-associated proteins.[22]

Fluorescent emissions used for image-guided surgery are classified into three categories according to the international union of pure and applied chemistry (IUPAC) regulations; near-infrared (NIR), far-red and visible fluorescence.[41] All three have demonstrated clinical potential.[42] Despite the popular demand for NIR analogues (e.g., ICG; $\lambda_{em\ max}$ 750-1000nm), there are clear arguments to be made for the surgical use of far red dyes (e.g., Cy5; $\lambda_{em\ max}$ 650-750nm). For example, Cy5 has a higher brightness and because of that superior tissue penetration.[43] Surprisingly, the latter is quite often falsely referred to as being a NIR dye.[33,44] Using a range of clinical-grade Cy5 camera prototypes has resulted in the successful in-patient use of far-red dyes.[33,35,36,45,46] The depiction of Cy5 fluorescence in vivo (Figure 5) has even been shown to be compatible with imaging of NIR dyes in the same patient allowing unique multicolor imaging strategies.[36,42]

Creating relevant *in vivo* models for the hepatobiliary resection of metastatic lesions is not trivial, especially in porcine models. To the best of our knowledge, this is the first report of such a model that can be used to evaluate image guidance technologies for hepatobiliary lesions. The lesions created displayed a ICG uptake that is in line with literature reports.[22,47] Nevertheless, clinical follow-up studies will be required to confirm the translational value of *h*HEPATO-Cy5.

Conclusion

By creating a small-molecule comprising a fluorescent Cy5 dye and a mas_3 chelate, a unique biliary excreted hybrid tracer has been created. A tracer that is capable of provide both fluorescence- and radio-guidance during excision of liver lesions. The hybrid nature of this tracer also paves the way for the future implementation of nuclear medicine roadmaps to plan and guide fluorescence-based hepatobiliary surgery.

References

1. Balasubramanya R, Selvarajan SK, Cox M, et al. Imaging of ocular melanoma metastasis. *Br J Radiol.* 2016;89:20160092.
2. Carvajal RD, Schwartz GK, Tezel T, Marr B, Francis JH, Nathan PD. Metastatic disease from uveal melanoma: treatment options and future prospects. *Br J Ophthalmol.* 2017;101:38-44.
3. Engstrand J, Nilsson H, Strömberg C, Jonas E, Freedman J. Colorectal cancer liver metastases - a population-based study on incidence, management and survival. *BMC Cancer.* 2018;18:78.
4. Riihimäki M, Hemminki A, Sundquist K, Sundquist J, Hemminki K. The epidemiology of metastases in neuroendocrine tumors. *Int J Cancer.* 2016;139:2679-2686.
5. Wang R, Zhu Y, Liu X, Liao X, He J, Niu L. The Clinicopathological features and survival outcomes of patients with different metastatic sites in stage IV breast cancer. *BMC Cancer.* 2019;19:1091.
6. Nordlinger B, Sorbye H, Glimelius B, et al. Perioperative chemotherapy with FOLFOX4 and surgery versus surgery alone for resectable liver metastases from colorectal cancer (EORTC Intergroup trial 40983): a randomised controlled trial. *Lancet.* 2008;371:1007-1016.
7. Jones AD, Wilton JC. Can intra-operative fluorescence play a significant role in hepatobiliary surgery? *Eur J Surg Oncol.* 2017;43:1622-1627.
8. Gavriilidis P, Roberts KJ, de'Angelis N, Aldrighetti L, Sutcliffe RP. Recurrence and survival following microwave, radiofrequency ablation, and hepatic resection of colorectal liver metastases: A systematic review and network meta-analysis. *Hepatobiliary & Pancreatic Diseases International.* 2021;20:307-314.
9. Lu Q, Zhang J, Gao WM, Lv Y, Zhang XF, Liu XM. Intraoperative Blood Transfusion and Postoperative Morbidity Following Liver Resection. *Med Sci Monit.* 2018;24:8469-8480.
10. Freitas PS, Janicas C, Veiga J, Matos AP, Herédia V, Ramalho M. Imaging evaluation of the liver in oncology patients: A comparison of techniques. *World J Hepatol.* 2021;13:1936-1955.
11. Piccolo G, Barabino M, Pesce A, et al. Role of Indocyanine Green Fluorescence Imaging in Minimally Invasive Resection of Colorectal Liver Metastases. *Surg Laparosc Endosc Percutan Tech.* 2022;32:259-265.
12. Kow AWC. Hepatic metastasis from colorectal cancer. *Journal of Gastrointestinal Oncology.* 2019;10:1274-1298.
13. Ishizawa T, Fukushima N, Shibahara J, et al. Real-time identification of liver cancers by using indocyanine green fluorescent imaging. *Cancer.* 2009;115:2491-2504.
14. Hu Y, Fu T, Zhang Z, Hua L, Zhao Q, Zhang W. Does application of indocyanine green fluorescence imaging enhance clinical outcomes in liver resection? A meta-analysis. *Photodiagnosis Photodyn Ther.* 2021;36:102554.
15. van Leeuwen FWB, Schottelius M, Brouwer OR, et al. Trending: Radioactive and Fluorescent Bimodal/Hybrid Tracers as Multiplexing Solutions for Surgical Guidance. *J Nucl Med.* 2020;61:13-19.
16. Snyder E KS, Lopez PP. Hepatobiliary Iminodiacetic Acid Scan. Accessed Feb 2023, 2023.

17. Marie S, Hernández-Lozano I, Langer O, Tournier N. Repurposing (99m)Tc-Mebrofenin as a Probe for Molecular Imaging of Hepatocyte Transporters. *J Nucl Med.* 2021;62:1043-1047.
18. Franz M, Arend J, Wolff S, et al. Tumor visualization and fluorescence angiography with indocyanine green (ICG) in laparoscopic and robotic hepatobiliary surgery - valuation of early adopters from Germany. *Innov Surg Sci.* 2021;6:59-66.
19. Winkel BMF, de Korne CM, van Oosterom MN, et al. A tracer-based method enables tracking of Plasmodium falciparum malaria parasites during human skin infection. *Theranostics.* 2019;9:2768-2778.
20. Hensbergen AW, Buckle T, van Willigen DM, et al. Hybrid Tracers Based on Cyanine Backbones Targeting Prostate-Specific Membrane Antigen: Tuning Pharmacokinetic Properties and Exploring Dye-Protein Interaction. *J Nucl Med.* 2020;61:234-241.
21. Wonganan P, Jonsson-Schmunk K, Callahan SM, Choi JH, Croyle MA. Evaluation of the HC-04 cell line as an in vitro model for mechanistic assessment of changes in hepatic cytochrome P450 3A during adenovirus infection. *Drug Metab Dispos.* 2014;42:1191-1201.
22. Bunschoten A, van Willigen DM, Buckle T, et al. Tailoring Fluorescent Dyes To Optimize a Hybrid RGD-Tracer. *Bioconjug Chem.* 2016;27:1253-1258.
23. Tanimizu N, Ichinohe N, Sasaki Y, et al. Generation of functional liver organoids on combining hepatocytes and cholangiocytes with hepatobiliary connections ex vivo. *Nat Commun.* 2021;12:3390.
24. Buckle T, Hensbergen AW, van Willigen DM, et al. Intraoperative visualization of nerves using a myelin protein-zero specific fluorescent tracer. *EJNMMI Res.* 2021;11:50.
25. Berehova N, van Meerbeek MP, Azargoshasb S, et al. A Truncated 14-Amino-Acid Myelin Protein-Zero-Targeting Peptide for Fluorescence-Guided Nerve-Preserving Surgery. *Biomolecules.* 2023;13.
26. de Vries HM, Bekers E, van Oosterom MN, et al. c-MET Receptor-Targeted Fluorescence on the Road to Image-Guided Surgery in Penile Squamous Cell Carcinoma Patients. *J Nucl Med.* 2022;63:51-56.
27. Buckle T, Kuil J, van den Berg NS, et al. Use of a single hybrid imaging agent for integration of target validation with in vivo and ex vivo imaging of mouse tumor lesions resembling human DCIS. *PLoS One.* 2013;8:e48324.
28. Gary Hong Chun C, Jemima JB, Maëlle L, Paul G, Christopher JS. ER-PM contacts regulate apical domain formation in hepatocytes. *bioRxiv.* 2020:2020.2004.2023.057521.
29. Wit EMK, KleinJan GH, Berrens AC, et al. A hybrid radioactive and fluorescence approach is more than the sum of its parts; outcome of a phase II randomized sentinel node trial in prostate cancer patients. *Eur J Nucl Med Mol Imaging.* 2023.
30. Meershoek P, van Oosterom MN, Simon H, et al. Robot-assisted laparoscopic surgery using DROP-IN radioguidance: first-in-human translation. *Eur J Nucl Med Mol Imaging.* 2019;46:49-53.
31. van Leeuwen FW, Hardwick JC, van Erkel AR. Luminescence-based Imaging Approaches in the Field of Interventional Molecular Imaging. *Radiology.* 2015;276:12-29.
32. van Willigen DM, van den Berg NS, Buckle T, et al. Multispectral fluorescence guided surgery; a feasibility study in a phantom using a clinical-grade laparoscopic camera system. *Am J Nucl Med Mol Imaging.* 2017;7:138-147.

33. Burggraaf J, Kamerling IM, Gordon PB, et al. Detection of colorectal polyps in humans using an intravenously administered fluorescent peptide targeted against c-Met. *Nat Med.* 2015;21:955-961.

34. Mieog JSD, Achterberg FB, Zlitni A, et al. Fundamentals and developments in fluorescence-guided cancer surgery. *Nat Rev Clin Oncol.* 2022;19:9-22.

35. Zanoni DK, Stambuk HE, Madajewski B, et al. Use of Ultrasmall Core-Shell Fluorescent Silica Nanoparticles for Image-Guided Sentinel Lymph Node Biopsy in Head and Neck Melanoma: A Nonrandomized Clinical Trial. *JAMA Netw Open.* 2021;4:e211936.

36. van Beurden F, van Willigen DM, Vojnovic B, et al. Multi-Wavelength Fluorescence in Image-Guided Surgery, Clinical Feasibility and Future Perspectives. *Mol Imaging.* 2020;19:1536012120962333

37. van der Vorst JR, Schaafsma BE, Hutteman M, et al. Near-infrared fluorescence-guided resection of colorectal liver metastases. *Cancer.* 2013;119:3411-3418.

8

The rise of molecular image-guided robotic surgery

Future perspectives

Adapted from:
Fijs W.B. van Leeuwen, Tessa Buckle, Matthias N. van Oosterom,
Daphne D.D. Rietbergen.

J Nucl Medicine 2024. Online ahead of print

Abstract

Following early acceptation by urologists, the use of surgical robotic platforms is rapidly spreading to other surgical fields of application. The fact that the empowerment of surgical perception via robotic advances occurs in parallel to the developments in intraoperative implementation of molecular imaging indicates there is a logical incentive to pursue image-guided robotics (IGR). A field that exploits the symbiosis between robotics and imaging to progress surgical precision with both advanced surgical dexterity and surgical decision making. In this review, topic related developments in chemistry (tracer development) and engineering (device development) are discussed and future (scientific) growth markets for molecular imaging are presented.

Introduction

Today's robotic surgery paradigm is the direct result of a decades long initiative towards minimally invasive treatment strategies. The enhanced dexterity and ergonomics that lie at the robot's core has motivated an increasing number of surgical disciplines to pursue its implementation. This has resulted in a global growth market for robotic surgery that already extends to the use of >7500 robotic systems in ≈11 million surgeries so far.[1] Currently the standard is set by the da Vinci platform, which standardly incorporates a stereoscopic fluorescence camera. However, an increasing number of alternative robotic platforms – none of them appear to display compelling disruptive features – are, or have already been, translated into the clinical setting.[2] The surgical use of robots has also evoked scientific interest; the number of publications related to robotic surgery has shown a steep upward trend since 2000 (2000-2004: 704 publications vs. 2019-2023: 19.018 publications; search term "robotic surgery" in Pubmed).

In parallel to the development of robotic platforms, the surgical field is benefitting from the rise of intraoperative molecular imaging (IMI). An imaging discipline that facilitates enhancement of the surgical perception by exploiting, most commonly, radio- and fluorescence guidance. This helps improve surgical accuracy and (oncological) outcomes but can also lead to a reduction of the number and severity of surgically-induced complications. Opportunely, the intents of robotic surgery to increase surgical dexterity, and IMI to augment surgical perception, converge, yielding the sub-discipline of image-guided robotics (IGR). Activities in this sub-discipline are exemplified with surgical guidance by the use of radiopharmaceuticals (e.g., for identification of nodal involvement in oncology)[3,4] and fluorescent dyes (e.g., visualization of physiological measures in anastomosis or lymphangiography)[5,6]. An over-arching factor herein is that all these approaches have proven to be highly reliant on the insights provided by preoperative 'roadmaps' based on SPECT-CT and/or PET-CT-images.[4] Herein the general emphasis seems to lie on the use of the gamma-emitting radioisotope ^{99m}Tc and the approved near-infrared (NIR) dye indocyanine green (ICG), but other isotopes and fluorescent dyes have also been successfully used.[6,7] Best-of-both worlds IMI scenarios are offered by approaches that combine the benefits provided by radiopharmaceuticals (quantitative (pharmacokinetic) measures and in-depth detection) and fluorescent dyes (video-rate imaging and <1cm superficial detection).[7,8] For example, the initial successes with hybrid sentinel node approaches in prostate cancer patients[9] have instigated the dissemination of this technique in other robotic-surgery indications such as cervical[10], vulvar[11], oral cavity[11], bladder[12] and penile cancer[11].

In a highly interactive environment such as surgery, decision making is based on the perception of the surgeon. This perception drives the surgical actions and is defined

by the surgeons' sensory responses in relation to the patient-environment. A concept that can be illustrated using an example provided by Bogh et al.[13] This example shows that shape recognition based on static imaging content only provides a 49% accuracy in object recognition, while rotating 3D vision was shown to enrich perception, with a corresponding increase to 72%. Addition of tactile information (sensing) was shown to result in an eventual 99% accuracy. These insights in interactive perception can be effectively translated to IGR. To this end, static images allow identification of (radio)pharmaceutical-avid surgical targets, but require complementary imaging/sensing technologies that support interactive tissue interpretation to enhance the level of perception. Digitization of multi-sensory data, combined with the use of artificial intelligence (AI), thereby offers additional advantages that pave the way towards a future wherein perception-enhanced performance helps realize robotic autonomy. For example, via autonomous implementation of image-guidance to a surgical perception level that precedes that of surgeons.

In this review key perception enhancing components in IGR are addressed that provide a means to advance the field of minimal invasive robotic surgery from an imaging perspective (Figure 1). Key components such as (radio)pharmaceuticals for target definition, perception enhancement, digitization of data streams, technology assessment and automation are discussed and their place in molecular image-guided surgery is emphasized.

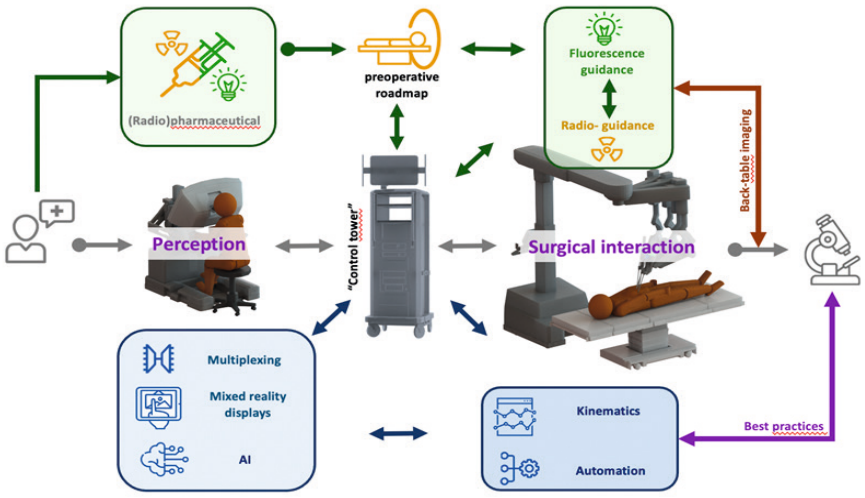

Figure 1. Systems engineering components in the field of image guided robotics

(Radio)pharmaceuticals for target definition

Perception starts with the ability to separate a target tissue from its surroundings. In IMI this separation is enabled via the use of (radio)pharmaceuticals that specifically highlight anatomical or disease-specific features. The development of such pharmaceuticals finds its origin in radioimmunoguided surgery, a concept that was introduced in the late nineties and that covers both receptor targeted and physiology-based approaches.[14] Physiology based imaging has particularly benefitted from the pharmacokinetic properties of clinically approved fluorescent dyes such as ICG and fluorescein.[6] Today, the use of fluorescence is actively being expanded towards receptor-targeted applications as well. This generally results in fluorescent analogues of receptor-targeted radiotracers used in diagnostic nuclear medicine. Emergence of new imaging targets supports dissemination of IGR to the indications that currently make up the robotic surgery market (Urology 23%, Gynecology 23%, General surgery 19%, Cardiothoracic surgery 9% and other indications 26%; Figure 2).

The ability to sensitively detect radiopharmaceuticals when applied within a micro-dosing regimen (≤100µg/patient) greatly facilitates the translational aspects of radioguided surgery efforts.[15] Studies in nuclear medicine indicate that accurate dosing influences the quality of imaging data, whereby an increase in dosing tends to negatively affect obtained results.[16] A word of caution herein is that a combination of small lesions, low receptor expression levels, and suboptimal tracer affinities could still result in false negative results. Fluorescent tracer derivatives tend to be more translationally impaired as their inferior detection sensitivity often needs to be compensated for by applying therapeutic dosing (mg/kg).[17] Recent dosing studies with the fluorescent PSMA-targeting agents IS-002 and OTL78 indicate that the use of high doses tends to result in oversaturation, which not only negatively affects signal-to-background-ratios (SBR), but also induces false positives.[18,19]

It is considered beneficial for the surgical perception when diagnostic 3D images, provided at nuclear medicine, can be substantiated with dynamic intraoperative tracing/imaging findings. The correlation between pre- and intra-operative findings is, among others, supported by the availability of theranostic pairs of (radio)pharmaceuticals that can be used at the same, or similar, dosing. A textbook example for such a "theranostic" pair is ^{68}Ga-/^{18}F-PSMA-PET (for diagnostics) and ^{99m}Tc- /^{111}In-PSMA (for surgical radiotracing).[3] Important to realize is that surgical radiotracing is not expected to reliably detect lesions not visible in, e.g., preoperative PET-CT roadmaps.[20] In a similar fashion, to facilitate the resection of gastroenteropancreatic neuroendocrine tumors, theranostic pairs that employ somatostatin-targeted (SSTR) neuroendocrine tumor (NET) targeting could be used withfor example ^{68}Ga-DOTATOC and ^{99m}Tc-EDDA/HYNIC-octreotate.[21] Looking ahead, various other diagnostic PET-radiopharmaceuticals have ^{99m}Tc containing analogues

and could therefore be exploited as theranostic pairs for surgery. Examples are ^{99m}Tc-Pentixafor (target: chemokine receptor-4 (CXCR4) expressed on e.g., glioblastoma)[22], ^{99m}Tc-FAPI 34 (target: fibroblast antigen protein (FAP), involved in >28 different cancer types)[23], ^{99m}Tc-folate (target: folate receptor)[24], ^{99m}Tc-DB15 (target: gastrin-releasing peptide receptor)[25], ^{99m}Tc-IMMU-4Fab' (target: Carcinoembryonic antigen)[26] and a variety of targets and radioisotopes previously pursued in radioimmunoguided surgery initiatives.[27] As sensitivity and dosing seem to play a critical role in achieving a correlated pre- and intraoperative accuracy, it will be complex to make well correlated theranostic pairs made up out of, e.g., PET- and purely fluorescent-agents. This is certainly true for small molecules, but may be less relevant for monoclonal antibodies, making it a topic in need of further investigation. Here hybrid agents that contain both a radioactive and fluorescent component can provide outcome.[8]

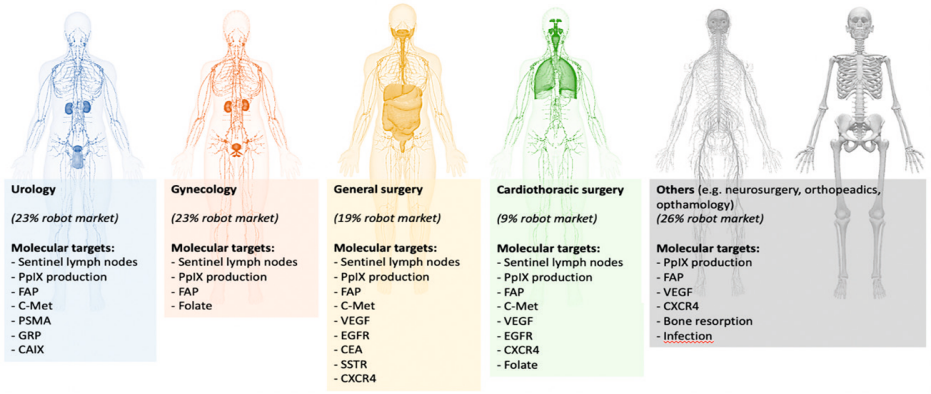

Figure 2. Targets for intraoperative molecular imaging in relation to the main surgical fields that employ robotics

Perception enhancing modalities

Technologies that enrich the robots' perceptual abilities (e.g., sensing and vision) will help improve the level of surgical perception. Given the fact that tissue tends to move during surgery, static images only provide limited guidance. Generating a demand for vision and sensing based intraoperative scanning technologies. To implement these modalities in the minimally invasive robotic setting, a variety of physical constraints need to be overcome, e.g., accessibility of the target, the perception of stiffness during the performance of surgical maneuvers (i.e., the fulcrum effect)[28], a remote center of motion and limited freedom of movement.

Robotic vision is facilitated via system-integrated endoscopes that provide three-dimensional (3D) video streams of the surgical field. These endoscopes include traditional white light imaging, and in some cases fluorescence imaging (e.g., the

Firefly™ cameras on the da Vinci Si, X, Xi and SP systems [29] and the TIPCAM® Rubina video-endoscope on the HUGO™ RAS system)[30]. The integration of fluorescence imaging and the ability to identify (moving) tissues at video-rate has instigated a paradigm shift towards the acceptance of fluorescence guidance in surgery.

As stated earlier, perception is optimal when vision is combined with a sense of touch (e.g., palpation/pressure, temperature sensation and/or pain). Unfortunately, the manipulating instruments of, e.g., the da Vinci platform are deprived of such sensations. A logical step in IGR design is to enrich robotic manipulators with a sense of 'touch' (Figure 3A). Allowing them to fulfill a role as surrogate for the surgeons' hands. An advantage of robot platforms is that they can be technically enhanced to allow molecular sensing capabilities. Thus, supporting detection of (radio)pharmaceuticals. This creates a sensory experience that is beyond human abilities. The first steps toward realizing such sensory-enrichment have already been made with the now CE-marked tethered drop-in gamma probe and the pursuit of click-on sensors that can be applied directly onto the surgical tool (Figure 3B). [31-33] The provided numerical and acoustic sensory readout demonstrated perception enhancing in applications that also employed fluorescence-vision.[34] (Pre)clinical evaluation indicates that sensory-enrichment can be applied for a variety of molecular imaging signatures, for example: beta particles, Raman spectroscopy, mass spectrometry, fluorescence and fluorescence lifetime.[31,35,36]

In contrast to the above stated efforts set to enhance the surgeon's perception during the intervention, off-line back-table (*ex vivo*) assessments are also increasingly being proposed for IGR.[37] Promising examples include the use of Cerenkov imaging, small-bore PET systems and freehand tissue scanning.[38,39] While presenting a confirmatory value regarding target removal, it remains difficult to relate these measurements to the context of the surgical wound.[37]

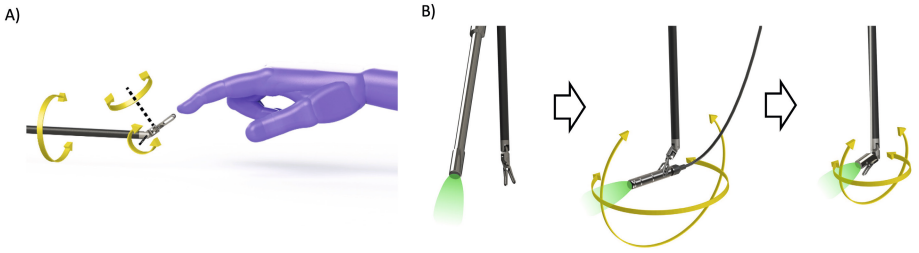

Figure 3. Enhancing perception by combining vision with sensory information: A) Vision and sensing, translating concepts from man-to-robot, B) Evoilution of (gamma) probes in an effort to molecular-sensing capapbilities in robotic instruments.

Digitization of data-streams

Uniquely, surgical robots provide the hardware and the computing power that supports data-integration. Digital operating platforms thereby provide a means to incorporate, and multiplex, multi-sensory device inputs.[40] Input that can be converted to outputs presented in forms such as highlighting of findings and sending of alerts. Digitization facilitates the merging and absorption of a wide range of data streams, including data streams that are not related to imaging. When combined with smart algorithms, pre-, intra- and post-surgical data streams can be processed to unmatched levels of complexity (Figure 4A). All these then come together in a single 'control tower' that helps to redefine how surgery is analyzed and (could be) performed.[41]

The most straightforward example of imaging data integration during robotic surgery is the split-screen visualization of preoperatively acquired imaging 'roadmaps' (e.g., CT, a lymphoscintigraphic or SPECT/CT images) directly next to the surgical video feed.[31] A strategy that helps to actively relate diagnostic imaging information (static images) to the dynamic surgical environment. This can be further enhanced via the employment of mixed reality (MR) overlays whereby the preoperative images are overlayed onto the surgical video-feed (Figure 4B).[42] Currently this strategy is most widely employed using radiological images (CT and MRI). Nevertheless, there are also examples where images generated at nuclear medicine are being displayed over a (fluorescence enhanced) video feed.[43] Active positional tracking of both instruments and the patient anatomy support "gps-like" directional guidance (Figure 4C). Such navigation strategies are already routinely applied during surgeries where image-to-patient registration can be realized using rigid landmarks (e.g., orthopedics-, skull-, and neurosurgery).[44] Unfortunately, implementation of image-to-patient registration during surgery in soft-tissue indications is still hampered by challenges related to deformations caused by positioning, insufflation, breathing, and the tissue movement caused by the surgical manipulation itself. This stresses the need for surgical modalities such as fluorescence imaging or gamma tracing that can confirm or correct the navigation accuracy in real-time.[43] Uniquely, the active tracking of the drop-in gamma probe during the surgical act has opened the possibility to register its intra-abdominal readout with its positional location. This feature, when complemented with "freehand" image-reconstruction algorithms, can enable an interaction-facilitated MR vision enhancement called robot-assisted SPECT (Figure 4B).[45] A tomographic form of digital vision enhancement that could in the future also benefit other robotic sensing modalities.

In surgical practice, it often remains challenging to interpret the collected data, leading to false-negative (missed lesions) or false-positive (resection healthy tissue) results. In this context computer vision algorithms, e.g., artificial intelligence (AI) strategies, can help support high-end feature extraction such as anatomy

recognition, instrument segmentation (Figure 4C-D) and fluorescence intensity interpretation.[46,47]

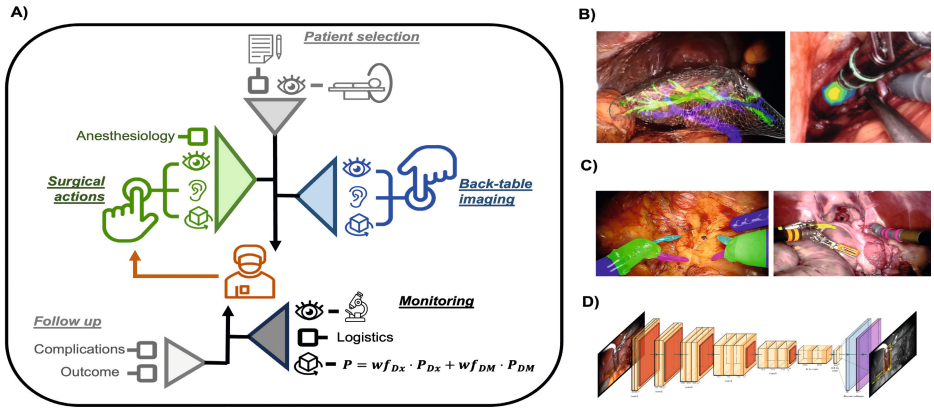

Figure 4. Digital surgery: A) Multiplexing of surgery related data-streams and their interaction with the surgeon, B) Robotic instrument tracking technologies, c) Mixed reality visualizations, and D) Use of Artificial intelligence (AI) for automated image analysis in surgical video feeds.

Technology assessment

The societal incentive for the use of robotics is to offer precision enhancement and a decrease in short- and long-term complications. These features are not defined by first-in-human proof-of-concept data, but rather by multivariate (health) technology assessments performed over a prolonged period of time.[48] Assessment of the patient benefit embodies traditional outcome measures such as (randomized) retrospective analysis of databases for complications, quality-adjusted life years (QALY's) and disease-free survival (DFS). For example, QALY's have been used to clarify for which indications robotic surgery may (e.g., for prostatectomy)[49] or may not (e.g., for cystectomy)[50] result in performance-enhancement. The ability to provide high-end evidence on benefits for the patient and/or the treating physicians not only drives technological dissemination, but also defines the ability to make a healthy business case for a technology.[51] In this respect, shifting focus to the field of IMI, immediately exposes a challenge as long-term technological assessments are rarely reported. Exceptions are SN, 5-ALA, and PSMA-RGS procedures, and only the latter has been evaluated in the context of IGR.[3,9,52] Therefore, further indicating steps towards the direction of performance assessment is still a necessity.

Unfortunately, traditional long-term patient outcome measures do not match well with the speed at which R&D activities are being conducted. Assuming the goal of IGR is to use perception-enhancement to advance the interaction between the

surgeon and the patient, one can even claim that traditional measures provide an indirect measure for the technological impact. Hence an alternative performance assessment strategy is desirable. If we look at the way technological enhancement is assessed in areas such as (motor) sports, it becomes clear that movement kinematics can help provide a wealth of quantitative readouts for efficiency optimization. As the surgeons' skills are defined by dexterity (gesture) and decision making (perception)[53], extraction of multi-dimensional kinematic metrics related to instrument movement (e.g. speed, pathlength, jerkiness, directionality) provides a means to objectively assess how technologies alter the surgeons interaction with the patient.[46,54] Recently, such strategies have been successfully exploited to quantify how ques based on (radio)pharmaceutical signal intensities and signal-to-background ratios impact the surgical decision making. [46,55]

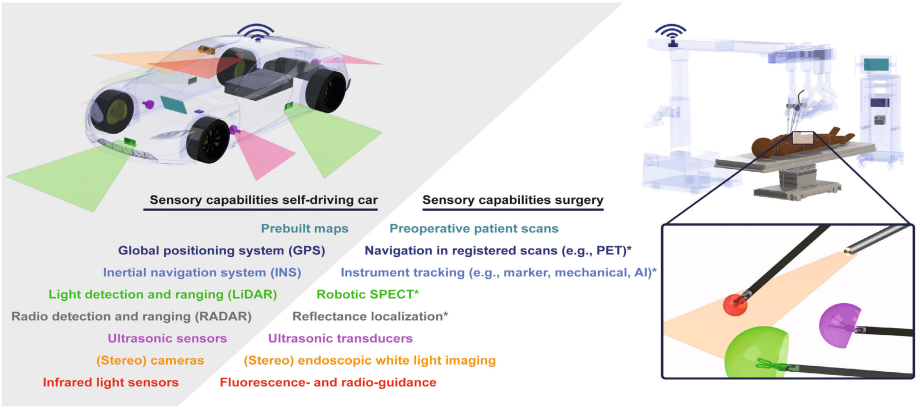

Figure 5. Sensory experiences in self-driving cars vs. the matching available, but often experimental, robotic surgery technologies. **Technology in research setting*

Automation

For most, the term robotics goes together with the term automation. Nevertheless, today's tele-operative systems are classified as having no Level of Autonomy (LoA-0). Meaning that the motions along the robotic links and joints remain fully controlled by the operating surgeon. This while the growing shortage in skilled surgical personnel, the ever-increasing procedural complexity, and rising healthcare costs provide an incentive to move decision-making away from human supervisors.[56] Fully autonomous robots (LoA-5), thereby, promise to democratize surgery, help make surgical quality ubiquitous, standardize outcomes, and reduce recurrences.

Beyond healthcare, perhaps the most well-known example of supervised autonomy is adaptive cruise control in a car (LoA-1). A clinical situation where specific surgical subtasks are outsourced to the robot is the use of the AquaBeam system for

treatment of the urinary tract.[56] For cars to advance to a higher LoA, they require an exceptional level of sensory-enrichment coupled to AI-advanced data-computing (Figure 5).[57] Subsequently, the active interaction between the components of data-acquisition, -processing and automated perception assessments (i.e., decision making) allow vehicles to cope with environmental variations. Translation of these concepts to a surgical robot demands a more intelligent interaction between the robot and the surgical environment, as facilitated by (molecular) imaging/sensing (Figure 5).[58] Considering how easy it is for surgeons to overlook tumor fragments during surgery, control strategies that raise the diagnostic accuracy seem to provide an obvious starting point when exploring surgical automation.[59] Over time such efforts will help, amongst others, to transfer the above mentioned 'freehand' IGR technologies into 'hands-free' technologies that empower surgeons in their perception.

The rise of autonomous vehicles poses obvious questions with regards to, e.g., liability and ethics.[60] These topics are critically being looked at by today's lawmakers, starting with the regulations concerning the use of AI. As the act of surgery is very fault intolerant, emphasis should be put on these dilemmas when entrusting robots to reliably identify, and quickly react to, unpredictable clinical situations.[56]

Conclusion

The rise of IGR offers the field of IMI unique (out-of-the-box) growth capabilities. Not only in the traditional terms of (radio)pharmaceuticals, engineering, physics and expanding clinical indications, but also in terms of embracing up-and-coming digital-, performance-guided, and autonomous-surgery paradigms. Exploration of these opportunities will expand the impact that nuclear medicine and molecular imaging have on the future of patient care.

References

1. Guthart G. J.P. Morgan Healthcare Conference. Accessed 03/08, 2024.
2. Bhandari M, Zeffiro T, Reddiboina M. Artificial intelligence and robotic surgery: current perspective and future directions. *Current Opinion in Urology.* 2020;30.
3. Berrens AC, Knipper S, Marra G, et al. State of the Art in Prostate-specific Membrane Antigen-targeted Surgery-A Systematic Review. *Eur Urol Open Sci.* 2023;54:43-55.
4. Valdés Olmos RA, Rietbergen DDD, Rubello D, et al. Sentinel Node Imaging and Radioguided Surgery in the Era of SPECT/CT and PET/CT: Toward New Interventional Nuclear Medicine Strategies. *Clinical Nuclear Medicine.* 2020;45.
5. Lee YJ, van den Berg NS, Orosco RK, Rosenthal EL, Sorger JM. A narrative review of fluorescence imaging in robotic-assisted surgery. *Laparosc Surg.* 2021;5.
6. van Beurden F, van Willigen DM, Vojnovic B, et al. Multi-Wavelength Fluorescence in Image-Guided Surgery, Clinical Feasibility and Future Perspectives. *Mol Imaging.* 2020;19:1536012120962333.
7. Van Oosterom MN, Rietbergen DDD, Welling MM, Van Der Poel HG, Maurer T, Van Leeuwen FWB. Recent advances in nuclear and hybrid detection modalities for image-guided surgery. *Expert Rev Med Devices.* 2019;16:711-734.
8. van Leeuwen FWB, Schottelius M, Brouwer OR, et al. Trending: Radioactive and Fluorescent Bimodal/Hybrid Tracers as Multiplexing Solutions for Surgical Guidance. *J Nucl Med.* 2020;61:13-19.
9. Mazzone E, Dell'Oglio P, Grivas N, et al. Diagnostic Value, Oncological Outcomes And Safety Profile Of Image-Guided Surgery Technologies During Robot-Assisted Lymph Node Dissection with Sentinel Node Biopsy For Prostate Cancer. *J Nucl Med.* 2021.
10. Paredes P, Vidal-Sicart S, Campos F, et al. Role of ICG-99m Tc-nanocolloid for sentinel lymph node detection in cervical cancer: a pilot study. *European journal of nuclear medicine and molecular imaging.* 2017;44:1853-1861.
11. KleinJan G, Van Werkhoven E, van Den Berg N, et al. The best of both worlds: a hybrid approach for optimal pre-and intraoperative identification of sentinel lymph nodes. *European journal of nuclear medicine and molecular imaging.* 2018;45:1915-1925.
12. Rietbergen DDD, van Gennep EJ, KleinJan GH, et al. Evaluation of the Hybrid Tracer Indocyanine Green–99mTc-Nanocolloid for Sentinel Node Biopsy in Bladder Cancer—A Prospective Pilot Study. *Clinical Nuclear Medicine.* 2022;47.
13. Bohg J, Hausman K, Sankaran B, et al. Interactive Perception: Leveraging Action in Perception and Perception in Action. *IEEE Transactions on Robotics.* 2017;33:1273-1291.
14. Sun D, Bloomston M, Hinkle G, et al. Radioimmunoguided surgery (RIGS), PET/CT image-guided surgery, and fluorescence image-guided surgery: Past, present, and future. *Journal of Surgical Oncology.* 2007;96:297-308.
15. Fleming GA. 12 Regulatory Considerations for Early Clinical Development. *Translational Research Methods for Diabetes, Obesity and Cardiometabolic Drug Development: A Focus on Early Phase Clinical Studies.* 2014:283.
16. Luurtsema G, Pichler V, Bongarzone S, et al. EANM guideline for harmonisation on molar activity or specific activity of radiopharmaceuticals: impact on safety and imaging quality. *EJNMMI Radiopharmacy and Chemistry.* 2021;6:34.

17. KleinJan GH, Bunschoten A, van den Berg NS, et al. Fluorescence guided surgery and tracer-dose, fact or fiction? *Eur J Nucl Med Mol Imaging.* 2016;43:1857-1867.
18. Nguyen HG, van den Berg NS, Antaris AL, et al. First-in-human Evaluation of a Prostate-specific Membrane Antigen-targeted Near-infrared Fluorescent Small Molecule for Fluorescence-based Identification of Prostate Cancer in Patients with High-risk Prostate Cancer Undergoing Robotic-assisted Prostatectomy. *Eur Urol Oncol.* 2023.
19. Stibbe JA, de Barros HA, Linders DGJ, et al. First-in-patient study of OTL78 for intraoperative fluorescence imaging of prostate-specific membrane antigen-positive prostate cancer: a single-arm, phase 2a, feasibility trial. *Lancet Oncol.* 2023;24:457-467.
20. van Leeuwen FWB, Winter A, van Der Poel HG, et al. Technologies for image-guided surgery for managing lymphatic metastases in prostate cancer. *Nat Rev Urol.* 2019;16:159-171.
21. Cockburn KC, Toumi Z, Mackie A, Julyan P. Radioguided Surgery for Gastroenteropancreatic Neuroendocrine Tumours: a Systematic Literature Review. *Journal of Gastrointestinal Surgery.* 2021;25:3244-3257.
22. Konrad M, Rinscheid A, Wienand G, et al. [(99m)Tc]Tc-PentixaTec: development, extensive pre-clinical evaluation, and first human experience. *Eur J Nucl Med Mol Imaging.* 2023;50:3937-3948.
23. Trujillo-Benítez D, Luna-Gutiérrez M, Ferro-Flores G, et al. Design, Synthesis and Preclinical Assessment of (99m)Tc-iFAP for In Vivo Fibroblast Activation Protein (FAP) Imaging. *Molecules.* 2022;27.
24. Galt JR, Halkar RK, Evans CO, et al. In vivo assay of folate receptors in nonfunctional pituitary adenomas with 99mTc-folate SPECT/CT. *J Nucl Med.* 2010;51:1716-1723.
25. Nock BA, Kaloudi A, Kanellopoulos P, et al. [(99m)Tc]Tc-DB15 in GRPR-Targeted Tumor Imaging with SPECT: From Preclinical Evaluation to the First Clinical Outcomes. *Cancers (Basel).* 2021;13.
26. Lechner P, Lind P, Snyder M, Haushofer H. Probe-guided surgery for colorectal cancer. *Recent Results Cancer Res.* 2000;157:273-280.
27. Povoski SP, Neff RL, Mojzisik CM, et al. A comprehensive overview of radioguided surgery using gamma detection probe technology. *World journal of surgical oncology.* 2009;7:1-63.
28. Nisky I, Huang F, Milstein A, Pugh CM, Mussa-Ivaldi FA, Karniel A. Perception of stiffness in laparoscopy - the fulcrum effect. *Stud Health Technol Inform.* 2012;173:313-319.
29. Meershoek P, KleinJan GH, van Willigen DM, et al. Multi-wavelength fluorescence imaging with a da Vinci Firefly-a technical look behind the scenes. *J Robot Surg.* 2021;15:751-760.
30. Raffaelli M, Gallucci P, Voloudakis N, et al. The new robotic platform Hugo™ RAS for lateral transabdominal adrenalectomy: a first world report of a series of five cases. *Updates in Surgery.* 2023;75:217-225.
31. van Oosterom MN, Azargoshasb S, Slof LJ, van Leeuwen FWB. Robotic radioguided surgery: toward full integration of radio- and hybrid-detection modalities. *Clinical and Translational Imaging.* 2023.
32. Azargoshasb S, van Alphen S, Slof LJ, et al. The Click-On gamma probe, a second-generation tethered robotic gamma probe that improves dexterity and surgical decision-making. *Eur J Nucl Med Mol Imaging.* 2021;48:4142-4151.
33. van Oosterom MN, van Leeuwen SI, Mazzone E, et al. Click-on fluorescence detectors: using robotic surgical instruments to characterize molecular tissue aspects. *Journal of Robotic Surgery.* 2023;17:131-140.

34. Dell'Oglio P, Meershoek P, Maurer T, et al. A DROP-IN Gamma Probe for Robot-assisted Radioguided Surgery of Lymph Nodes During Radical Prostatectomy. *Eur Urol.* 2021;79:124-132.
35. Collamati F, Morganti S, van Oosterom MN, et al. First-in-human validation of a DROP-IN β-probe for robotic radioguided surgery: defining optimal signal-to-background discrimination algorithm. *European Journal of Nuclear Medicine and Molecular Imaging.* 2024:1-11.
36. Gorpas D, Phipps J, Bec J, et al. Autofluorescence lifetime augmented reality as a means for real-time robotic surgery guidance in human patients. *Scientific reports.* 2019;9:1187.
37. Dell'Oglio P, Mazzone E, Buckle T, et al. Precision surgery: the role of intra-operative real-time image guidance - outcomes from a multidisciplinary European consensus conference. *Am J Nucl Med Mol Imaging.* 2022;12:74-80.
38. Fragoso Costa P, Shi K, Holm S, et al. Surgical radioguidance with beta-emitting radionuclides; challenges and possibilities: a position paper by the EANM. *European journal of nuclear medicine and molecular imaging.* 2024:1-19.
39. van Oosterom MN, Meershoek P, Welling MM, et al. Extending the Hybrid Surgical Guidance Concept With Freehand Fluorescence Tomography. *IEEE Trans Med Imaging.* 2020;39:226-235.
40. Wendler T, van Leeuwen FWB, Navab N, van Oosterom MN. How molecular imaging will enable robotic precision surgery. *European Journal of Nuclear Medicine and Molecular Imaging.* 2021;48:4201-4224.
41. Lam K, Abràmoff MD, Balibrea JM, et al. A Delphi consensus statement for digital surgery. *npj Digital Medicine.* 2022;5:100.
42. Parekh P, Patel S, Patel N, Shah M. Systematic review and meta-analysis of augmented reality in medicine, retail, and games. *Visual Computing for Industry, Biomedicine, and Art.* 2020;3:21.
43. van Oosterom MN, van der Poel HG, Navab N, van de Velde CJH, van Leeuwen FWB. Computer-assisted surgery: virtual- and augmented-reality displays for navigation during urological interventions. *Current Opinion in Urology.* 2018;28.
44. Picard F, Deakin AH, Riches PE, Deep K, Baines J. Computer assisted orthopaedic surgery: Past, present and future. *Medical Engineering & Physics.* 2019;72:55-65.
45. Azargoshasb S, Berrens A-C, Slof LJ, et al. Robot-assisted Single Photon Emission Computed Tomography: Integrating Nuclear Medicine in Robotic Urologic Surgery. *European urology.* 2024:S0302-2838 (0324) 00064-00062.
46. Azargoshasb S, de Barros HA, Rietbergen DDD, et al. Artificial Intelligence-Supported Video Analysis as a Means to Assess the Impact of DROP-IN Image Guidance on Robotic Surgeons: Radioguided Sentinel Lymph Node versus PSMA-Targeted Prostate Cancer Surgery. *Advanced Intelligent Systems.* 2023;5:2300192.
47. Madani A, Namazi B, Altieri MS, et al. Artificial Intelligence for Intraoperative Guidance: Using Semantic Segmentation to Identify Surgical Anatomy During Laparoscopic Cholecystectomy. *Ann Surg.* 2022;276:363-369.
48. Reeves B. Health-technology assessment in surgery. *The Lancet.* 1999;353:S3-S5.
49. Lindenberg MA, Retèl VP, van der Poel HG, Bandstra F, Wijburg C, van Harten WH. Cost-utility analysis on robot-assisted and laparoscopic prostatectomy based on long-term functional outcomes. *Sci Rep.* 2022;12:7658.

50. Michels CTJ, Wijburg CJ, Hannink G, Witjes JA, Rovers MM, Grutters JPC. Robot-assisted Versus Open Radical Cystectomy in Bladder Cancer: An Economic Evaluation Alongside a Multicentre Comparative Effectiveness Study. *Eur Urol Focus.* 2022;8:739-747.
51. Farinha R, Puliatti S, Mazzone E, et al. Potential Contenders for the Leadership in Robotic Surgery. *J Endourol.* 2022;36:317-326.
52. Gandhi S, Tayebi Meybodi A, Belykh E, et al. Survival outcomes among patients with high-grade glioma treated with 5-aminolevulinic acid–guided surgery: A systematic review and meta-analysis. *Frontiers in oncology.* 2019;9:620.
53. Spencer F. Teaching and measuring surgical techniques: the technical evaluation of competence. *Bull Am Coll Surg.* 1978;63:9-12.
54. Hung AJ, Ma R, Cen S, Nguyen JH, Lei X, Wagner C. Surgeon automated performance metrics as predictors of early urinary continence recovery after robotic radical prostatectomy—a prospective bi-institutional study. *European urology open science.* 2021;27:65-72.
55. Azargoshasb S, Boekestijn I, Roestenberg M, et al. Quantifying the Impact of Signal-to-background Ratios on Surgical Discrimination of Fluorescent Lesions. *Mol Imaging Biol.* 2023;25:180-189.
56. Jamjoom AAB, Jamjoom AMA, Thomas JP, et al. Autonomous surgical robotic systems and the liability dilemma. *Front Surg.* 2022;9:1015367.
57. Babak S-J, Hussain SA, Karakas B, Cetin S. Control of autonomous ground vehicles: a brief technical review. *IOP Conference Series: Materials Science and Engineering.* 2017;224:012029.
58. Hashimoto DA, Rosman G, Rus D, Meireles OR. Artificial Intelligence in Surgery: Promises and Perils. *Ann Surg.* 2018;268:70-76.
59. Attanasio A, Scaglioni B, Momi ED, Fiorini P, Valdastri P. Autonomy in Surgical Robotics. *Annual Review of Control, Robotics, and Autonomous Systems.* 2021;4:651-679.
60. Pattinson J-A, Chen H, Basu S. Legal issues in automated vehicles: critically considering the potential role of consent and interactive digital interfaces. *Humanities and Social Sciences Communications.* 2020;7:153.

9

Summary, discussion and future perspectives

Summary, discussion and future perspectives

Preoperative imaging of solid tumors is the cornerstone of adequate staging in cancer diagnosis. Patients with cN0 or preoperative staging imaging without lymph node involvement (iN0M0) may undergo curative surgery. In many solid tumors, the sentinel lymph node procedure (SN) helps to determine if micrometastatic lymph nodes are involved, leading to adequate staging and appropriate treatment choices.

During surgical procedures, the surgeon explores the operating field for target lesions of interest; both the primary tumor and the SN. In the bloodied operating field, small targets, such as the SN, are not always easy to find. Especially not in areas with difficult anatomy or richly vascularized and nerve-fed areas. Searching for this SN in these challenging areas can lead to unnecessary removal of healthy tissue with associated morbidities, incomplete resections (R1 resections), or a longer duration of surgery.

Accurate preoperative imaging, surgical planning, and intraoperative tools to guide the surgeon to the desired lesion can overcome these problems. Hybrid SN tracers have been shown to offer the best in both pre- and intraoperative lesion detection.

Section 1 of this thesis focuses on clinical application with combined pre- and intraoperative imaging, using the hybrid SN-tracer ICG-^{99m}Tc-nanocolloid, alone or in comparison to other radioactive tracers, for novel potential clinical indications. This section also focuses on ^{99m}Tc-Tilmanocept, a new generation SN tracer.

Chapter 2 provides an overview of interventional nuclear medicine using existing and new tracers and different detection modalities that discuss the needs for and key indications of radioguided surgery (e.g., lymphatic mapping, creator delivery, and targeted tracer development) with respect to chemical and engineering initiatives.

Chapters **3 and 4** compare other radiocolloids of different particle sizes with the hybrid tracer ICG-^{99m}Tc nanocolloid, which is based on the most widely used colloid particle size in Europe. In the clinical study, described in **Chapter 3**, lymphoscintigraphic drainage patterns, including SN and non-SLN of ^{99m}Tc-Senti-Scint and the standard tracer ICG-^{99m}Tc-nanocolloid, are compared in patients with melanoma of the head and neck and truck.

In **Chapter 4**, drainage patterns, SN visualization and non-SN visualization of a relatively new kid on the block, ^{99m}Tc-Tilmanocept, a manose receptor binding tracer, are presented and discussed for SN procedures in patients with breast cancer and melanoma.

Based on a prospective pilot study in patients with muscle-invasive bladder cancer, **Chapter 5** describes the feasibility of SN targeting using the hybrid tracer indocyaninegreen (ICG)^{99m}Tc-nanocolloid for preoperative imaging and concomitant intraoperative radioconduction and fluorescence conduction.

Section 2 describes innovations in the field of radioguided surgery.

In a preclinical setting, **Chapter 6** describes the sensitivity of using a freehand mobile SPECT gamma camera with 3D navigation to identify ^{99m}Tc-HDP positive lesions in bone scintigraphy. Furthermore, the possible use for future radioguided biopsy osseous and non-osseous applications is discussed.

Chapter 7 describes the preclinical tracer development of a novel hybrid tracer for liver surgery. This approach is based on fluorescence-guided minimally invasive hepatobiliary surgery for liver cancer, including the use of preoperative imaging to visualize the lesions well in advance.

Section 2 concludes with future perspectives in radioguided surgery as discussed in **Chapter 8**, which also contains additional suggestions for expanding the hybrid surgical guidance concept in robot-assisted surgery.

In conclusion, radioguided surgery (RGS) has led to better preoperative surgical planning and a more personalized surgery approach for the patient. The development of tracers and instruments for the pre- as well as the intraoperative procedure has contributed to standardize SN biopsy, replacing extended lymph node dissections in numerous malignancies; this has led to significantly reduce complications such as nerve damage, bleeding, lymphedema and lymphatic leakage. RGS stands and falls with the proper use of tracer for both pre- and intraoperative purposes. Hybrid versions of the radiotracer shows the additional value of visual input during surgery besides the preoperative imaging and intraoperative radioguidance. Nowadays, some surgeons prefer the fluorescent SN procedure as single modality instead of the hybrid version. However, the use of fluorescence alone shows a trend of removing, in addition to the SN, a greater number of resected nodes than needs, drifting away from personalized surgery. In this context, the use of a hybrid approach with bimodal detection technology may solve the limitations of fluorescence alone. For the radioactive component the logistics is the same as used for radioguided surgery and additional investments in this regard are not necessary. Nevertheless, either resting on novel devices or original radiotracers gradual technological advances and subsequent clinical validations are necessary for continuous improving radioguided precision surgery in the future

The results described in this thesis demonstrate the added value of hybrid imaging in various indications and the potential of new hybrid tracers and medical devices in the operating room. Current expansion of use in other indications, development of targeted hybrid tracers and intra-operative devices will further increase the field of RGS and interventional Nuclear Imaging.

The rise of IGR offers the field of IMI unique (out-of-the-box) growth capabilities. Not only in the traditional terms of (radio)pharmaceuticals, engineering, physics and expanding clinical indications, but also in terms of embracing up-and-coming digital-, performance-guided, and autonomous-surgery paradigms. Exploration of these opportunities will expand the impact that nuclear medicine and molecular imaging have on the future of patient care.

10

Nederlandse samenvatting

Preoperatieve beeldvorming van solide tumoren is de cornerstone van adequate stadiëring bij de diagnose van kanker. Patiënten met cN0 of preoperatieve stadiëringsbeeldvorming zonder betrokkenheid van lymfeklieren of metastasen op afstand (iN0M0) ondergaan in opzet curatieve chirurgie. Bij solide tumoren wordt de schildwachtklierprocedure (SN) ingezet om te bepalen of er ondanks iN0M0, micrometastatische ziekte is, wat leidt tot een adequate stadiëring en aangepaste behandelingskeuzes.

Tijdens radiogeleide, chirurgische ingrepen verkent de chirurg het operatieveld op targetlaesies die voor adequate stadiëring van belang zijn; zowel de primaire tumor als de SN(s). In het bebloede operatieveld zijn kleine targets, zoals de SN, niet altijd gemakkelijk te vinden. Vooral niet in gebieden met een moeilijke anatomie, rijk gevasculariseerde of door zenuwen omgeven gebieden. Het zoeken naar deze SN kan in deze uitdagende gebieden leiden tot onnodige verwijdering van gezond weefsel met de bijbehorende complicaties, onvolledige resecties (R1-resecties) of een langere duur van de operatie.

Nauwkeurige preoperatieve beeldvorming, chirurgische planning en intra-operatieve hulpmiddelen om de chirurg naar de gewenste target laesie te leiden, kunnen deze problemen overwinnen. Daarnaast hebben hybride SN-tracers aangetoond dat ze het beste bieden bij zowel pre- als intra-operatieve laesiedetectie.

Sectie 1 van dit proefschrift is gericht op klinische toepassing met gecombineerde pre- en intra-operatieve beeldvorming, waarbij gebruik wordt gemaakt van de hybride SN-tracer ICG-^{99m}Tc-nanocolloïd, alleen of in vergelijking met andere radioactieve tracers, voor nieuwe potentiële klinische indicaties. In deze sectie wordt ook aandacht besteed aan ^{99m}Tc-Tilmanocept, een SN-tracer van de nieuwe generatie.

Hoofdstuk 2 geeft een overzicht van interventionele nucleaire geneeskunde met behulp van bestaande en nieuwe tracers, verschillende detectiemodaliteiten en de belangrijkste indicaties van radiogeleide chirurgie (bijvoorbeeld lymfatische mapping en gerichte tracerontwikkeling).

In **hoofdstuk 3 en 4** worden andere radiocolloïden van verschillende deeltjesgrootte vergeleken met de hybride tracer ICG-^{99m}Tc-nanocolloïd, die is gebaseerd op de meest gebruikte colloïddeeltjesgrootte in Europa. In de klinische studie, beschreven in **hoofdstuk 3**, worden lymfoscintigrafische drainagepatronen, waaronder SN en niet-SLN van ^{99m}Tc-Senti-Scint en de standaard gebruikte tracer ICG-^{99m}Tc-nanocolloïd, met elkaar vergeleken bij patiënten met melanoom van het hoofd-hals gebied en de romp.

In **hoofdstuk 4** worden drainagepatronen, SN-visualisatie en niet-SN-visualisatie van de nieuwere ^{99m}Tc-Tilmanocept, een manose receptor bindende radiocolloid, gepresenteerd en besproken voor SN-procedures bij patiënten met borstkanker en melanoom.

Op basis van een prospectieve pilotstudie bij patiënten met spierinvasief blaaskanker, beschrijft **hoofdstuk 5** de haalbaarheid van SN-targeting met behulp van de hybride tracer indocyanine groen (ICG)^{99m}Tc-nanocolloïde voor preoperatieve beeldvorming en gelijktijdige intra-operatieve radiogeleiding en fluorescentiegeleiding.

In **sectie 2** worden innovaties op het gebied van radiogeleide chirurgie beschreven.

In een preklinische setting beschrijft **hoofdstuk 6** de gevoeligheid van het gebruik van een mobiele (freehand) SPECT-gammacamera om radioactieve (^{99m}Tc-HDP-positieve) laesies gezien op een botscintigrafie te identificeren. Verder wordt het mogelijke gebruik voor toekomstige radiogeleide biopsie in ossale en niet-ossale toepassingen besproken.

In **hoofdstuk 7** wordt de tracerontwikkeling en preklinische evaluatie van een nieuwe, hybride tracer voor leverchirurgie beschreven. Deze aanpak is gebaseerd op fluorescentiegeleide minimaal invasieve hepatobiliaire chirurgie voor leverkanker, waarbij het gebruik van radioactiviteit preoperatieve beeldvorming genereert om de laesies preoperatief te visualiseren.

Toekomstperspectieven in radiogeleide robotchirurgie worden besproken in **hoofdstuk 8**, dat ook aanvullende suggesties bevat voor uitbreiding van het hybride chirurgische geleidingsconcept.

Kortom, radiogeleide chirurgie (RGS) heeft geleid tot een betere preoperatieve chirurgische planning en een meer gepersonaliseerde chirurgische aanpak voor de patiënt. De ontwikkeling op het gebied van zowel tracers als chirurgische instrumenten, voor zowel pre- als intra-operatieve procedures, hebben bijgedragen aan een standaardisering van SN procedure, ter vervanging van uitgebreide klierdissecties bij talrijke solide tumoren. Dit heeft ertoe geleid tot aanzienlijk vermindering van complicaties zoals zenuwbeschadiging, bloedingen, lymfoedeem en lymflekkage. RGS valt en staat bij het juiste gebruik van de tracer, zowel voor pre- als intra-operatieve doeleinden. De hybride versie van de radiotracers tonen toegevoegde waarde van visuele input tijdens operatie naast de preoperatieve beeldvorming en intra-operatieve radiogeleiding. Tegenwoordig geven sommige chirurgen de voorkeur aan fluorescente SN procedure als enkele modaliteit in plaats van de hybride versie. Het gebruik van alleen fluorescentie laat echter een trend zien waarbij, naast de SN, een groter aantal gereseceerde klieren wordt verwijderd dan

nodig. Het gebruik van de hybride benadering met bimodale detectietechnologie zal de beperking van het gebruik van de fluorescentie alleen oplossen. Desalniettemin zijn technologische ontwikkelingen (op het gebied van apparatuur en tracers) en daaropvolgende klinische validaties noodzakelijk voor het voortdurend verbeteren van radiogeleide precisie chirurgie in de toekomst.

De in dit proefschrift beschreven resultaten demonstreren de toegevoegde waarde van hybride beeldvorming bij verschillende indicaties en het potentieel van nieuwe hybride tracers en medisch apparatuur in de operatiekamer. De huidige uitbreiding van het gebruik bij andere indicaties, de ontwikkeling van (targeted) hybride tracers en intra-operatieve apparatuur zal het terrein van RGS en interventionele nucleaire geneeskunde verder vergroten. De opkomst van image guided robotics biedt het gebied van interventional moleculaire imaging unieke groeimogelijkheden. Niet alleen in de traditionele termen van (radio)farmacie, engineering, fysica en groeiende klinische indicaties, maar ook in termen van omarmen van de opkomende digitale, prestatiegeleide en autonome chirurgische paradigma's. Het verkennen van deze mogelijkheden zal de impact, die nucleaire geneeskunde en moleculaire beeldvorming hebben op de toekomst van de patiëntenzorg, vergroten.

A

Appendices

About the author
List of publications
Dankwoord

ABOUT THE AUTHOR

Daphne Rietbergen werd geboren op 27 januari 1981 te Den Haag. Na het behalen van het gymnasiumdiploma aan het Adelbert College in Wassenaar in 2000 behaalde ze in 2005 haar doctoraal en in 2006 het artsexamen in Leiden. Hierna ging ze in opleiding tot Nucleair Geneeskundige in het LUMC, met stages interne geneeskunde en oncologie onder andere in het Slotervaart, NKI en VUMC, waarbij ze haar opleiding voltooide in 2010. Na een jaar fellowship werd ze vast staflid Nucleaire Geneeskunde en trad toe tot de afdeling Radiologie, sectie Nucleaire Geneeskunde LUMC. In 2018 werd Daphne benoemd tot sectiehoofd van de Nucleaire Geneeskunde. Naast haar baan als medisch specialist en sectiehoofd, is ze actief in onderwijs en startte ze in 2018 een PhD research traject bij de Interventional Molecular Imaging (IMI) groep, dat leidde tot deze thesis. Na haar promotie gaat Daphne door met het combineren van zorg, onderwijs en innovatie in samenwerking met de onderzoeksgroepen binnen de Nucleaire Geneeskunde en IMI.

LIST OF PUBLICATIONS

Droste MF, van Velden FHP, van Oosterom MN, Luijk VJ, Burgmans MC, Buckle T, van Leeuwen FWB, **Rietbergen DDD**. Augmenting CT-Guided Bone Biopsies Using ^{18}F-FDG PET/CT Guidance. *Cancers 2024; 16: 2693-2704*

Pisano G, Wendler T, Valdés Olmos RA, Garganese G, **Rietbergen DDD,** Giammarile F, Vidal-Sicart S, Oonk MHM, Frumovitz M, Abu-Rustum NR, Scambia G, Rufini V, Collarino A. Molecular image-guided surgery in gynaecological cancer: where do we stand? *Eur J Nucl Med Mol Imaging. 2024 Aug;51(10):3026-3039*

Leeuwen FWB, Buckle T, van Oosterom MN, **Rietbergen DDD**. The rise of molecular image-guided robotic surgery. *J Nucl Medicine 2024. Online ahead of print*

Tessa Buckle; **Daphne D. D. Rietbergen;** Linda de Wit -van der Veen; Margret Schottelius. Lessons learned in application driven imaging agent design for image-guided surgery. *European Journal of Nuclear Medicine and Molecular Imaging. 2024; 51: 3040-3054*

Fijs W.B. van Leeuwen; Tessa Buckle; **Daphne D.D. Rietbergen**; Matthias N. van Oosterom. The realization of medical devices for precision surgery – development and implementation of 'stop-and-go' imaging technologies. *Expert Review of Medical Devices 2024; 21: 349-358*

Vreeburg MTA, Azargoshasb S, van Willigen D, Molenaar T, van Oosterom MN, Buckle T, Slof LJ, Klop M, Karakullukcu B, Donswijk M, van der Poel H, van Leeuwen FWB, Brouwer OR, **Rietbergen DDD**. Comparison of two hybrid sentinel node tracers: indocyanine green (ICG)-^{99m}Tc-nanocolloid vs. ICG-^{99m}Tc-nanoscan from a nuclear medicine and surgical perspective. *European Journal of Nuclear Medicine and Molecular Imaging 2024; 50 (8): 2282-2291*

Valdés Olmos RA, Collarino A, **Rietbergen DDD**, Pereira Arias-Bouda L, Giammarile F, Vidal-Sicart S. Setting-up a training programme for intraoperative molecular imaging and sentinel node mapping: how to teach? How to learn? *Eur J Nucl Med Mol Imaging. 2024;51(10):2878-2892*

Berrens AC, Scheltema M, Maurer T, Hermann K, Hamdy FC, Knipper S, Dell'Oglio P, Mazzone E, de Barros HA, Sorger JM, van Oosterom MN, Stricker PD, van Leeuwen PJ, **Rietbergen DDD**, Valdés Olmos RA, Vidal-Sicart S, Carroll PR, Buckle T, van der Poel HG, van Leeuwen FWB.Delphi consensus project on prostate-specific membrane antigen (PSMA)-targeted surgery-outcomes from an international multidisciplinary panel. *Eur J Nucl Med Mol Imaging. 2024;51(10):2893-2902*

Daphne D.D. Rietbergen, Tessa Buckle, Leon J. Slof, Maarten P. van Meerbeek, Clarize M. de Korne, Mick M. Welling, Matthias N. van Oosterom, Kevin Bauwens, Meta Roestenberg, Julia Kloetzl, Fijs W.B. van Leeuwen. hHEPATO-Cy5, a bi-modal tracer for image-guided hepatobiliary surgery. *JNM. 2024; 65(8):1301-1306*

Pim Hendriks, **Daphne D. D. Rietbergen**, Arian R. van Erkel, Minneke J. Coenraad, Mark J. Arntz, Roel J. Bennink, Andries E. Braat, Stijn Crobach, Otto M. van Delden, Petra Dibbets-Schneider et al. Adjuvant holmium-166 radioembolization after radiofrequency ablation in early-stage hepatocellular carcinoma patients: a dose-finding study (HORA EST HCC trial). *European Journal of Nuclear Medicine and Molecular Imaging 2024; 51: 2085-2097*

Renato A. Valdés Olmos, **Daphne D.D. Rietbergen**, Sergi Vidal-Sicart. About disruptive innovations in radioguided precision surgery. *Clin Trans Imaging 2023;11: 509-512*

Welling MM, Duszenko N, van Meerbeek MP, Molenaar TJM, Buckle T, van Leeuwen FWB, **Rietbergen DDD**. Microspheres as a Carrier System for Therapeutic Embolization Procedures: Achievements and Advances. *J Clin Med. 2023 Feb; 12(3): 918*

Welling MM, Warbroek K, Khurshid C, van Oosterom MN, **Rietbergen DDD**, de Boer MGJ, Nelissen RGHH, van Leeuwen FWB, Pijls BG, Buckle T. A radio- and fluorescently labelled tracer for imaging and quantification of bacterial infection on orthopaedic prostheses: a proof of principle study. *Bone Joint Res. 2023 Jan;12(1):72-79*

Rietbergen DDD, van Gennep EJ, KleinJan GH, Donswijk M, Olmos RAV, van Rhijn BW, van der Poel HG, van Leeuwen FWB. Evaluation of the Hybrid Tracer Indocyanine Green–99mTc-Nanocolloid for Sentinel Node Biopsy in Bladder Cancer—A Prospective Pilot Study. *Clinical Nuclear Medicine 2022; 47 (9): 774-780*

Azargoshasb S, Boekestijn I, Roestenberg M, KleinJan GH, van der Hage JA, van der Poel HG, **Rietbergen DDD**, van Oosterom MN, van Leeuwen FWB. Quantifying the Impact of Signal-to-background Ratios on Surgical Discrimination of Fluorescent Lesions. *Mol Imaging Biol. 2023 Feb;25(1):180-189*

Imke Boekestijn, Matthias N. van Oosterom, Paolo Dell'Oglio, Floris H. P. van Velden, Martin Pool, Tobias Maurer, **Daphne D. D. Rietbergen**, Tessa Buckle, Fijs W. B. van Leeuwen. The current status and future prospects for molecular imaging-guided precision surgery. *Cancer Imaging. 2022; 22: 48*

Hendriks P, **Rietbergen DDD**, van Erkel AR, Coenraad MJ, Arntz MJ, Bennink RJ, Braat AE, Crobach ASLP, van Delden OM, van der Hulle T, Klümpen HJ, van der Meer RW, Nijsen JFW, van Rijswijk CSP, Roosen J, Ruijter BN, Smit F, Stam MK, Takkenberg RB, Tushuizen ME, van Velden FHP, de Geus-Oei LF, Burgmans MC; Dutch Hepatocellular Cholangiocarcinoma Group. Study Protocol: Adjuvant Holmium-166 Radioembolization After Radiofrequency Ablation in Early-Stage Hepatocellular Carcinoma Patients-A Dose-Finding Study (HORA EST HCC Trial). *Cardiovasc Intervent Radiol. 2022 Aug;45(8):1057-1063*

Bijlstra OD, Boreel MME, van Mossel S, Burgmans MC, Kapiteijn EHW, Oprea-Lager DE, **Rietbergen DDD**, van Velden FHP, Vahrmeijer AL, Swijnenburg RJ, Mieog JSD, de Geus-Oei LF. The Value of ^{18}F-FDG-PET-CT Imaging in Treatment Evaluation of Colorectal Liver Metastases: A Systematic Review. *Diagnostics (Basel). 2022 Mar 15;12(3):715*

Dotinga M, Vriens D, van Velden FHP, Stam MK, Heemskerk JWT, Dibbets-Schneider P, Pool M, **Rietbergen DDD**, de Geus-Oei LF, Kapiteijn E. Reinducing Radioiodine-Sensitivity in Radioiodine-Refractory Thyroid Cancer Using Lenvatinib (RESET): Study Protocol for a Single-Center, Open Label Phase II Trial. *Diagnostics (Basel). 2022 Dec 14;12(12):3154*

Grootjans W, **Rietbergen DDD**, van Velden FHP. Added Value of Respiratory Gating in Positron Emission Tomography for the Clinical Management of Lung Cancer Patients. *Semin Nucl Med. 2022 Nov;52(6):745-758*

Daphne D.D. Rietbergen, Erik J. van Gennep, Gijs H. KleinJan, Maarten Donswijk, Renato A.Valdés Olmos, Bas W. van Rhijn, Henk G. van der Poel, Fijs W.B. van Leeuwen. Evaluation of the Hybrid Tracer Indocyanine Green–^{99m}Tc-Nanocolloid for Sentinel Node Biopsy in Bladder Cancer—A Prospective Pilot Study. *Clin Nucl Med. 2022 Sep; 47(9): 774–780*

Imke Boekestijn, Samaneh Azargoshasb, Matthias N. van Oosterom, Leon J. Slof, Petra Dibbets-Schneider, Jenny Dankelman, Arian R. van Erkel, **Daphne D. D. Rietbergen**, Fijs W. B. van Leeuwen. Value-assessment of computer-assisted navigation strategies during percutaneous needle placement. *Int J Comput Assist Radiol Surg. 2022; 17(10): 1775–1785*

Mostert JM, Romeijn SR, Dibbets-Schneider P, **Rietbergen DDD**, Pereira Arias-Bouda LM, Götz C, DiFranco MD, Dimai HP, Grootjans W. Inter-observer agreement of vertebral fracture assessment with dual-energy x-ray absorptiometry equipment. *Arch Osteoporos. 2021 Dec 10;17(1):4*

Welling MM, Duszenko N, van Willigen DM, Hensbergen AW, Buckle T, **Rietbergen DDD,** Roestenberg M, van Leeuwen FWB. Interventional nuclear medicine: "click" chemistry as an in vivo targeting strategy for imaging microspheres and bacteria. *Biomater Sci. 2021 Mar 10;9(5):1683-1690*

Diederick J. van Doorn, Pim Hendriks, Mark C. Burgmans, **Daphne D. D. Rietbergen**, Minneke J. Coenraad, Otto M. van Delden, Roel J. Bennink, Tim A. Labeur, Heinz-Josef Klümpen, Ferry A. L. M. Eskens, Adriaan Moelker, Erik Vegt, Dave Sprengers, Nahid Mostafavi, Jan Ijzermans, R. Bart Takkenberg. Liver Decompensation as Late Complication in HCC Patients with Long-Term Response following Selective Internal Radiation Therapy. *Cancers (Basel) 2021 Nov; 13(21): 5427.*

Boekestijn I, Azargoshasb S, Schilling C, Navab N, **Rietbergen D**, van Oosterom MN. PET- and SPECT-based navigation strategies to advance procedural accuracy in interventional radiology and image-guided surgery. Q *J Nucl Med Mol Imaging. 2021 Sep;65(3):244- 260*

Rietbergen DD, Pereira Arias-Bouda LM, van der Hage J, Valdés Olmos RA. Does ^{99m}Tc-tilmanocept, as next generation radiotracer, meet with the requirements for improved sentinel node imaging? *Rev Esp Med Nucl Imagen Mol. 2021; 40(5):275-280*

Daphne D. Rietbergen, Matthias N. van Oosterom, Gijs H. KleinJan, Oscar R.Brouwer,Renato A. Vald és-Olmos, Fijs W. Van leeuwen, Tessa Buckle. Interventional nuclear medicine: a focus on radioguided intervention and surgery. *The Quarterly Journal of nuclear Medicine and Molecular imaging 2021 March;65(1):4-19*

Valdés Olmos RA, **Rietbergen DDD,** Rubello D, Pereira Arias-Bouda LM, Collarino A, Colletti PM, Vidal-Sicart S, van Leeuwen FWB. Sentinel Node Imaging and Radioguided Surgery in the Era of SPECT/CT and PET/CT: Toward New Interventional Nuclear Medicine Strategies. *Clin Nucl Med. 2020 Oct;45(10):771-777*

Deken MM, van Doorn HC, Verver D, Boogerd LSF, de Valk KS, **Rietbergen DDD**, van Poelgeest MIE, de Kroon CD, Beltman JJ, van Leeuwen FWB, Putter H, Braak JPBM, de Geus-Oei LF, van de Velde CJH, Burggraaf J, Vahrmeijer AL, Gaarenstroom KN. Near- infrared fluorescence imaging compared to standard sentinel lymph node detection with blue dye in patients with vulvar cancer - a randomized controlled trial. *Gynecol Oncol. 2020 Dec;159(3):672-680*

Rietbergen DDD, Meershoek P, KleinJan GH, Donswijk M, Valdés Olmos RA, van Leeuwen FWB, Klop MWMC, van der Hage JA. Head-to-head comparison of the hybrid tracer indocyanine green-^{99m}Tc-nanocolloid with ^{99m}Tc Senti-Scint using sentinel node lymphoscintigraphy and single-photon emission computed tomography combined

with computer tomography in melanoma. *Nucl Med Commun. 2020 Oct;41(10):1010-1017*

Burgmans MC, Hendriks P, **Rietbergen DDD**. Does a Widely Adopted Approach Need Reconsideration: Embolization of Parasitized Extrahepatic Tumor Feeders in Patients Undergoing Transarterial Liver-Directed Therapy? *Cardiovasc Intervent Radiol. 2020 Jul;43(7):1103-1104*

Rietbergen DDD, Meershoek P, van Oosterom MN, Roestenberg M, van Erkel AR, Smit F, van der Hage JA, Valdés Olmos RA, van van Leeuwen FWB. Freehand-SPECT with ^{99m}Tc-HDP as tool to guide percutaneous biopsy of skeletal lesions detected on bone scintigraphy. *Rev Esp Med Nucl Imagen Mol (Engl Ed). 2019; 38(4):218-223*

Welling MM, Spa SJ, van Willigen DM, **Rietbergen DDD,** Roestenberg M, Buckle T, van Leeuwen FWB. In vivo stability of supramolecular host-guest complexes monitored by dual-isotope multiplexing in a pre-targeting model of experimental liver radioembolization. *J Control Release. 2019 Jan 10; 293: 126-134*

Van Oosterom MN, **Rietbergen DDD**, Welling MM, Van Der Poel HG, Maurer T, Van Leeuwen FWB. Recent advances in nuclear and hybrid detection modalities for image-guided surgery. *Expert Rev Med Devices. 2019 Aug;16(8):711-734*

Spa SJ, Welling MM, van Oosterom MN, **Rietbergen DDD**, Burgmans MC, Verboom W,Huskens J, Buckle T, van Leeuwen FWB. A Supramolecular Approach for Liver Radioembolization. *Theranostics. 2018; 8(9): 2377–2386*

Andrés Perissinotti, **Daphne DD Rietbergen**, Sergi Vidal-Sicart, Ana A Riera, Renato A Valdés Olmos. Melanoma & nuclear medicine: new insights & advances. *Melanoma Manag. 2018 Jun; 5(1): MMT06*

KleinJan GH, Brouwer OR, Mathéron HM, Rietbergen DD, Valdés Olmos RA, Wouters MW, van den Berg NS, van Leeuwen FW. Hybrid radioguided occult lesion localization (hybrid ROLL) of F-18-FDG-avid lesions using the hybrid tracer indocyanine green-Tc- 99m-nanocolloid. *Rev Esp Med Nucl imagen Mol 2016; 35 (5): 292-297*

Floris P.R. Verbeek, Quirijn R.J.G. Tummers, **Daphne D.D. Rietbergen**, Alexander A.W. Peters, Boudewijn E. Schaafsma, Cornelis J.H. van de Velde, John V. Frangioni, Fijs W.B. van Leeuwen, Katja N. Gaarenstroom, Alexander L. Vahrmeijer. Sentinel Lymph Node Biopsy in Vulvar Cancer using Combined Radioactive and Fluorescence Guidance. *Int J Gynecol Cancer. J Gynecol Cancer. 2015; 25(6): 1086–1093*

Thijs Engelen, Beatrice MF Winkel, **Daphne DD Rietbergen**, Gijs H KleinJan, Sergi Vidal-Sicart, Renato A Valdés Olmos, Nynke S van den Berg, Fijs WB van Leeuwen. The next evolution in radioguided surgery: breast cancer related sentinel node localization using a freehandSPECT-mobile gamma camera combination. *Am J Nucl Med Mol Imaging. 2015; 5(3): 233–245*

Andele D de Zwart, Frank JP Beeres, **Daphne DD Rietbergen,** Pieta Krijnen, Inger B Schipper. Initial experience of SPECT/CT in the diagnosis of occult scaphoid fracture. *Acta Radiol Open. 2015 Oct; 4(10): 2058460115602729*

Valdés Olmos RA, **Rietbergen DD,** Vidal-Sicart S, Manca G, Giammarile F, Mariani G. Contribution of SPECT/CT imaging to radioguided sentinel lymph node biopsy in breast cancer, melanoma, and other solid cancers: from "open and see" to "see and open". *Q J Nucl Med Mol Imaging. 2014 Jun;58(2):127-39.* Review

Rietbergen D. D. D., Engelen T, Winkel B., et al. A new method for preoperative sentinel node identification and localization: a prototypical combination of freehandSPECT with a handheld gamma camera. *Eur J Nucl Med Mol Imaging 2014; 4: S264-S264*

Rietbergen Daphne, Winkel Beatrice, van den Berg Nynke, Pouw B, Engelen T, Valdes Olmos R, van Leeuwen FWB. 3D Freehand SPECT of the sentinel node using a navigated handheld gamma imaging probe.*Journal of Nuclear Medicine 2014; 55 (1): 1543*

Boudewijn E. Schaafsma, Floris P.R. Verbeek, **Daphne D.D. Rietbergen**, Bernies van der Hiel, Joost R. van der Vorst, Gerrit-Jan Liefers, John V. Frangioni, Cornelis J.H. van de Velde, Fijs W.B. van Leeuwen, Alexander L. Vahrmeijer. Clinical trial of combined radio- and fluorescence-guided sentinel lymph node biopsy in breast cancer. *Br J Surg 2013 Jul; 100(8): 1037–1044*

van den Berg N. S., KleinJan G. H., **Rietbergen D. D. D.,** et al. An opto-nuclear probe for combined radio- and fluorescence guided sentinel node biopsy. *Eur J Nucl Med Mol Imaging 2013; 40: S154*

Rietbergen D. D. D., Schaafsma BE, Liefers GJ et al. Dose optimization of ICG-Tc-99m-nanocolloid for combined radioguided and optical sentinel biopsy of the breast. *European Journal of Nuclear Medicine and Molecular Imaging 2012; 39: 176-177*

Bookchapters
Leerboek Nucleaire Geneeskunde. Chapter: Sentinel Node procedure

Renato A. Valdés Olmos, Lenka M. Pereira Arias-Bouda, **Daphne D.D. Rietbergen**, Jos A. van der hage. Breast Cancer. In Nuclear Medicine Manual in Female Cancer, Collarino A. Vidal-Sicart S, Valdés Olmos RA (eds), Springer Nature Switzerland, 2022.

Renato A. Valdés Olmos, Sergi Vidal-Sicart, **Daphne DD Rietbergen**. Sentinel node detection in melanoma. In Nuclear Medicine and Molecular Imaging, Signore A (ed), Elsevier, Oxford, 2022.

Dankwoord

Na jaren van samenwerking in het wetenschappelijke domein mag mijn promotieboek dan eindelijk gebonden worden. Het is een mooie reis geweest die een jaar of 10 geleden begon, aan de vooravond van de bevalling van mijn tweede kind. Het is een reis geworden van zaadjes planten, ideeën uitvoeren, studies opzetten tussen de bedrijven door van het bestaan als medisch specialist, sectiehoofd en uiteraard als CEO van een gezin van 4, samen met mijn man. Het waren uitdagende tijden en dit alles was dan ook niet mogelijk geweest zonder alle steun en samenwerking die ik heb mogen ontvangen van een fantastisch team zowel op werk als privé. Samenwerkingen binnen de sectie Nucleaire Geneeskunde, Klinische Fysica, de afdeling Radiologie, collega verwijzers in het LUMC en andere centra zoals het NKI-AvL. Maar bovenal zou dit promotieboekje niet voor u liggen zonder de fantastische begeleiding en steun van de IMI-researchgroep en de onvoorwaardelijke steun en afleiding van mijn gezin, familie en vrienden.

Beste Fijs, bedankt voor jouw bedrevenheid, jouw vertrouwen en geloof in mij en de projecten waar we samen aan hebben gewerkt. Door de samenwerking met jou heb ik oog gehad voor meer dan alleen mijn eigen PhD traject waar ik inzicht heb gekregen in het gehele spectrum en alle facetten die komen kijken bij het beoefenen van research.

Beste Renato, maestro, sinds mijn stage bij jou in het NKI zie ik jou als voorbeeld van de beeldgeleide SN chirurgie binnen de Nucleaire Geneeskunde. Het is een hele eer dat ik met jou heb mogen samenwerken, veel dank daarvoor Renato.

Beste Tessa, de grote steun en toeverlaat, zeer bekwaam en gedreven. Dank voor de fijne samenwerking, onze goede gesprekken en het toevertrouwen van jouw/ onze toekomstige projecten.

Beste Fijs, Renato, Tessa, op naar nog meer vele mooie projecten en samenwerkingen!

Beste collega's van de IMI, Nucleaire Geneeskunde, Klinische Fysica en Radiologie, dank voor jullie steun, jullie luisterend oor, momenten van sparren en jullie oplossende vermogen.

Lieve broers, familie & schoonfamilie, dank jullie wel voor jullie steun en goede zorgen, voor mij, Rutger en onze kinderen. Het is altijd fijn te weten dat de kinderen het naar hun zin hebben als ik weer eens moest werken of een praatje op congres gegeven moest worden. Lieve vrienden, dank voor al jullie interesse in mijn promotie, het geduld dat jullie moesten tonen als ik weer zei "het is bijna klaar, nog even…", de gezellige momenten met de meiden, gezinnen of stellen. Ook heeft dit zo nu en dan

wel eens geknaagd, als ik weer een keer niet kon aanhaken bij een borrel of diner. Als het goed zal er vanaf nu meer tijd zijn om er meer bij te zijn. Lieve paranimfen, dank voor jullie steun naar aanloop van en tijdens de verdediging.

Lieve mam en pap, bedankt dat ik er ben, voor al die jaren die jullie voor mij klaar stonden en voor wie ik ben geworden. Ik had het niet beter met jullie kunnen treffen. Lieve Beau, Feline, Tijn en Tom, zonder jullie kanjers waren de dagen stukken minder zonnig geweest. Jullie zijn samen met pappa de liefdevolle afleiding geweest tussen al het schrijven en analyseren door. Lieve Rut, zonder jouw steun, hulp en afleiding was dit nooit gelukt, dank je wel. En nu is mijn proefschrift dan ook eindelijk klaar ;-).